I

666

MULTINUCLEAR (TIN-119, CARBON-13, DEUTERIUM) N.M.R. SPIN-LATTICE RELAXATION STUDIES ON ORGANOTIN COMPOUNDS

A thesis submitted by

ANDREW FRANGOU

in candidature for

the degree of Doctor of Philosophy

of the University of London

The Bourne Laboratory
Royal Holloway College
University of London
Egham Hill
Egham
Surrey

Feb 1979

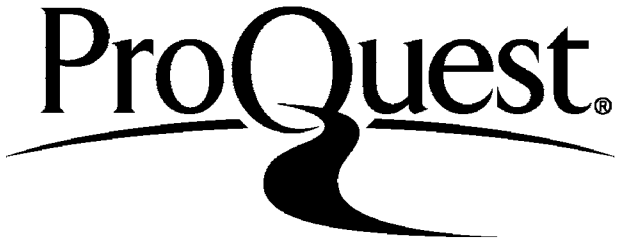

Acknowledgements

The author would like to express his gratitude to Dr Duncan Gillies for his guidance and encouragement during the course of this work and to Dr Peter Beynon of Jeol Ltd. and Dr Ian Stenhouse for the measurements carried out on the Jeol FX100Q and the Bruker HX90 respectively. Thanks are also due to Mr Ian Cresshull for the software development relating to the spectrometer in this laboratory.

In addition the author wishes to thank all the staff and research students of the Bourne Laboratory whose seemingly constant good humour and friendship have made the author's stay a very happy one.

A research studentship from the Science Research Council is gratefully acknowledged.

Finally the author would like to thank Mrs E I Kearsey for typing this thesis.

This thesis is dedicated to my wife, Sally, for her constant support and encouragement especially during the latter stages of this work.

Abstract

The carbon-13, tin-119 and deuterium NMR spectra of a number of organo tin compounds have been detected by direct observation. The compounds fall into two main classes consisting of organo tin hydrides and organo tin chlorides. Tin-119 spin-lattice relaxation data for nPr_3SnCl, nBu_3SnCl, Sn_2Me_6 and nBu_4Sn were measured, the first three over a temperature range. Measurements of tin-119 T_1 values were carried out with proton decoupling using the inversion-recovery technique. NOE factors were measured by comparing spectra resulting from continuous and gated proton decoupling. For the n-alkyl tin compounds the T_1 and NOE data indicated contributions to the total rate arising from the dipole-dipole interactions of tin-119 with remote protons. The competing mechanism was spin-rotation. T_1 values were typically less than 5 seconds. Measurements of tin-119 T_1 values in the hydrides were complicated by the magnitude of $^1J_{^{119}Sn-H}$ (>1500 Hz) and only for nBu_3SnH and Ph_3SnH have T_1 and NOE factors been determined.

Carbon-13 T_1 measurements have been made for Sn_2Me_6, nPr_3SnH, nBu_3SnH, nPr_3SnCl, nBu_3SnCl and Ph_3SnH. NOE factors have been determined for the last four molecules. Segmental motion was apparent in the n-alkyl chains. For Ph_3SnH rotation of the phenyl groups about the tin-carbon bond was indicated and the ratio of $D_{||}/D_{\perp}$ has been determined.

The spin-lattice relaxation time of ^2H in nBu_3SnD over a range of temperature was measured and the quadrupole coupling constant of deuterium in the $^{119}Sn-D$ bond was estimated as 88 ± 10 kHz.

The variation of the tin-119 chemical shift of $nBu_2Sn(OAc)_2$ with temperature and concentration has been investigated and the data can be adequately explained in terms of a monomer-dimer equilibrium. Equilibrium constants and the enthalpy for the dissociation of the dimer have been evaluated. The tin-119 T_1 and NOE data for this molecule at 1.4 and 2.3 T indicated a significant contribution to the relaxation from a field dependent mechanism.

CONTENTS

CHAPTER 1

Basic NMR Theory

Section 1

A. Basic Principles

A characteristic of all nuclei is the possession of a positive charge. Nuclei of odd mass number and odd atomic number also possess angular momentum, characterised by the spin quantum number I (in units of $\hbar$). For nuclei of this type $I = \frac{1}{2}$. The nuclear spin has associated with it a magnetic moment μ which acts in the direction of the axis of rotation. In the presence of a magnetic field Bo, applied in the z direction the magnetic moment has an energy E given by

$$E = -\underline{\mu} \cdot \underline{B} = -\mu_z \underline{B}_o \qquad 1$$

where μ_z is the z component of μ. In the case of nuclear spin this component is defined by m_I given by

$$\mu_z = \gamma \hbar m_I \qquad 2$$

So equation 1 becomes

$$E = -\gamma \hbar m_I B_o \qquad 3$$

For a nucleus of spin $I = \frac{1}{2}$ in the presence of a magnetic field there exist $2I + 1$ non-degenerate energy levels which correspond to the $2I + 1$ allowed values of m_I. Clearly the levels are separated by $\gamma \hbar Bo$.

In principle, therefore to induce transitions between the levels all that is required is electromagnetic radiation of the appropriate frequency. This is the condition of resonance. For a single nucleus

$$\nu = \frac{\gamma}{2\pi} B_o \qquad 4$$

where ν is known as the Lamor frequency. In radians $\omega_o = \gamma B_o$.

Pulse experiments, with which this thesis is mainly concerned can be more readily appreciated in terms of a classical treatment concerning the equation of motion of the magnetic moments in a magnetic field.

B

The Bloch Equations

A nucleus of spin I and $\mu = \gamma I$ placed in a magnetic field Bo (in the z direction) experiences a torque which causes it to move in a manner described by

$$\frac{d\mu}{dt} = \gamma (\mu \times \underline{B}) \qquad 5$$

where $\mu = (\mu_x + \mu_y + \mu_z)$ and $B = (0,0,B_o)$

$$\mu \times B = \begin{bmatrix} i & j & k \\ \mu_x & \mu_y & \mu_z \\ B_x & B_y & B_z \end{bmatrix} \qquad 6$$

Expanding equation 6 we may write

$$\frac{d\mu_x}{dt} = (\mu_y B_z - \mu_z B_y) \qquad 7a$$

$$\frac{d\mu_y}{dt} = (\mu_z B_x - \mu_x B_z) \qquad 7b$$

$$\frac{d\mu_z}{dt} = (\mu_x B_y - \mu_y B_x) \qquad 7c$$

Since $B_x = B_y = 0$ and $B_z = B_o$ equation 7 can be written as

$$\frac{d\mu_x}{dt} = \gamma \mu_y B_o \qquad 8a$$

$$\frac{d\mu_y}{dt} = -\gamma \mu_x B_o \qquad 8b$$

$$\frac{d\mu_z}{dt} = 0 \qquad 8c$$

Equation 8 describes the precession of a single magnetic moment about the z axis at an angular frequency ω_o. In a sample of only one chemically shifted nucleus (see section 3) there will be many magnetic moments all precessing at ω_o. However the phase of the precessing nuclei will be randomly distributed (Figure 1).

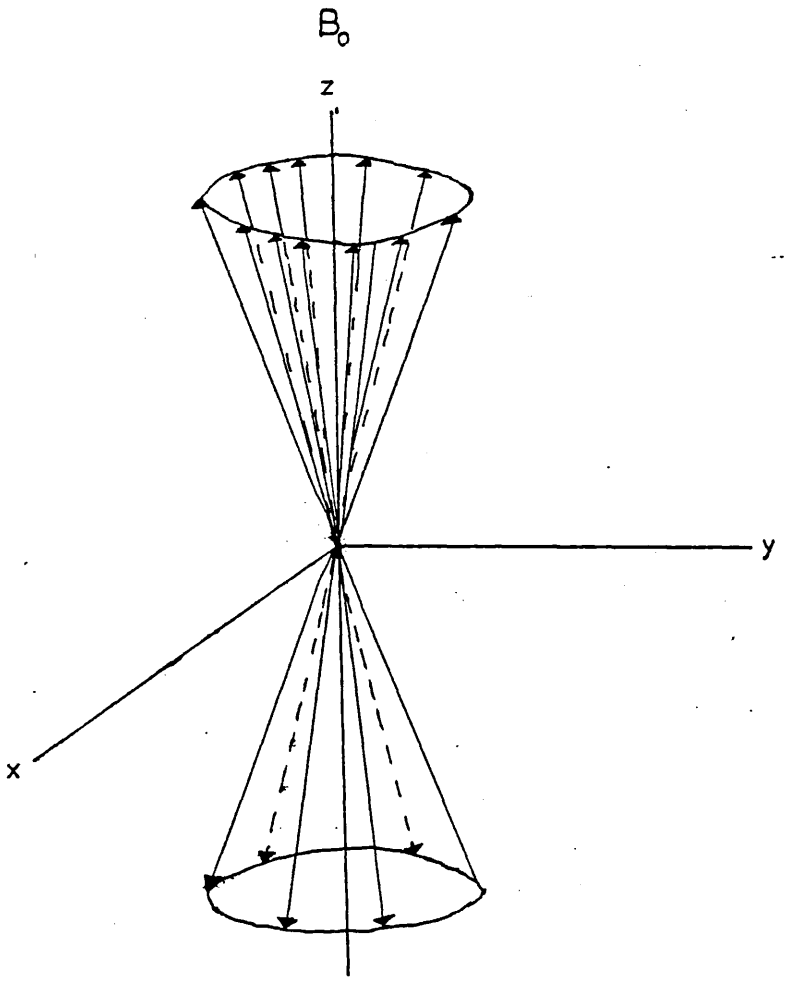

Figure 1

At equilibrium more nuclei are aligned in the direction of the magnetic field than against since the Boltzmann distribution will

always favour the lower energy state. So a net macroscopic magnetisation M exists having a resultant only in the +ve z direction. There is no magnetisation in the x or y direction since the moments are randomly phased in the xy plane.

So we may write

$$\underline{M} = (0, 0, M_o)$$

To observe the NMR spectrum of such a system it is necessary to disturb the system by a smaller time dependent radiofrequency field B_1, which is itself rotating with angular frequency, ω in the same sense as the precessing nuclei. Under such conditions the x and y components of the magnetisation become non zero as ω approaches ω_o.

The rotating field is provided by a linear radiofrequency in the x direction. This field can be resolved into two components rotating in the xy plane with angular frequency ω in opposite senses. Only the component with the correct sense of rotation interacts with the precessing nuclei to a detectable extent. The equation of motion may now be written in terms of the macroscopic magnetisation M and the total field B.

$$\frac{d\underline{M}}{dt} = \gamma(\underline{M} \times \underline{B}) \qquad 9$$

where $\underline{M} = (M_x, M_y, M_z)$ $\quad \underline{B} = (B_1 \cos\omega t, -B_1 \sin\omega t, B_o)$

So

$$\frac{dM_x}{dt} = \gamma(M_y B_o + M_z B_1 \sin\omega t) \qquad 10a$$

$$\frac{dM_y}{dt} = \gamma (M_z B_1 \cos\omega t - M_x B_o) \qquad 10b$$

$$\frac{dM_z}{dt} = -\gamma (M_x B_1 \sin\omega t + M_y B_1 \cos\omega t) \qquad 10c$$

These are the Bloch equations, as yet incomplete since to describe the system correctly terms must be added to account for the relaxation of the x, y and z components of the magnetisation back to their equilibrium values. Two first order rate constants are required $\frac{1}{T_1}$ and $\frac{1}{T_2}$, where T_1 describes the decay of the longitudinal magnetisation Mz and T_2 the decay of the transverse magnetisation Mx and My. So the Bloch equations in full are

$$\frac{dM_x}{dt} = \gamma (M_y B_o + M_z B_1 \sin\omega t) - M_x/T_2 \qquad 11a$$

$$\frac{dM_y}{dt} = \gamma (M_z B_1 \cos\omega t - M_x B_o) - M_y/T_2 \qquad 11b$$

$$\frac{dM_z}{dt} = -\gamma (M_x B_1 \sin\omega t + M_y B_1 \cos\omega t) - (M_z - M_o)/T_1 \qquad 11c$$

The transverse relaxation processes (T_2 processes) cause dephasing of the nuclear spins which become phased as ω approaches ω_o and the resonance condition is met. The dephasing results from the variation of local magnetic fields of individual nuclei. The longitudinal relaxation time, T_1 depends on how effectively the spin system is coupled with the lattice. T_1 processes will be discussed in more detail in Chapter 2.

C

The Rotating Frame

The above derivation of the Bloch equation has been carried out in the laboratory frame of reference. This fixed coordinate system may be replaced by a coordinate system that rotates about Bo in the direction of the magnetisation. In such a system certain pulse experiments (see section 5) are more readily understood.

In the rotating frame u is defined as the component of M along the B_1 direction (in phase) and v is the component of M perpendicular to B_1 (out of phase by 90°). It should be noted that in the rotating frame B_1 is stationary (see Figure 2).

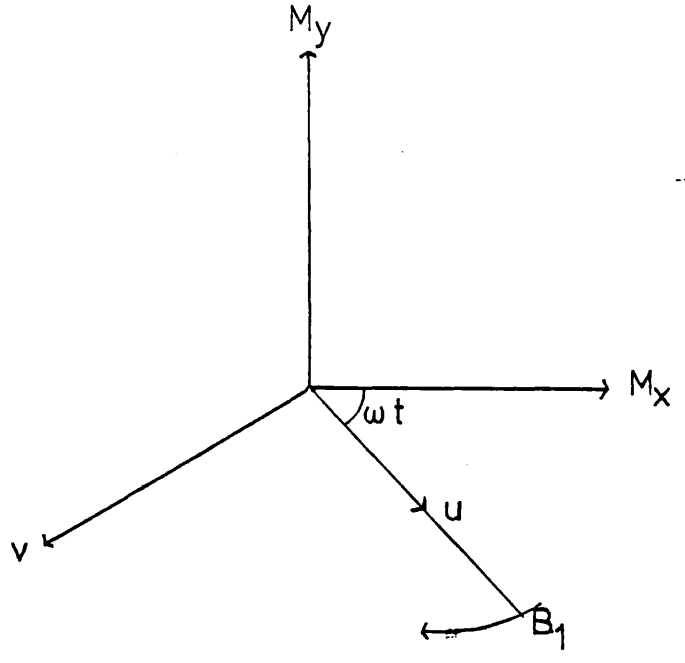

Figure 2

In the rotating frame the magnetic field B is given by

$$\underline{B} = (B_1, 0, B_o) \qquad 12$$

and the magnetisation by

$$\underline{M} = (u, -v, M_z) \qquad 13$$

Also ω_o should be replaced by $(\omega_o - \omega)$. So the Bloch equations in the laboratory frame may be rewritten in the rotating frame as

$$\frac{du}{dt} = -(\omega_o - \omega)v - u/T_2 \qquad 14a$$

$$\frac{dv}{dt} = (\omega_o - \omega)u - \gamma M_z B_1 - v/T_2 \qquad 14b$$

$$\frac{dM_z}{dt} = \gamma B_1 v - (M_z - M_o)/T_1 \qquad 14c$$

Equations 14a - 14c can be solved for various limiting conditions to obtain the familiar Lorentzian equation that describes the NMR line shape, In section 2 the effect of chemical exchange on the Bloch equations will be considered and following the treatment of Sutherland (see refs.) the concept of a complex magnetisation G in the xy plane will be developed here to facilitate discussion later.

$$G = u + iv \text{ and } \frac{dG}{dt} = \frac{du}{dt} + \frac{idv}{dt} \qquad 15$$

where the imaginary component of G describes the absorption spectrum. Combining equations 14 and 15 we may write

$$\frac{dG}{dt} = i(\omega_o - \omega)G - i\gamma B_1 M_z - G/T_2 \qquad 16a$$

$$\frac{dM_z}{dt} = \gamma B_1 v - (M_z - M_o)/T_1 \qquad 16b$$

So the variation of the complex magnetisation G may be obtained from equation 16a, the imaginary component of which is the absorption intensity at ω. In the cw experiment the observing radiofrequency

(RF) ω is swept slowly (so called steady state conditions) so that the time derivatives above are set to zero. Also the RF is so small that the equilibrium value of the magnetisation M_o is used as the z component. Thus equation 16a can be rewritten as

$$\frac{dG}{dt} = i(\omega_o - \omega)G - iC - G/T_2 = 0 \qquad 17$$

where $C = \gamma B_1 Mz$

Rearranging yields

$$G = \frac{-iC}{1/T_2 - i(\omega_o - \omega)} \qquad 18$$

We note that G is of the form $(a + ib)/(c + id)$ so it is a simple step to extract the imaginary part of G.

$$\text{Im}G = \frac{-C\,T_2}{1 + T_2^{\,2}(\omega_o - \omega)^2} \qquad 19$$

This is the familiar Lorentzian line shape equation for the absorption NMR signal centred at ω_o.

Section 2

Introduction

In section 1 the derivation of the Bloch equations was described. For a two site exchange where spin coupling is absent the original equations may be quite simply modified to account for this exchange. For such a simple case it is unnecessary to carry out a full density matrix treatment.[1,2]

The effect on the line shape of such a two site exchange processes will now be considered following the approach of Hahn, Maxwell and McConnell.[3,4]

A

The Bloch Equations Modified by Exchange

Consider the case of a nucleus exchanging between two sites which we label A and B, the site populations being p_A and p_B respectively. The kinetics of the exchange process are described by two first order rate constants k_A and k_B where k_A is the transfer rate from site A to site B and k_B from site B to site A. At equilibrium then

$$k_A p_A = k_B p_B$$

The simplifying assumption that exchange of sites is instantaneous is made. In other words a nucleus "jumping" from site A to site B does so in a time short enough that nuclear precession does not occur. The effect of a nucleus jumping from site A to site B will be a decrease in the transverse magnetisation at site A which occurs at a rate $k_A G_A$ and an increase of the magnetisation at site B at the same rate. For jumps from site B to A the magnetisation at B decreases at a rate $k_B G_B$ and increases at A by the same amount. These changes in the complex magnetisation at the two sites can be incorporated into the Bloch equations

Written separately for sites A and B

$$\frac{dG_A}{dt} + \alpha_A G_A = -i \quad B_1 M_{2A} + k_B G_B - k_A G_A \qquad 2a$$

$$\frac{dG_B}{dt} + \alpha_B G_B = -i \quad B_1 M_{zB} + k_A G_A - k_B G_B \qquad 2b$$

where

$$\alpha_A = \frac{1}{T_{2A}} - 2\pi i(\nu_A - \nu)$$

$$\alpha_B = \frac{1}{T_{2B}} - 2\pi i(\nu_B - \nu)$$

As described in section 1 under steady state conditions the z components of the magnetisation, M_z are not appreciably changed from their equilibrium value Mo. In particular we may write

$$M_{zA} = M_{oA} = p_A M_o$$

$$M_{zB} = M_{oB} = p_B M_o$$

Also the time derivatives in equations 2a, 2b can be set to zero, so they may be rewritten

$$\alpha_A G_A = -i\gamma B_1 p_A M_o + k_B G_B - k_A G_A \qquad 3a$$

$$\alpha_B G_B = -i\gamma B_1 p_B M_o + k_A G_A - k_B G_B \qquad 3b$$

Setting $\gamma B_1 M_o = C$ and rearranging yields

$$\alpha_A G_A + k_A G_A - k_B G_B = -ip_A C \qquad 4a$$

$$\alpha_B G_B + k_B G_B - k_A G_A = -ip_B C \qquad 4b$$

Hence the total magnetisation $G = G_A + G_B$ may be obtained from equations 4a and 4b. This may be more conveniently expressed in terms of the lifetime τ of a particular site where

$$\tau_A = \frac{1}{k_A} \quad \text{and} \quad \tau_B = \frac{1}{k_B}$$

The measured absorption intensity at a frequency ν is proportional to the imaginary component of G given by the line shape equation[5,6]

$$G = G_A + G_B = \frac{-iC[\tau_A + \tau_B + \tau_A \tau_B (\alpha_A p_B + \alpha_B \tau_A)]}{(1+\alpha_A \tau_A)(1+\alpha_B \tau_B) - 1} \qquad 5$$

from which the imaginary component may be extracted.[13]

Equation 5 may be simplified for particular cases depending on the ratio of the exchange rate to the chemical shift difference of the two sites in Hz ($\nu_A - \nu_B$). Normally three cases are considered

i) when $k_A, k_B \ll (\nu_A - \nu_B)$ termed slow exchange.

ii) when $k_A, k_B \simeq (\nu_A - \nu_B)$ termed intermediate exchange.

iii) when $k_A, k_B \gg (\nu_A - \nu_B)$ termed fast exchange.

In the particular case of $nBu_2Sn(OAc)_2$ only case (iii) need be considered since only one signal is observed whose shift is temperature dependent. This is indicative of fast exchange.

B

Fast Exchange

In the limit of fast exchange the lifetimes at the two sites τ_A and τ_B are short. So equation 5 will reduce to equation 6 if all terms involving the products of τ_A and τ_B are ignored.

$$G = \frac{-iC(\tau_A + \tau_B)}{\alpha_A \tau_A + \alpha_B \tau_B} \qquad 6$$

From which the imaginary part may be extracted

$$\mathrm{Im}\, G = \frac{-C\,(p_A/T_{2A} + p_B/T_{2B})}{(p_A/T_{2A} + p_B/T_{2B})^2 + 4\pi^2(p_A\nu_A + p_B\nu_B - \nu)^2} \qquad 7$$

Comparison of this equation to equation 17 of Chapter 1 shows that equation 7 describes a Lorentzian line at the weighted mean frequency of ν_A and ν_B with an apparent width w^* given by

$$w^* = p_A w_{AO} + p_B w_{BO}$$

where w_{AO}, w_{BO} are the line widths at half height of the A and B resonances when the exchange rate is zero.

Piette and Anderson[8] have shown that if τ_A and τ_B are too large to ignore the product terms but $k \gg (\nu_A - \nu_B)$ then the resulting line shape equation describes a line of width w, and that k_A and k_B are given by the simple expression:

$$k_i = \frac{p_i p_j^2 \, 4\pi (\nu_A - \nu_B)^2}{(w - w^*)} \qquad 8$$

In the case of two equally populated sites this becomes

$$k = \frac{\pi . (\nu_A - \nu_B)^2}{2(w - w^*)} \qquad 9$$

Section 3

The Chemical Shift

In the preceding section the discussion has assumed that all the nuclei of a given species resonate at the same field; the applied laboratory field, B_o. This is not the case. The local chemical environment modifies this field slightly so that

$$B_{loc} = B_o (1 - \sigma)$$

where σ is the screening constant. This constant is not generally isotropic except in spherical molecules so σ differs along the different molecular axes. In fact it is a tensor quantity but the rapid molecular motion characteristic of normal fluids renders only the trace observable.

$$\sigma = 1/3 \, (\sigma_{xx} + \sigma_{yy} + \sigma_{zz})$$

where $\sigma_{xx,yy,zz}$ are the screening constants along the x, y and z molecular axes respectively.

It is prudent at this point to inquire as to the origin of the screening term.

When a nucleus is chemically bound a number of terms can contribute to σ. The most important for small nuclei is the local diamagnetic term and for heavier nuclei the local paramagnetic term do minates.

A

Diamagnetic Term σ_d

Consider a nucleus with an s electron. In the applied magnetic field the electron will precess at the appropriate Larmor frequency. This circulating current will generate a magnetic field opposed to B_o (in accordance with Lenz's law) and hence the field felt at the nucleus is decreased. σ_d may be calculated from

$$\sigma_d = \frac{e}{3 M_e} \int_0^\infty r\rho(r)\,dr$$

where (r) describes the electron density as a function of the distance r. This is the Lamb term.

Since σ_d depends on the magnitude of the field induced (which is itself dependent on the electron density at the nucleus) any electronegative group on a molecule which tends to withdraw electron density from the nucleus will decrease the shielding and the resonance will appear at lower field.

B

Paramagnetic Term σ_p

The local paramagnetic term arises from the circulation of electrons in the bonds of the molecule. It is a much more complicated task to calculate this quantity, but a simplified expression due to Jameson and Gutowsky[9] is useful for semiquantitative interpretation

of shifts of heavy nuclei:

$$\sigma_p = \frac{2e^2h^2}{3\Delta E m^2 c^2} \left[\langle r^{-3} \rangle_p Qnp + \langle r^{-3} \rangle_d Qnd \right]$$

where

ΔE is the mean electronic excitation energy. This determines the extent to which the ground and excited states are mixed by the field Qnp, Qnd are the amounts of electron imbalance associated with the valence p and d orbitals.

$\langle r^{-3} \rangle_p$, $\langle r^{-3} \rangle_d$ are the average values of the appropriate radial functions.

For a series of related tin compounds ΔE is normally taken to be constant.[10,11]

Qnp and Qnd depend on the coordination number at tin, the hybridisation and the bond ionicity.[12] For many four coordinate tin compounds Q_{5d} may be ignored and Q_{5p} will dominate the tin shielding.[13] For tin Qp has a maximum value when one p orbital is filled and the other two are empty, or vice versa and a minimum when all are filled or all are empty.

The term $\langle r^{-3} \rangle$ increases with increasing atomic number in a given group of the periodic table.[13] It is for this reason that the chemical shift range of ^{119}Sn is much larger than that of ^{29}Si or ^{13}C.

Section 4

Spin-Spin Coupling

In high resolution NMR spectra more lines may be observed than can be accounted for by consideration of equivalent groups of nuclei.

The magnitudes of these splittings are independent of the applied field and are due to interactions of the magnetic moments of neighbouring non-equivalent nuclei; the energy of interaction is given by

$$E_{ij} = hJ_{ij} [\hat{\underline{I}}(i) \cdot \hat{\underline{I}}(j)]$$

where Jij is the spin-spin coupling constants, in hertz. The coupling constant has sign as well as magnitude. Relative signs can be determined by double resonance experiments on suitable spin systems. Detailed spectral analysis can also yield relative signs of coupling constants in second order spectra. By definition J is positive when the antiparallel orientation of two nuclear spins is a more stable state than the parallel orientation.[14] Pople and Santry[15] have defined a reduced coupling constant Kij

$$K_{ij} = J_{ij} \frac{2\pi}{\hbar \gamma_i \gamma_j}$$

to eliminate the contribution of the magnetic moments to Jij.

Section 5

Methods of NMR detection

Two main methods exist for the detection of NMR signals; the most striking differences being the domains in which detection occurs and the mode of excitation of the various resonances in the spectrum.

A

Continuous Wave (CW)

The CW experiment is done in the frequency domain. It is a technically simple experiment. The frequencies of interest in the

spectrum are swept from the lower to the upper limit (or vice versa); essentially only one frequency at a time can be excited. One disadvantage is that the experimenter spends time searching in regions where there is no signal. Also slow sweep times are normally used so that the so called steady state conditions apply.

For nuclei other than protons the range of chemical shifts is much larger and increases with atomic weight (e.g. ^{1}H, 20 ppm; ^{13}C, 200 ppm; ^{119}Sn, 2000 ppm). Many of these other nuclei have low sensitivity resulting from low magnetic moments and/or low natural abundance. In the least favourable cases the CW method may not be practicable even with signal averaging. In more favourable cases the pulsed operation is almost always more advantageous in terms of signal to noise achieved in a given time.

B

Pulse Fourier Transform

The pulse method utilises a short burst of radiofrequency to tip the magnetisation away from the z' direction. The angle through which the magnetisation is displaced is given by

$$\theta = \gamma B_1 \tau_p$$

where τ_p is the length of the RF pulse. B_1 is normally kept constant and θ is controlled by varying τ_p. With $\theta = 90^\circ$ the so called "90° pulse" is obtained and in the above case the magnetisation immediately after the pulse is in the x'y' plane.

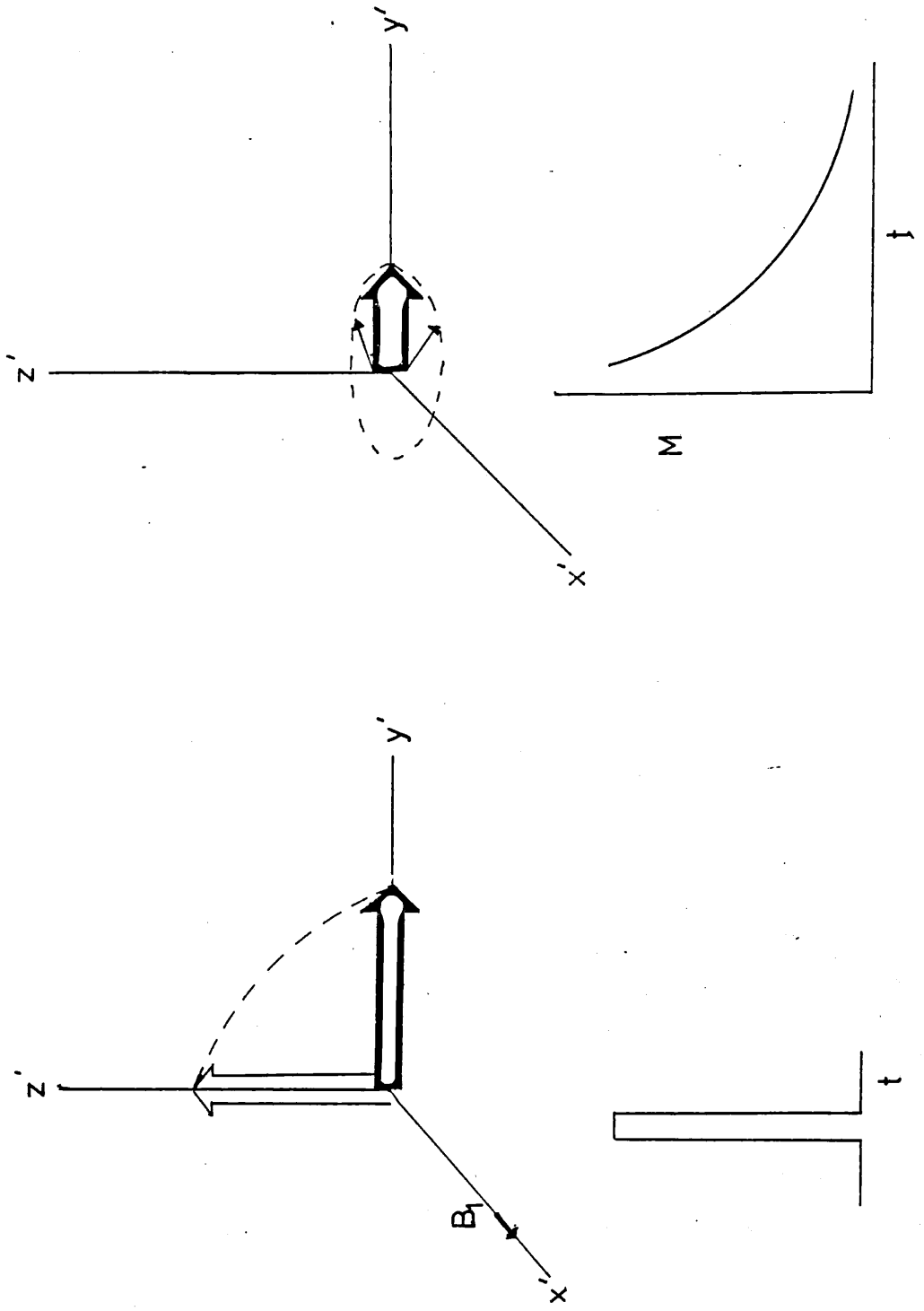

Figure 3

This pulse is normally short enough (say 10 - 100 μ s) so that no relaxation occurs during the pulse. Figure 3 shows the effect of a 90° pulse at resonance along x' on the magnetisation. When the pulse is switched off relaxation begins and dephasing in the x'y' plane occurs and the magnetisation returns to its equilibrium value over a period of time. The signal is detected as a decay (normally exponential) along y' and is termed the free induction decay (F.I.D.) Figure 3. This signal is in the time domain and, except in the simplest cases is not conducive to interpretation by eye. The requirement is for a frequency spectrum. Happily the two domains are related by a standard mathematical relationship the Fourier transform (FT)

$$F(\omega) = \int_{-\infty}^{\infty} f(t) \exp(-i\omega t)\, dt$$

The spectrometer is interfaced to a computer that detects the F.I.D. and carries out the Fourier transform.

A pulse of RF lasting τ_p seconds at a frequency ν_o excites not only ν_o but a range of frequencies defined by τ_p. Figure 4 shows the Fourier transform of a pulse to have the form sin x/x. If the usable frequency range is $\nu_o \pm \frac{1}{4\tau_p}$ then in principle a 10 μ s pulse excites $\nu_o \pm 25$ kHz. Herein lies the intrinsic advantage of the pulse method in that all frequencies of interest can be excited at the same time. The CW analogy of this would be multiple receivers (and obviously multiple transmitters). Hardly a practical proposition.

Ernst and Anderson[16] have obtained a signal to noise improvement of ten for progesterone using the pulse method compared to CW. This seems to be a typical improvement. Since the signal

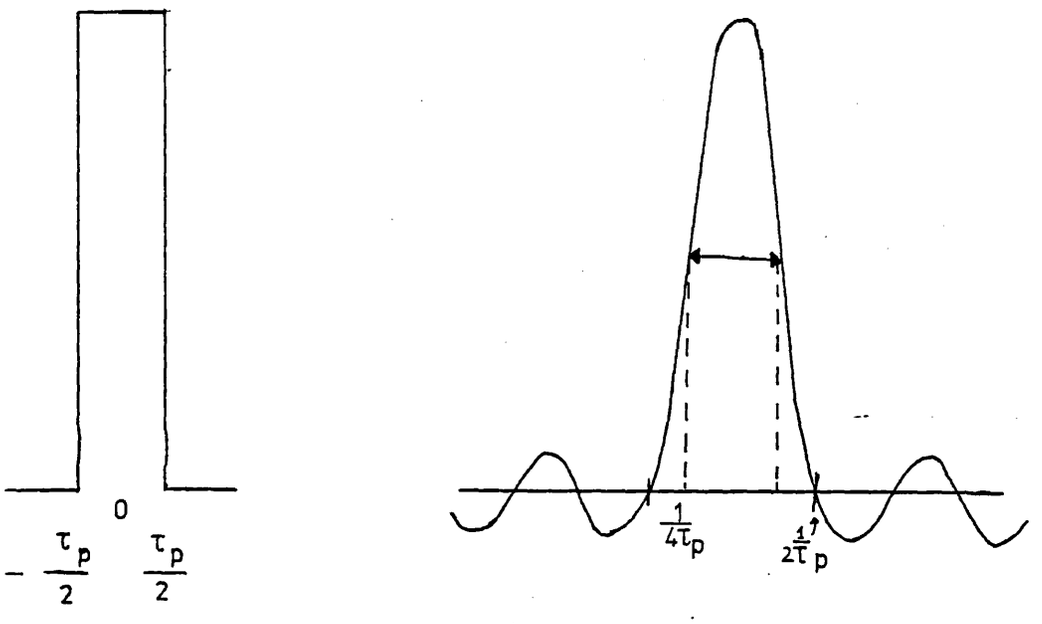

Figure 4

to noise ratio (S/N) improves according to $\sqrt{n}$, where n is the number of spectra taken the same S/N can be obtained in one hundreth of the time using pulsed excitation. A more detailed discussion of this topic is given by D. Shaw in his book.[17]

Basic Texts/Reviews

D.G. Gillies, D. Shaw, Ann. Report NMR Spect. (1972) 5A 557

R. Lynden-Bell, R.K. Harris, NMR Spectroscopy.

A. Carrington, A.D. McLachlan, Introduction to Magnetic Resonance.

D. Shaw, Fourier Transform NMR.

T.C. Farrar, E.D. Becker, Pulse and Fourier Transform NMR.

I.O. Sutherland, Ann. Reports. NMR Spect. (1971) 4 71.

References

1 L.M. Jackman, T.E. Kavanagh, R.C. Hadden, Org. Magn. Resonance (1969) 1 109.

2 R.M. Lynden-Bell, Prog. in Nucl. Magn. Reson. (1967) 2 163.

3 E.L. Hahn, D.G. Maxwell, Phys. Rev. (1952) 88 1070.

4 H.M. McConnell, J. Chem. Phys. (1958) 28 430.

5 H.S. Gutowsky, D.W. McCall, C.P. Slichter, J. Chem. Phys. (1953) 21 279.

6 H.S. Gutowsky, A. Saika, J. Chem. Phys. (1953) 21 1688.

7 M.T. Rogers, J.C. Woodbrey, J. Phys. Chem. (1962) 66 540.

8 L.H. Piette, W.A. Anderson, J. Chem. Phys. (1959) 30 899.

9 C.J. Jameson, H.S. Gutowsky, J. Chem. Phys. (1964) 40 1714.

10 B.K. Hunter, L.W. Reeves, Can. J. Chem. (1968), 46, 1399.

11 A.G. Davies, P.G. Harrison, J.D. Kennedy, T.N. Mitchell, R.J. Puddephatt, W. McFarlane, J. Chem. Soc. C.(1969),1136.

12 P.J. Smith, A.P. Tupciauskas, in press.

13 J.D. Kennedy, W. McFarlane, Revs. Si, Ge, Sn, Pb (1974) 1, 235.

14 J. Karplus, J. Chem. Phys. (1962) 84 2458.

15 J.A. Pople, D.P. Santry, Mol. Phys. (1964) 8 1.

16 R.R. Ernst, W.A. Anderson, Rev. Sci. Intrum. (1966) 37 93.

17 D. Shaw, Fourier Transform NMR Chapter 5.

CHAPTER 2

Relaxation

Section 1 Introduction

A Molecular Motion

B Spectral Density Functions

Section 2 Relaxation Mechanisms

A Dipole-Dipole

B Spin Rotation

C Chemical Shift Anisotropy

D Scalar

E Quadrupole

F Electron-Nuclear

Section 3A Measurement of T_1 by Inversion-Recovery

B Separation of spin-lattice mechanisms

C Nuclear Overhauser Effect

D Separation of Intermolecular Dipole-Dipole Contributions to T_1

E Gated Decoupling

References

Section 1

Introduction

In general NMR has been used very successfully as a powerful analytical tool and to this end the chemist has been most interested in chemical shift determinations and magnitude (and sometimes signs) of coupling constants (Chapter 1). Relaxation times(Chapter 1) have to an extent been ignored and only since the advent of high resolution pulse spectrometers, where T_1 is easily measured has interest grown. Much of the available T_1 data is for ^{13}C where relaxation arises almost exclusively from intramolecular interactions and is further simplified by the absence of homonuclear couplings.

The interest in relaxation data of nuclei other than ^{13}C has, to an extent grown in parallel with that shown in ^{13}C although the amount of data published is still quite small compared to that on ^{13}C. The appearance of commercial multinuclear pulsed NMR spectrometers will no doubt further stimulate work in this field.

A

Molecular Motion

In a liquid sample the frequencies of motions cover a large range. The ensemble obviously contains some molecules which are moving very fast and others moving much more slowly. We may consider on the average a molecule to remain in a given state of motion for 10^{-12}S and hence expect frequency components of the motion up to 10^{12}Hz.

Spin-spin and spin lattice relaxation occur by the interaction of the nuclear spin system with fluctuating local magnetic fields.

These microscopic fields are generated by individual magnetic moments on molecules as they move about in solution. They behave in much the same way as the applied RF, B_1. If the macroscopic magnetisation, M is perturbed from its equilibrium position so that it has components along the x',y' and z' axes then the interaction of the microscopic field b with M is given by

$$(\underline{b} \times \underline{M}) = i(b_{y'} M_{z'} - b_{z'} M_{y'}) + j(b_{z'} M_{x'} - b_{x'} M_{z'}) + k(b_{x'} M_{y'} - b_{y'} M_{x'})$$

From this equation it is apparent that in the rotating frame $b_{x'}$ fields provide relaxation mechanisms for $M_{y'}$ and $M_{z'}$, $b_{y'}$ fields for $M_{x'}$ and $M_{z'}$. The $b_{z'}$ component however interacts only with $M_{x'}$ and $M_{y'}$. That is, the x' and y' components of the fluctuating microscopic field are efficient for spin-lattice (T_1) and spin-spin (T_2) relaxation whereas $b_{z'}$ is effective for T_2 relaxation only.

A static component of b in the z' direction is static in the laboratory frame also. Consequently in the laboratory frame there is a zero frequency contribution to T_2. However a static component of b in the x' or y' direction necessarily corresponds to a high frequency (ω_o) component of b in the laboratory frame so that only high frequencies (of the order of the resonance frequency) will affect T_1. If the microscopic fields have components at the appropriate frequencies they can cause spin relaxation and the larger such components are the more efficient in the relaxation and the shorter are the relaxation times. The range of relevant frequencies for spin-lattice relaxation is in the MHz region so motions that are important are rotation and diffusion. Electronic and vibrational motions occur on much shorter timescales and are thus unimportant when considering magnetic relaxation.

A useful concept to describe random molecular motion is that of the correlation time which can be defined in a number of ways according to the motion to which it relates. For translational motion τ_c is the average time between molecular collisions and for rotational motion it is the average time for the molecule to rotate one radian. For nuclei such as ^{13}C where the intermolecular contribution to relaxation is small, the correlation times derived from relaxation data are rotational.

B

Spectral Density Functions

For a more quantitative understanding of relaxation behaviour we need to introduce the correlation function, $K(\omega)$ and the spectral density function $J(\omega)$. These functions are related by the Fourier transform:

$$J(\omega) = \int_{-\infty}^{\infty} k(\tau)\exp(-i\omega\tau)d\tau \qquad 1$$

In fact the spectral density function relates the intensities of the frequency components of the molecular motion. It is analogous to the Fourier transform of the F.I.D. analysing the intensities at different frequencies.

It can be shown[1] that the correlation functions $K_i(i=0,1,2)$ have the form

$$K_i(\tau) = K_i(0)\exp(-|\tau|/\tau_c) \qquad 2$$

Also for the case of dipole-dipole relaxation

$$K_o(0) = \frac{12}{15} r^{-6} \quad K_1(0) = \frac{2}{15} r^{-6} \quad K_2(0) = \frac{8}{15} r^{-6} \qquad 3$$

Equation 2 merely states that a system characterised by short τ_c loses phase coherence in a short time. Substituting equation 3 into 1 and integrating yields the spectral density functions at zero frequency, single frequency and double frequency

$$J_0(\omega) = \frac{24}{15} r^{-6} \quad \frac{\tau_c}{1+\omega^2 \tau_c^2}$$

$$J_1(\omega) = \frac{4}{15} r^{-6} \quad \frac{\tau_c}{1+\omega^2 \tau_c^2} \qquad 4$$

$$J_2(\omega) = \frac{16}{15} r^{-6} \quad \frac{\tau_c}{1+\omega^2 \tau_c^2}$$

In Figure 1 it is seen how $J_0(\omega)$ depends on $\omega_0 \tau_c$. Three curves are shown, for $\omega_0 \tau_c \ll 1$, $\omega_0 \tau_c \simeq 1$ and $\omega_0 \tau_c \gg 1$. They are drawn for constant B_0 so the different curves arise from different τ_c.

If τ_c is short all motional frequencies (0 to τ_c^{-1}) have a small but equal probability of occurring. For long τ_c low frequencies have large Fourier components whereas high frequencies are almost entirely absent. In both cases the components at the resonance frequency (ω_0) are smallest. For $\omega_0 \tau_c \simeq 1$ the component at ω_0 is largest and most efficient relaxation occurs when this condition holds. The time scales for molecular motion and precession are matched. This was demonstrated by Bloembergen Purcell and Pound[2] for glycerine. The area under the curves in Figure 1 is constant, reflecting the fact that the power available for molecular motion is constant and that changing τ_c only alters the frequency distribution of this power.

When $\omega_0 \tau_c \ll 1$ all frequencies have an equal probability of occurring. This is termed the extreme narrowing condition. When this condition holds the measured T_1's are field independent. However if τ_c is long

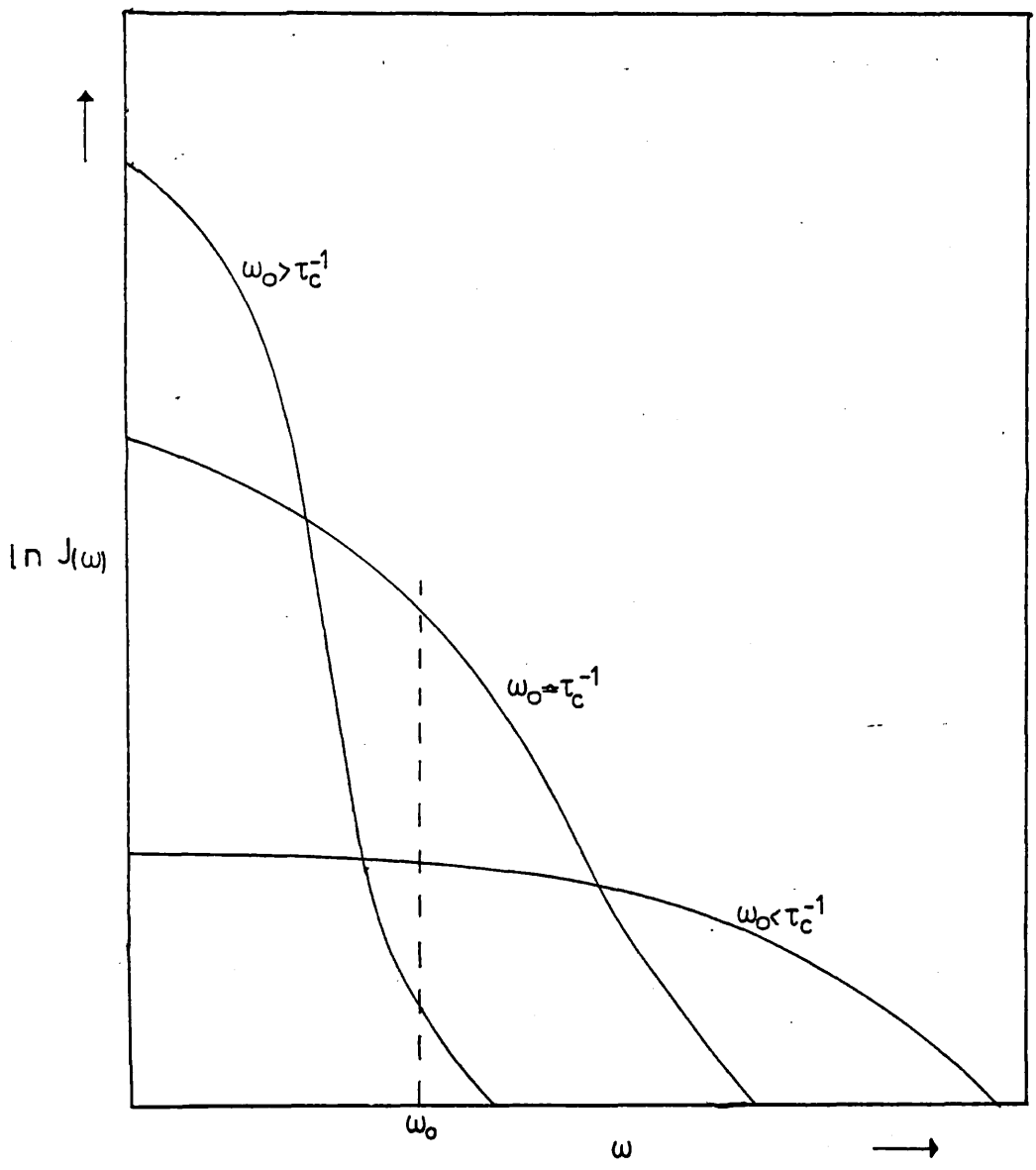

Figure 1

enough and/or ω_o is large (due to the use of a high applied field) the extreme narrowing condition no longer holds and T_1 and any NOE become field dependent with a minimum in T_1 at $\omega_o \tau_c \simeq 1$.

Section 2

Spin Lattice Relaxation Mechanism

A number of different mechanisms exist that enable the spin system and the lattice to exchange energy, allowing excess Zeeman energy to be dissipated. These are:

a) Magnetic dipole-dipole

b) Spin-rotation

c) Chemical shift anisotropy

d) Scalar Coupling

e) Electric quadrupole

A

Dipole-Dipole Relaxation

This is the most important relaxation mechanism for nuclei of spin $I = \frac{1}{2}$ in the liquid state.

Consider two nuclei I and S on the same molecule. If the molecule is stationary then the nucleus I will have two contributions to the total magnetic field B_t it experiences. The first is from the applied laboratory field, B_o and the second a local field B_{loc} from the magnetic moment of nucleus S. The energy of interaction of two magnetic moments μ_I, μ_S depends on their separation, r and their relative orientation θ, to the magnetic field B_o.[3] (see Figure 2).

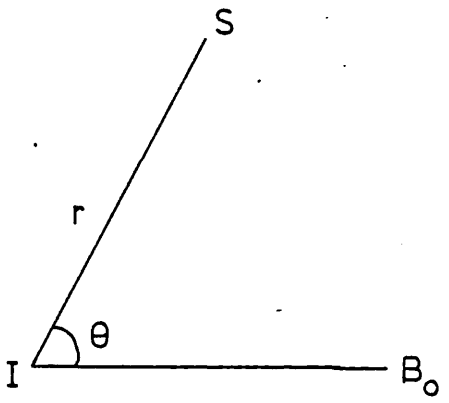

Figure 2

The local field at nucleus I is given by

$$B_1 = \pm \frac{\mu_s}{r^3} (3\cos^2\theta - 1) = \frac{\gamma_s I_s \hbar}{r^3} (3\cos^2\theta - 1)$$

If the molecule is now allowed to move about, θ becomes time dependent. If the motion is fast enough the local field averages to zero and the dipolar coupling will vanish resulting in narrow lines in the spectrum. Since θ is time dependent then the local field is also time dependent and consequently a potential relaxation mechanism.

For a nuclear spin I interacting with some other physical quantity described by the operator O the Hamiltonian may be written as

$$\mathcal{H} = -hI \cdot T \cdot O$$

where T is the tensor which describes the interaction. As the molecule moves in solution the elements t_{ij} of T become time dependent. For a spin I interacting with a spin S we may write

$$\mathcal{H} = -hI \cdot T \cdot S$$

For a two spin system of the same species Abragam[3] has shown that

$$R_1 = \frac{3}{2} \gamma^4 \hbar^2 I(I+1) \left\{ J_1(\omega_I) + J_2(2\omega_I) \right\} \qquad 5$$

and $$R_2 = \gamma^4 \hbar^2 I(I+1) \left\{ 3/8\, J_o(0) + \frac{15}{4} J_1(\omega_I) + 3/8\, J_2(2\omega_I) \right\} \qquad 6$$

The important point to note here is that R_2 has a term at zero frequency whereas R_1 is only affected by frequencies in the region of the resonance frequency. For a heteronuclear spin system of spins

I and S, R_1^S and R_2^S are given by

$$R_1^S = \gamma_I^2 \gamma_s^2 I(I+1)\left\{\frac{1}{12} J_o(\omega_s-\omega_I) + \frac{3}{2} J_1(\omega_s) + \frac{3}{4} J_2(\omega_I+\omega_s)\right\}$$

$$R_2^S = \gamma_I^2 \gamma_s^2 I(I+1)\left\{\frac{1}{6} J_o(0) + \frac{1}{24} J_o(\omega_s-\omega_I) + \frac{3}{4} J_1(\omega_s) + \frac{3}{8}(\omega_I+\omega_s)\right\}$$

For intramolecular dipole-dipole interactions, we need only consider rotational motion. The spectral densities at the relevant frequencies for like spins, are given by equation 4. Substitution into equations 5 and 6 yields

$$R_1^{Rot} = \frac{2\gamma^4 \hbar^2 I(I+1)}{5 r^6}\left[\frac{\tau_c}{1+\omega^2\tau_c^2} + \frac{4\tau_c}{1+4\omega^2\tau_c^2}\right] \quad 7$$

$$R_2^{Rot} = \frac{\gamma^4 \hbar^2 I(I+1)}{5 r^6}\left[3\tau_c + \frac{5\tau_c}{1+\omega^2\tau_c^2} + \frac{2\tau_c}{1+4\omega^2\tau_c^2}\right] \quad 8$$

For mobile liquids $\omega_o \tau_c \ll 1$ and equations 7 and 8 reduce to

$$R_1^{Rot} = R_2^{Rot} = \frac{2\gamma^4 \hbar^2 I(I+1)}{r^6}\tau_c$$

This is known as the extreme narrowing condition. For viscous liquids or at very low temperature $\omega_o \tau_c \gg 1$ and $R_1^{Rot} \neq R_2^{Rot}$. From the equations it can be seen that under such condition the relaxation times are frequency dependent.[2]

The dependence of the dipole-dipole mechanism on the inverse sixth power of the separation of the nuclei indicates that it is only effective over very short distances. The dipole-dipole mechanism can be intermolecular as well as intramolecular. That is the I and S nuclei are on separate molecules. In such a case equations 7 and 8 still hold except that τ_c is not a rotational correlation time,

rather it is a translational correlation time. Due to the r^{-6} dependence of the dipolar mechanism the intermolecular mechanism is normally ineffective in relaxing the I nucleus especially of the S nucleus is directly attached to I thereby making the intramolecular mechanism dominant.

B

Spin Rotation

This mechanism is the next most important mode of relaxation for spin $\frac{1}{2}$ nuclei. This is especially so for nuclei of large chemical shift range (^{13}C, ^{19}F, ^{15}N) in small symmetric molecules. Even in much larger molecules[4,5] spin rotation has been shown to be important.

The interaction arises from the magnetic fields generated at a nucleus by the motion of a molecular magnetic moment arising from the distribution of electrons in the molecule. As the molecule rotates a particular electron will rotate about a nucleus at some radius R, the rotational frequency being given by

$$V = hJ/2\pi I$$

where J is the rotational state of the molecule and I its moment of inertia. The magnetic moment μ_J generated by the resulting current is given by

$$\mu_J = \frac{eh}{2\pi Mc} J \simeq \mu_N J$$

where M is the nuclear mass and μ_N the nuclear magneton. This magnetic moment produces a local magnetic field at the nucleus which is modulated by collisions causing changes in both direction and rotation

thus enabling it to be an effective relaxation pathway. The Hamiltonian for the interaction is given by

$$\mathcal{H} = -hI \cdot C \cdot J$$

where J is the angular momentum operator and C the spin rotation tensor. For liquids undergoing isotropic reorientation the relaxation rate is given by

$$R_1 = (2\pi\ IkT/\hbar^2)\,1/3(2C_{\perp}^2 + C_{||}^2\ )\tau_j$$

where τ_j is the angular momentum correlation time and C the appropriate spin-rotation constants. Hubbard[6] and McClung[7] have shown that τ_j is inversely proportional to τ_c

$$\tau_c\ \tau_j = \frac{I}{6kT}$$

where k is the Boltzmann constant and T the absolute temperature. The relationship of the spin rotation relaxation rate and the chemical shift range is due to the fact that both the chemical shift and the spin rotation tensor depend on the electron distribution in the molecule. This point is further discussed by Maryott[8] and Deverell[9].

C

Chemical Shift Anisotropy

In Chapter 1 (section 3) it was pointed out that the field at the nucleus is given by

$$B_1 = B_o(1\ -\sigma)$$

where σ is the screening tensor. In mobile liquids the average value of the tensor is observed

$$\sigma = 1/3\ (\sigma_{xx} + \sigma_{yy} + \sigma_{zz})$$

If the components of σ are not equal the chemical shift is said to be anisotropic and molecular motion produces a fluctuating magnetic field at the nucleus which can act as a relaxation mechanism. For the case of axial symmetry R_1^{CSA} and R_2^{CSA} are given by

$$R_1^{CSA} = \frac{1}{15}\gamma^2 B_o^2(\sigma_{||} - \sigma_\perp)^2 \left\{\frac{2\tau_c}{1+\omega^2\tau_c^2}\right\}$$

and

$$R_2^{CSA} = \frac{1}{90}\gamma^2 B_o^2 (\sigma_{||} - \sigma_\perp)^2 \left\{8\tau_c + \frac{6\tau_c}{1+\omega^2\tau_c^2}\right\}$$

where $\sigma_{||}$, $\sigma_\perp$ are the screening constants parallel and perpendicular to the symmetry axis respectively. In the extreme narrowing condition these equations reduce to

$$R_1^{CSA} = \frac{6}{45}\gamma^2 B_o^2(\sigma_{||} - \sigma_\perp)^2 \tau_c$$

and

$$R_2^{CSA} = \frac{7}{45}\gamma^2 B_o^2(\sigma_{||} - \sigma_\perp)^2 \tau_c$$

We see that $R_1^{CSA}/R_2^{CSA} = 6/7$ and also that this mechanism is field dependent.

Chemical shift anisotropy is an inefficient mechanism and is rarely observed to contribute to spin relaxation except in liquid crystal solvents. It has been shown to be effective in $CH_3{}^{13}COOH$,[10] $Ph-C\equiv{}^{13}C-C\equiv C-Ph$ and $Me_2{}^{205}TlNO_3$.[12] Due to its square dependence on the field we may anticipate more examples of this mechanism now that high fields (up to 14.1 T[13]) are more generally available.

D

Scalar Relaxation

A nucleus I which is spin coupled to a nucleus S can be relaxed by fluctuating magnetic fields via scalar interaction involving the bonding electrons. The Hamiltonian for the interaction may be written as

$$\mathcal{H} = hI \cdot A \cdot S$$

where A is the spin-spin coupling tensor. It is evident that the local field at nucleus I can become time dependent in one of two ways: the coupling constant A (in rad s^{-1}) may be time dependent or the excited state of S may be time dependent. The first case is termed scalar relaxation of the first kind and the latter is scalar relaxation of the second kind. The equations for R_1^{SC} and R_2^{SC} applicable for the two types are analogous.

Scalar Relaxation of the first kind

The coupling constant can become time dependent by chemical exchange. The local field at I is AS/γ_I when I and S are covalently bound and zero otherwise and is consequently fluctuating. If the rate of exchange $\frac{1}{\tau_e}$ is large compared to A or to R_1^{SC} for either nucleus and the exchange is characterised by instantaneous jumps then the multiplet structure of the resonance disappears and a single line is observed. It has been shown[3] that the equations for scalar relaxation of nucleus I are given by

$$R_1^{SC} = \frac{2}{3} A^2 S(S+1) \left\{ \frac{\tau_e}{1+(\omega_I-\omega_S)^2 \tau_e^2} \right\} \qquad 9$$

and

$$R_2^{SC} = \frac{A^2}{3} S(S+1) \left\{ \tau_e + \frac{\tau_e}{1+(\omega_I-\omega_S)^2 \tau_e^2} \right\} \qquad 10$$

Scalar Relaxation of the second kind

For scalar relaxation of the second kind B_{loc} is modulated by the relaxation of the S nucleus. Equations 9 and 10 still apply but τ_e is replaced by T_{1s}.

From the equations it can be seen that to be effective for R_1^{SC} the exchange rate must be large, in fact comparable to the difference of the resonance frequencies. This proviso is also applicable to second kind relaxation in so far as the relaxation rate must be large. This is normally the case for quadrupolar nuclei and one only expects to observe this mechanism for a nucleus coupled to a spin $S > \frac{1}{2}$. The contribution to R_2^{SC} is more likely since a zero frequency term exists that does not involve this stringent matching of time scales to be effective.

E

Quadrupolar Relaxation

The interaction Hamiltonian is given by

$$\mathcal{H} = I \cdot Q \cdot I$$

where Q is the quadrupole coupling tensor.

So far we have only discussed the mechanisms available to relax spin $\frac{1}{2}$ nuclei and have limited ourselves to fluctuating magnetic fields. For nuclei with spin I $\frac{1}{2}$ an additional mechanism is available involving interactions with fluctuating electric fields.

Nuclei of spin $\frac{1}{2}$ have a spherical nuclear charge distribution whereas for nuclei of spin larger than $\frac{1}{2}$ the distribution is non-spherical and a quadrupole moment Q exists. Such quadrupolar nuclei do not have an electric dipole moment hence their energy is

independent of orientation in a uniform electric field. Where an electric field gradient exists the nuclei precess about the net electric field. As the molecule reorients the elements of Q become random functions of time thereby providing a relaxation pathway. In the limit of extreme narrowing it has been shown[3] that

$$R_1^Q = R_2^Q = \frac{3}{40} \frac{2I+3}{I^2(2I-1)} \left(1+\frac{\eta^2}{3}\right)\left(\frac{e^2Qq}{\hbar}\right)^2 \tau_c$$

where η is the asymmetry parameter, q is the electric field gradient and $(e^2Qq/\hbar)$ is the quadrupole coupling constant. The relaxation rates are thus governed not only by τ_c but also by the quadrupole coupling constant.

The electric field gradient at the nucleus will vary according to the molecular environment and consequently the quadrupole coupling constant can take a wide range of values. In the NH_4^+ ion and other particles of tetrahedral symmetry for instance, q is zero as is the quadrupole coupling constant. In molecules of lower symmetry q is non-zero and in CH_3CN in fact $(e^2Qq/\hbar)$ is 4MHz.[14]

For nuclei of spin $I > \frac{1}{2}$ the quadrupolar mechanism dominates the relaxation unless the electric field gradient is zero. The mechanism is so effective for such nuclei that there is no need to degass samples when measuring T_1.[15] It is an entirely intramolecular effect so if the quadrupole coupling constant is known (say from NQR or liquid crystal studies) measurement of T_1 enables τ_c to be calculated. A review[15] discussing relaxation times of deuterium (the most commonly studied quadrupolar nucleus) in a variety of compounds has recently appeared.

F

Electron Nuclear Relaxation

For completeness we should consider the intermolecular electron nuclear interaction as a cause of relaxation.

The electron has spin $\frac{1}{2}$ and therefore a magnetic moment. An unpaired electron will generate fluctuating magnetic fields as the molecule moves in solution and can thus be a cause of relaxation. This interaction is dipolar in nature and hence depends on the size of the magnetic moment (see section 2A). For the electron this is 10^3 times bigger than that of the proton and consequently electron-nuclear relaxation is 10^6 times more efficient than nuclear-nuclear relaxation. So even small amounts of paramagnetic species in a sample will significantly affect measured relaxation times. The most common paramagnetic species in samples is dissolved oxygen so care should be taken to degass samples to avoid any paramagnetic relaxation.

Section 3

A

Measurement of T_1

The most common method of measuring T_1 is by the $180^\circ-\tau-90^\circ$ pulse sequence, sometimes termed inversion recovery. The 180° pulse (Chapter 1, section 5B) inverts the magnetisation along the z' axis. Spin-lattice relaxation now occurs causing M_z to recover to its equilibrium value M_o. If a 90° pulse is applied at some time after the 180° pulse the magnetisation is rotated onto the y' axis and can be observed as an FID which can be transformed in the normal way.

After a suitable delay ($5T_1$ to allow the magnetisation to recover fully) the experiment is repeated for different values of τ. The recovery of the magnetisation is described by

$$M_\tau = M_o\left\{1-2\ \exp(-\tau/T_1)\right\}$$

For short τ ($< 0.69\ T_1$) the magnetisation is inverted and as τ is increased becomes positive till it reaches its equilibrium value, M_o (Figure 3). A plot of $-\ln(M_\infty - M_\tau)$ vs τ allows T_1 to be calculated.

B

Separation of spin-lattice Relaxation Mechanisms

It has been shown in the preceding sections of this Chapter the different relaxation mechanisms that may contribute to spin lattice relaxation times (R_1). Any measured rate can, in theory have a contribution from each of these mechanisms and if any quantitative relaxation studies are to be carried out some method of separating the different contributions is required. The problem is not as complicated as it seems at first sight. Very few nuclei will have contributions from all mechanisms and mere inspection of the relevant equations can indicate whether a particular mechanism is likely to contribute. For instance the chemical shift anisotropy mechanism is seen to be dependent on the square of the field and can therefore be readily separated. Scalar coupling requires stringent matching of time scales, the main requirements being a fast relaxing nucleus or rapid chemical exchange. If both are absent there will be no scalar coupling contribution to the relaxation time. For spin $\frac{1}{2}$ nuclei this leaves the most common contributing mechanisms to

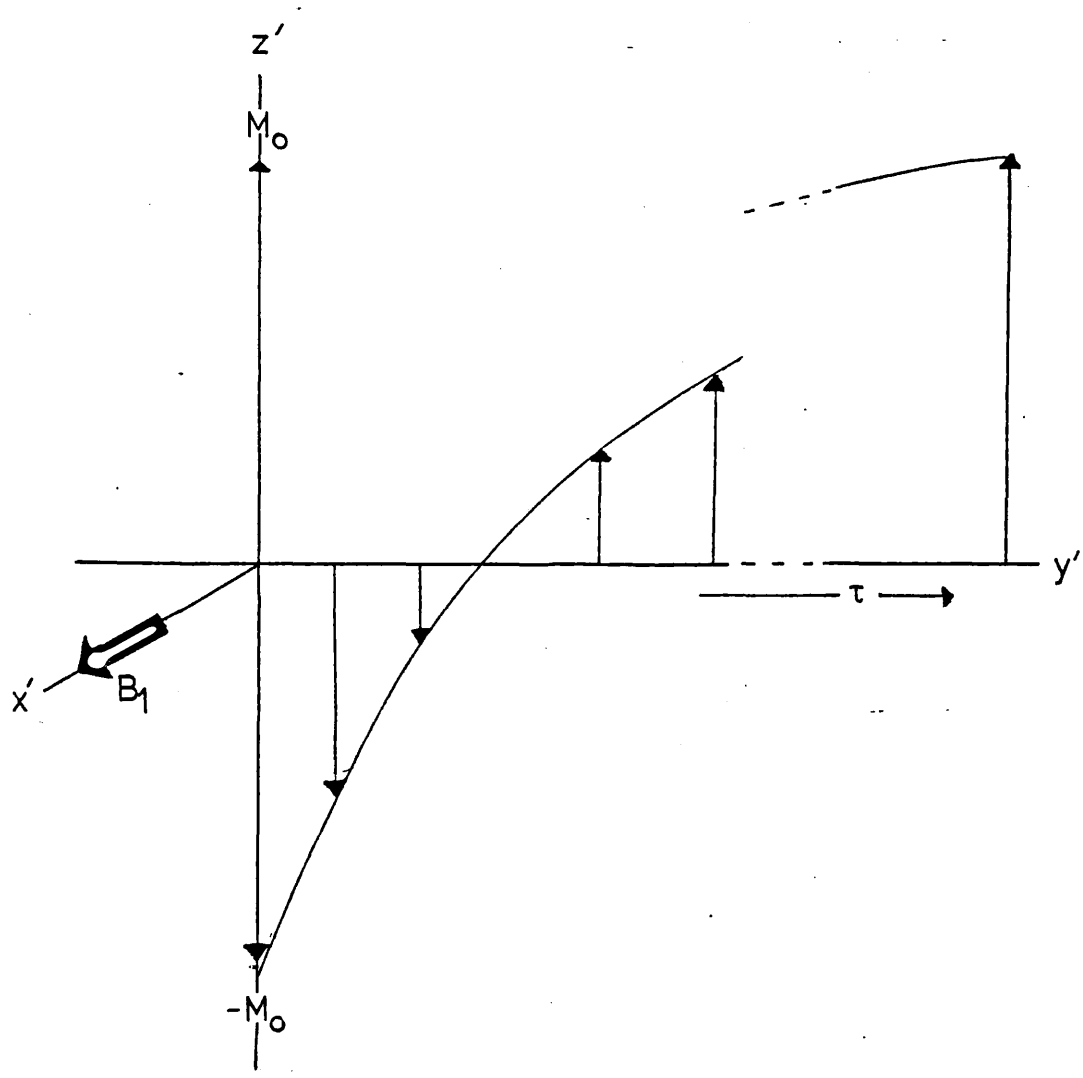

Figure 3

separate spin-rotation and dipole-dipole. Here two properties come to our aid. First these two mechanisms have an opposite temperature dependence, dipole-dipole having the same dependence as all other mechanisms. Consequently a nucleus having contributions from spin-rotation and any other mechanisms will exhibit a non-linear Arrhenius plot (Figure 4). It is possible to analyse such a curve

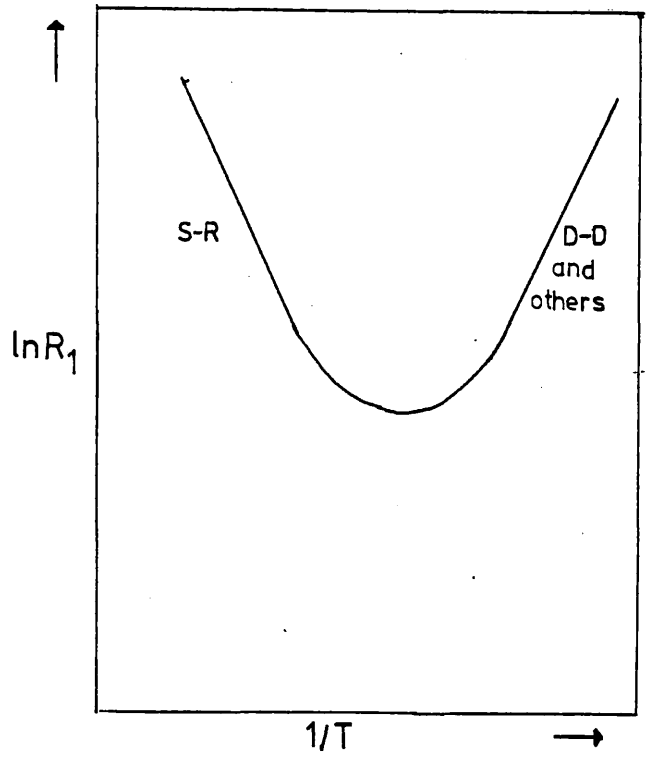

Figure 4

to extract spin rotation rates. However the best method of separating the dipole-dipole mechanisms from all others (irrespective of temperature dependence) is to utilise the nuclear Overhauser effect (NOE).[16]

C

The Nuclear Overhauser Effect

The NOE is a change in the integrated nuclear magnetic resonance (NMR) signal of a spin when the NMR absorption signal of another spin (whether spin coupled to the former or not) is saturated by a strong second radiofrequency. The spins may be heteronuclear or chemically shifted homonuclear spins.

Consider a two spin $\frac{1}{2}$ system[17] I, S (where S = proton) the equation of motion for $\langle I_z \rangle$, the expectation value of I_z[18] is

$$d\langle I_z \rangle /dt = -(W_o+2W_{1I}+W_2)(\langle I_z \rangle - I_o)-(W_2-W_o)(\langle S_z \rangle - S_o) \qquad 15$$

where the W_j's are the transition probabilities in Figure 5, I_o, S_o are the equilibrium values of $\langle I_z \rangle$ and $\langle S_z \rangle$, and $\langle S_z \rangle$ the expectation value of S_z. If the populations of the proton energy levels are equalised by irradiation using a strong radiofrequency then $\langle S_z \rangle = 0$ and equation 15 becomes

$$d\langle I_z \rangle /dt = -(W_o+2W_{1I}+W_2)[\langle I_z \rangle - I_o(1+\eta)] \qquad 16$$

where

$$\eta = \frac{(W_2-W_o)\gamma_S}{(W_o+2W_{1I}+W_2)\gamma_I} \qquad 17$$

It follows from equation 16 that $\langle I_z \rangle$ decays exponentially with a time constant R_1 given by

$$R_1 = W_o + 2W_{1I} + W_2 \qquad 18$$

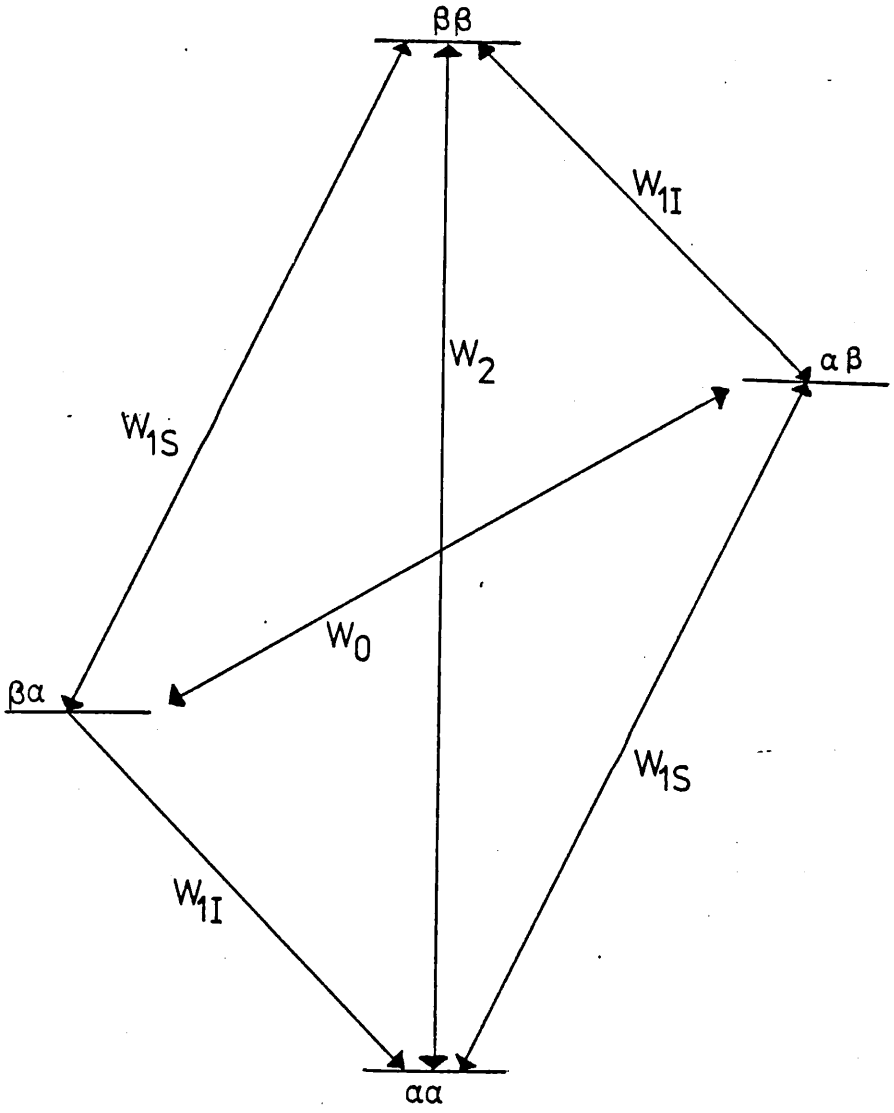

Figure 5

For dipolar relaxation the transition probabilities in Figure 5 are given by

$$\begin{aligned} W_o &= (1/20)k^2 J_o(\omega_I - \omega_S) \\ W_{1I} &= (3/40)k^2 J_1(\omega_I) \\ W_{1S} &= (3/40)k^2 J_1(\omega_S) \\ W_2 &= (3/10)k^2 J_2(\omega_I + \omega_S) \end{aligned} \qquad 19$$

where $k = \gamma_S \gamma_I \hbar$ and $J_i(\omega)$ are the spectral densities at the appropriate frequencies. Substituting equation 19 into 17 gives the nuclear Overhauser enhancement factor η as

$$\eta = \frac{[6J_2(\omega_S+\omega_I) - J_o(\omega_S-\omega_I)}{\Omega} \frac{\gamma_S}{\gamma_I} \qquad 20$$

where $\Omega = J_o(\omega_S-\omega_I) + 3J_1(\omega_I) + 6J_2(\omega_S+\omega_I)$

In the extreme narrowing limit it has been shown that all possible frequencies are equally probable (Figure 1) in other words the spectral densities are equal. So equation 20 becomes

$$\eta = \frac{\gamma_S}{2\gamma_I}$$

and the observed signal has intensity given by

$$NOE = 1 + \frac{\gamma_S}{2\gamma_I} \qquad 21$$

The most common example of this experiment is to irradiate protons and observe ^{13}C giving an enhancement factor, η for 100% dipole-dipole relaxation via the irradiated protons of 1.99. From equation 21 it is apparent that for a nucleus I of negative magnetogyric ratio (^{29}Si , ^{119}Sn), γ_I the NOE will be negative and consequently a decreased signal intensity will be observed.

It should be stressed that the NOE arises only from the dipole-dipole mechanism. A relaxation rate of which only half is due to the dipolar mechanism will show only half of the possible NOE as defined in equation 21. It is this fact that enables the dipolar rate to be extracted from the total.

The NOE is the subject of a book by Noggle and Schirmer[20] and the reader is referred to this for more detailed discussion.

D

Separation of Intermolecular Dipole-Dipole Contribution

For ^{13}C the intermolecular contribution to R_1 is insignificant. For ^{29}Si and ^{119}Sn also authors are generally agreed that this mechanism is unimportant. However for ^{1}H the intermolecular dipole-dipole mechanism can be important since protons, being univalent are essentially on the "surface" of the molecule and consequently can interact effectively with other magnetic nuclei on nearby molecules. In fact protons are not only the most affected by this mechanism but also the most common in providing the mechanism due to the large magnetogyric ratio.

Unfortunately the NOE does not distinugish between the inter- and intramolecular mechanisms. The method employed is to carry out a dilution study of the molecule in questi .on in its perdeutero analogue (this ensures that the details of the molecular motion are essentially identical at all concentrations). Any difference in dipolar relaxation rates over the concentration range studied enables the intermolecular contribution to be estimated. Obviously, synthesis of a fully deuterated molecule is not always practical and some authors use deuterated solvents. This latter procedure can be prone to large errors.

Gated Decoupling

The increased intensity of a resonance due to the NOE can be determined by comparing the spectra obtained with and without the Overhauser enhancement. Such a comparison is possible because decoupling of the S nucleus is essentially instantaneous and in fact occurs on a time scale of the order of $(\omega/2\pi)^{-1}$.[21] The I magnetisation resulting from this irradiation however, develops with a time constant of the spin lattice relaxation time T_1. This difference in time scales enables decoupled spectra with and without NOE to be obtained. The technique was first demonstrated by Kuhlmann and Grant[22] and later exploited in the pulse mode by Freeman et al.[23]

In practice a timing scheme as shown in Figure 6 is used to obtain a decoupled spectrum without the NOE.

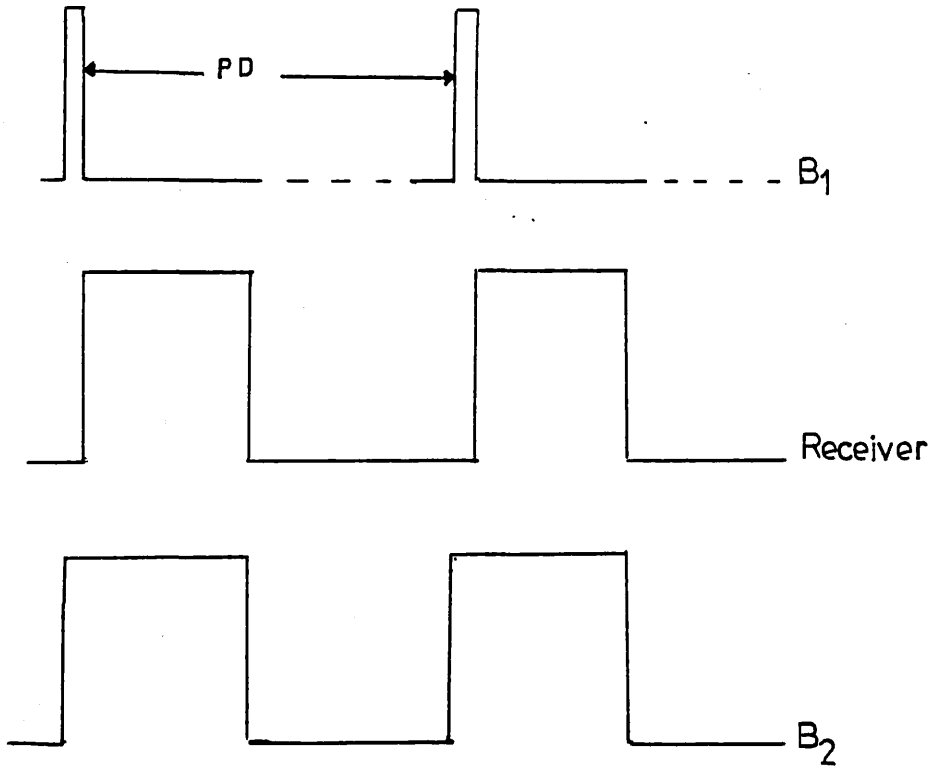

Figure 6

A decoupled spectrum with the NOE is obtained in the normal manner by leaving the decoupling field, B_z on during the whole experiment.

Due to the dynamics of the Overhauser effect the pulse delay (PD) should be $8 \times T_1$.[24]

If the intensity of the spectrum obtained using gated decoupling is denoted by I_g and that of the normally decoupled spectrum is I_N then the nuclear Overhauser factor η is given by

$$\eta = \frac{I_N}{I_g} - 1$$

For the nuclei discussed in this thesis I = ^{13}C, ^{119}Sn and S = ^{1}H. If η_{max} is the maximum enhancement factor then the dipolar relaxation rate (R_1^{DD}) can be extracted from the total rate R_1^{Tot} from

$$R_1^{DD} = \left(\frac{\eta}{\eta_{max.}}\right) R_1^{Tot}$$

where $\eta_{max.}$ = 1.99 for ^{13}C relaxed by protons and -1.34 for ^{119}Sn relaxed by protons.

1 J.L. Doob, Ann. Math. Statistics (1944) 15 229.

2 N. Bloembergen, E.M. Purcell, R.V. Pound, Phys. Rev. (1948) 73 679.

3 A. Abragam, Principles of nuclear magnetism.

4 I.D. Cresshull, D.G. Gillies, unpublished results.

5 J. Puskar, T. Saluvare, E. Lippma, A.B. Permin, V.S. Petrosyan, Proc. 18th Congress Ampere on Magnetic Resonance and Related Phenomena p. 509.

6 P.S. Hubbard, Phy. Rev. (1963) 131 1155.

7 R.E.D. McClung, J. Chem. Phys. (1969) 51 3842.

8 A.A. Maryott, T.C. Farr, M.S. Malberg, J. Chem. Phys. (1971) 54 64.

9 C. Deverell, Mol. Phys. (1970) 17 319.

10 T.C. Farrar, E.D. Becker, Pulse and FTNMR.

11 G.C. Levy, D.M. White, F.A.L. Anet, J. Magn. Res. (1972) 6 453.

12 I.D. Cresshull, D.G. Gillies, unpublished results.

13 J. Dadok, Fourth International Meeting on NMR Spectroscopy (1978).

14 W.B. Moniz, H.S. Gutowsky, J. Chem. Phys. (1963) 38 1155.

15 H.H. Mantsch, H. Saito, I.C.P. Smith, Prog. in NMR Spect. (1977) 11.

16 A.W. Overhauser, Phys. Rev. (1953) 92 411.

17 D. Doddrell, V. Glushko, A. Allerhand, J. Chem. Phys. (1972) 56 3683.

18 I. Solomon, Phys. Rev. (1955) 99 559.

19 K.F. Kuhlmann, D.M. Grant, R.K. Harris, J. Chem. Phys. (1970) 52 3439.

20 The Nuclear Overhauser Effect, Noggle and Shirmer, Academic Press 1971, Chemical Application.

21 F.T. NMR Spectroscopy, D. Shaw, Cahpter 9, Elsevier 1976.

22 K.F. Kuhlmann, D.M. Grant, J. Chem. Phys. (1971) 55 2998.

23 R. Freeman, H.D.W. Hill, R. Kaptein, J. Magn. Reson. (1972) 7 327.

24 S.J. Opella, D.J. Nelson, O. Jardetzky, J. Chem. Phys. (1976) 64 2533.

CHAPTER 3

The Spectrometer System

Section 1A Observe

B Field-Frequency Lock

C Proton Decoupling

A

Observe (see Figure 1)

The spectrometer has been developed in this laboratory by D.G. Gillies and is based on a Varian HA60-IL magnet system (gap 15"). I.D. Cresshull wrote the computer software and implemented some interfaces. Some aspects have been described previously.[1] The observing frequency was generated by a frequency synthesiser (normally General Radio Type 1061). The RF pulses, alternating in phase (two at 0°, two at 180° etc.), were amplified using a wide band amplifier (Amplifier Research Type 10 LA) to drive a 150W tuned amplifier (Polaron). A 2 kW tuned amplifier (Heathkit Type SB220) assembled in this laboratory was added during the course of this work. This reduced the 90° pulse length from around 100 μs to 25 μs. The pulses were applied to the sample using the cross-coil arrangement of the Varian XL-100 probe. The NMR signal was initially amplified in the probe by a Varian type preamplifier and further amplified by a Decca preamplifier and Polaron wide band amplifier. A balanced modulator (Hatfield Type MD4) was used to phase detect the signals which were then further amplified and passed through a low pass Butterworth filter. The signal was digitised by a 10 bit ADC (Digital Equipment Corporation, Type AR11) which was interfaced to the computer (DEC PDP 11, 28 K memory). Dual cassettes (DEC TU16) enabled up to six FID's with the accompanying parameter listings to be stored. The cassettes have subsequently been replaced by dual drive floppy discs. After digitisation the FID could be apodised (using a cosine function) and filtered (using an exponential weighting function) and finally Fourier transformed. The resulting frequency spectrum was displayed on the VDU and could be phased. The various display parameters could be changed interactively facilitating more detailed

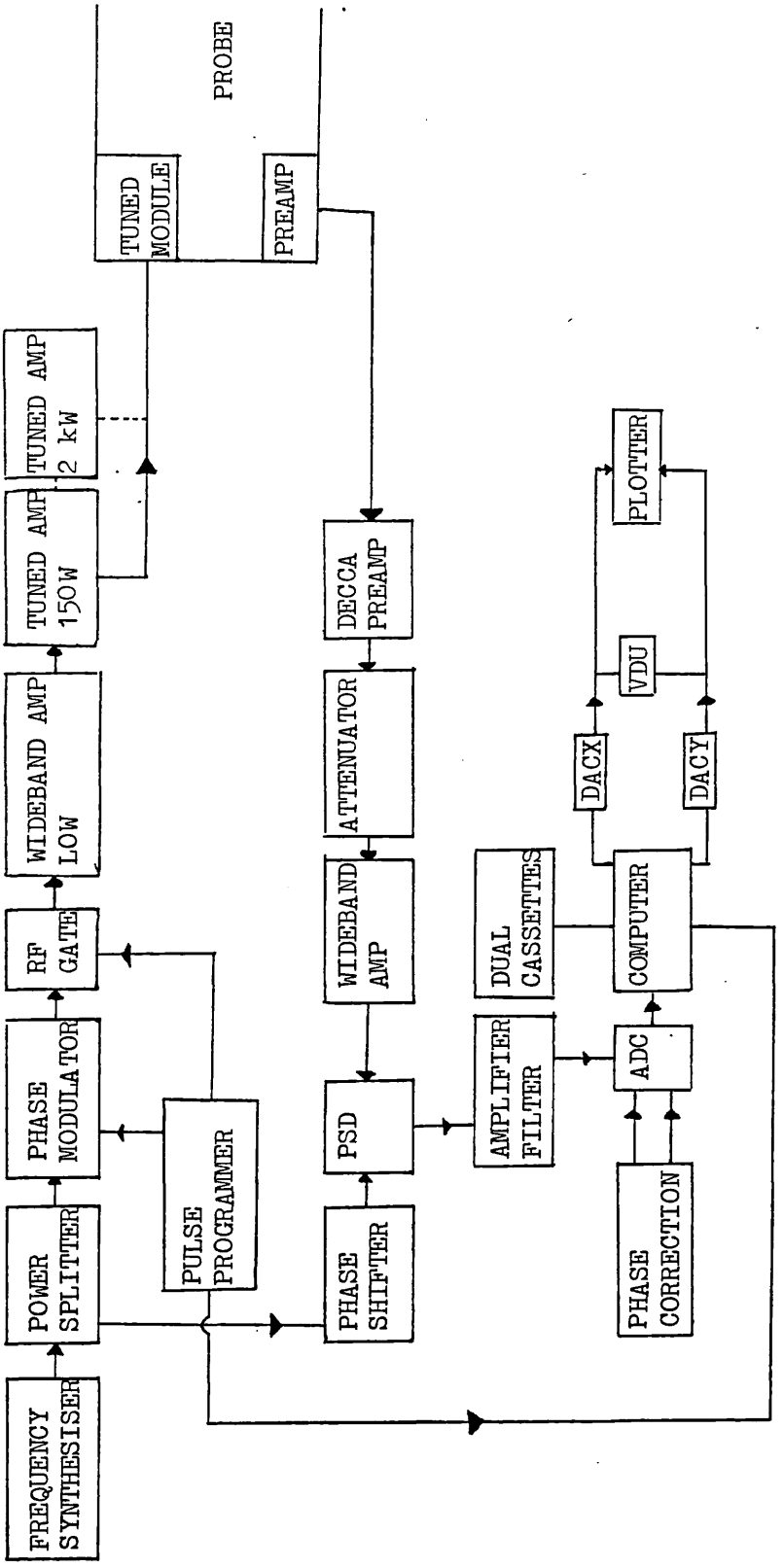
FREQUENCY SYNTHESISER
POWER SPLITTER
PHASE MODULATOR
RF GATE
WIDEBAND AMP LOW
TUNED AMP 150W
TUNED AMP 2 kW
PULSE PROGRAMMER
PHASE SHIFTER
PSD
WIDEBAND AMP
ATTENUATOR
DECCA PREAMP
PREAMP
TUNED MODULE
PROBE
AMPLIFIER FILTER
DUAL CASSETTES
ADC
PHASE CORRECTION
COMPUTER
DACX
DACY
VDU
PLOTTER

Figure 1

study of the spectrum. Hard copies of spectra were obtained from the XY plotter (Bryans).

The pulse programmer consists of five identical digital timers controlling the 90 and 180° pulse lengths, the value of τ (delay in the inversion recovery experiment), the acquisition rate and the overall repetition rate of the experiment. For the normal $(90 - \tau)_n$ experiment the timer controlling the 180° pulse and the delay timer were obviously inoperative. The timers were set manually, different pulse sequences being generated by manually changing the interconnection of the timers.

B

The Field-Frequency Lock System

Apart from a few early spectra which utilised a fluorine resonance, field-frequency lock was established using a deuterium resonance. A simplified block diagram is shown in Figure 2.

The system employed time shared modulation produced by transmitter pulses with a repetition rate of 1kHz and a 10% duty cycle. These pulses were amplified and applied to the decoupler coil through a double tuned network. The lock channel of the standard Varian V4354A internal reference controller was used to provide the dispersive signal for locking and the absorption signal to the recorder (shim switch on) and to a meter in order to monitor the lock. The lock was always to the first upfield sideband (at 1kHz) and could be conveniently set up prior to locking by sweeping through the resonance using the recorder since the latter produced a ramp voltage to drive the FSX 3006S frequency synthesiser.

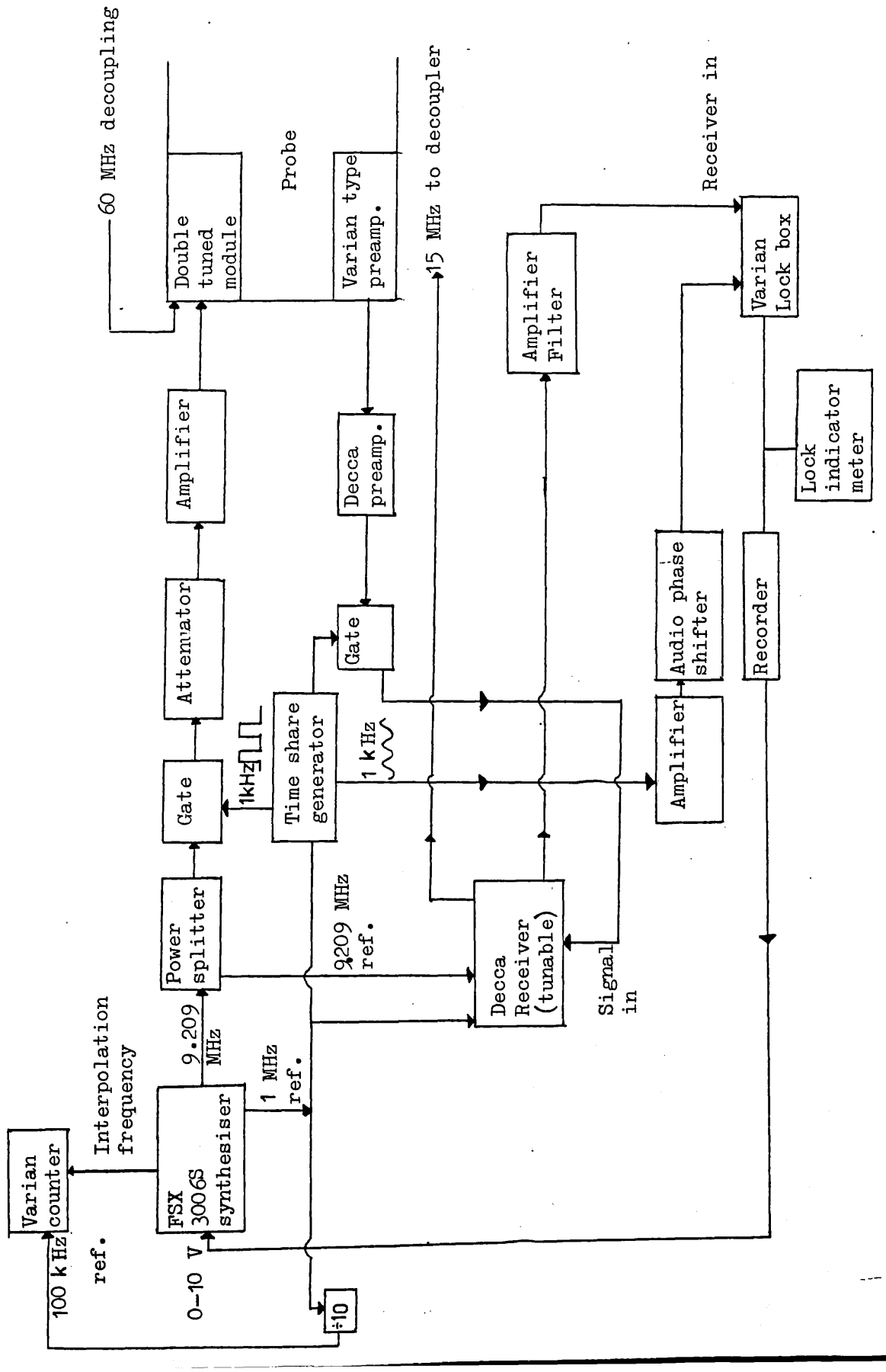

Figure 2

^{2}H Lock system

The exact frequency was read from the standard Varian counter which monitored the interpolation frequency in the synthesiser. This was particularly important as only a fixed frequency of 60 MHz (derived from the 1 MHz standard of the synthesiser) was available for proton decoupling. This meant that the deuterium lock frequency had to be changed in order to adjust the field for optimum decoupling.

Recently[2] this inconvenience has been eliminated by the use of an additional synthesiser in the decoupler channel.

C

The Proton Decoupler (see Figure 3)

The 60 MHz was provided by a Varian RF unit (V 4311) which was referenced to a standard 15 MHz. Power amplification was by a 10W broadband amplifier (Marconi Type TF 2167). For proton noise decoupling a pseudo random noise generator (12 bit) driving a phase inverter was used, the bandwidth of which was controlled by an oscillator (Wavetek Type 134). If CW decoupling was required the amplitude of the Wavetek was minimised so that the noise generator was not triggered and hence the RF phase not modulated. To enable NOE measurements to be carried out a diode gate was introduced into the 15 MHz line. The decoupler could be gated on during the acquisition time so as to produce NOE suppressed decoupled spectra whose intensity could be compared to spectra obtained with the decoupler on all the time.

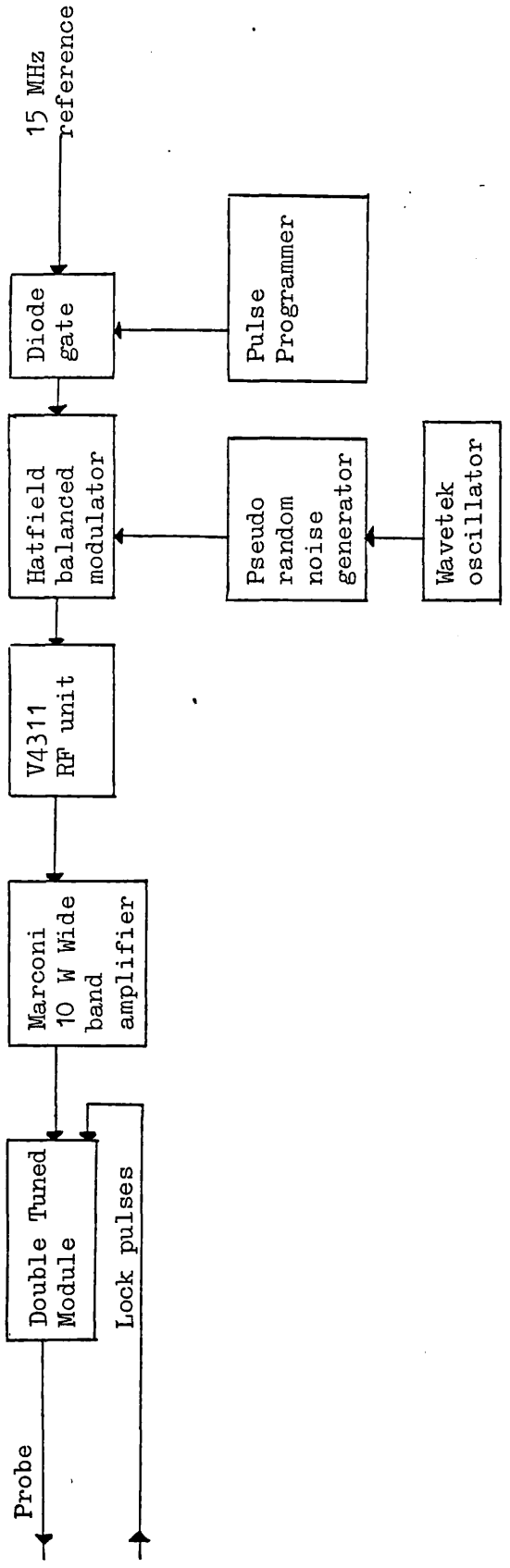

Figure 3

Block diagram of proton decoupler

References

1 D.G. Gillies, Specialist Periodical Reports NMR (1971) 1 Chapter 4.

2 D.G. Gillies, Private Communication.

CHAPTER 4

Spin-Lattice Relaxation Times and NOE Factors for ^{119}Sn

Part I

Section 1 Introduction

A Review

B Results and General Discussion of ^{119}Sn Relaxation Data

Part II

The ^{119}Sn Relaxation Data for nPr_3SnCl, nBu_3SnCl, nPr_4Sn and nBu_4Sn

Section 1 Discussion

Part III

The ^{119}Sn Relaxation Data for nBu_3SnH

Section 1 Introduction

A Discussion

Part IV

The ^{119}Sn Relaxation Data for $nBu_2Sn(OAc)_2$

Section 1 Discussion

A Effect of Exchange on R_1

Part V

The ^{119}Sn Relaxation Data for Sn_2Me_6

Section 1 Discussion

Part VI

The Spin-Rotation Contribution to ^{119}Sn R_1 values

Section 1 Discussion

Part VII

The Activation Energy

Part VIII

Microviscosity Theory

Part IX

Part I

1A Introduction

B Review

C Results and General Discussion of ^{119}Sn Relaxation Data

Section 1

Introduction

The majority of the available ^{119}Sn literature is concerned with shift and coupling constant determinations. Very little has been published relating to the spin-lattice relaxation behaviour of tin and to the knowledge of this author only five publications have appeared on this subject. Although the ^{119}Sn nucleus is twenty five times more sensitive to NMR detection than ^{13}C, the NOE effect (positive for ^{13}C and negative for ^{119}Sn) usually reduces this to a factor of about 8 at best (i.e. where η for ^{119}Sn is zero). In fact we now find that non-bonded dipolar interactions are more important than previously was thought and cases of severely reduced intensity may well be quite common. From the point of view of sensitivity and T_1 measurement the advent of commercial Fourier transform instruments should have stimulated interest in ^{119}Sn as a probe nucleus. This has not been so. In an effort to redress the balance and to extend the data base of more fundamental NMR information on ^{119}Sn spin-lattice relaxation times and NOE factors are presented and discussed in this chapter.

A

Review

Puskar et al[1] were the first to carry out a detailed spin-lattice relaxation study of organo tin compounds in the liquid state. They measured the ^{119}Sn and ^{13}C spin-lattice relaxation times in the series R_4Sn (R = Me, Et, Pr) over a range of temperature. The reported T_1 values for ^{119}Sn were in the range 0.5s to 5.0s at ambient temperature and hence much shorter than one typically finds for carbon and silicon.

The temperature dependence of the relaxation indicated that spin-rotation was the dominant mechanism over the whole temperature range only in the case of $SnMe_4$. The relaxation in $SnEt_4$ and $SnPr_4$ was dominated by the spin-rotation mechanism only at higher temperatures. At lower temperatures the dipole-dipole mechanism dominated. In the same paper the relaxation behaviour of ^{119}Sn in the series Me_3SnX (X = Cl, Br, I) was also reported and found to be dominated by the spin-rotation mechanism. Scalar relaxation contributes to the total rate only when X = I.

More recently Lassigne and Wells[2,3] have studied tetramethyl tin and its isotopic modifications $(CH_3)_{4-n}Sn(CD_3)_n$ and found that the spin-rotation relaxation rate varies according to the square root of the moment of inertia I where I = 1/3 (Ixx + Iyy + Izz), confirming the Hubbard relationship. They also showed a correlation between the spin-rotation relaxation rate and the paramagnetic term of the shielding tensor of the ^{119}Sn nucleus.

Sharp[4] has measured the spin-spin and spin-lattice relaxation times as a function of temperature for $SnCl_4$ and SnI_4. For $SnCl_4$ T_1 is dominated by the spin rotation mechanism over the entire temperature range. For SnI_4 a maximum in T_1 is observed at 190°C. Such behaviour is attributed to competition between spin-rotation and scalar coupling to the ^{127}I nucleus. For both liquids $T_2 \ll T_1$ and scalar coupling of the second kind dominates T_2. An absolute shielding scale for ^{119}Sn was also estimated.

Ahmed[5] has used the differential relaxation rates of the central and satellite features in the proton spectrum of a number or organo tin hydrides to derive correlation times (τ_c) for the tin-hydride proton

vector. Isotropic motion was assumed and τ_c showed a trend with molecular size.

In a paper not directly concerned with relaxation Mitchell[5] notes that significant NOE factors were observed for hexabutylditin and hexaoctylditin. Chromium tris(acetylacetonate) was found to partially eliminate the NOE without significantly affecting shifts.

B

Results and General Discussion of ^{119}Sn Relaxation Data

The spin-lattice relaxation rates (R_1) and NOE factors for the ^{119}Sn nucleus over a range of temperatures of a number of different molecules are tabulated in Table 1-4. The data are summarised in figures 1-4. Table 5 shows the observed rate and NOE factors for nPr_4Sn, nBu_4Sn, nPr_2SnCl, nBu_3SnCl and nBu_3SnH at 307°K. Figure 1a shows typical results from a (180-τ-90) experiment for nPr_3SnCl. Figure 1b shows the NOE measurement.

The data now reported may be interpreted in terms of two contributing mechanisms, spin-rotation and dipole-dipole (tin-proton). In the case of the chlorides the possibility of a contribution from scalar relaxation of the second kind was considered and found to be negligible in agreement with the observations of Sharp[4] and Puskar et al.[1] A significant contribution would obviously modify the ln R_1 vs 1/Temp plot and degrade the fit of the NOE deduced straight lines representing the dipole-dipole and spin-rotation contributions. In particular the maximum NOE could not have been observed for a nBu_3SnCl at low temperature and the NOE value of -0.67 (corresponding to 50% dipole-dipole relaxation) would not have corresponded to the minimum in the curves. Obviously then the

Tables 1 and 1a show the T_1 and NOE data for neat nPr_3SnCl. All measurements at 22.37 MHz using spectrometer described in Chapter 3.

Table 1

Temp/K	R_1^{Tot}/s^{-1}
279.5	0.21
299.3	0.22
313.6	0.20
331.2	0.26
344.0	0.31
358.9	0.33
385.0	0.44

Table 1a

Temp/K	η
253.5	-1.08
266.5	-0.75
276.6	-0.72
285.0	-0.62
300.4	-0.34
317.2	-0.19
330.6	-0.22
368.3	-0.05
394.5	-0.12

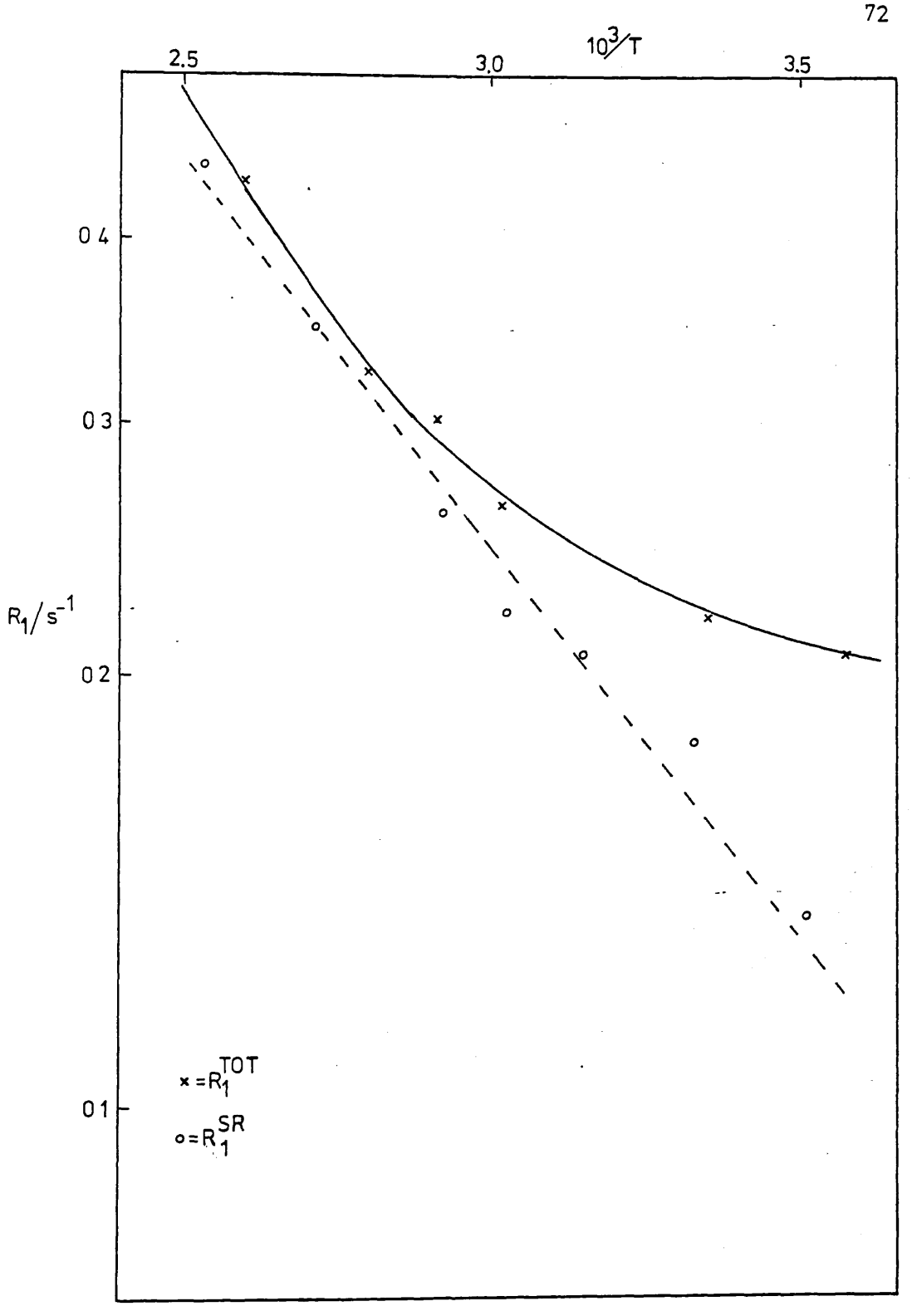

Figure 1

Arrhenius plot of data in Tables 1 and 1a

for nPr_3SnCl

Figure 1a

Typical results of (180-τ-90) experiment measured at 22.374 MHz using spectrometer described in Chapter 3. These results are for nPr_3SnCl (neat) at 299.3°K using 16 transients

$T_1 = 4.53s \quad \eta = -0.34$

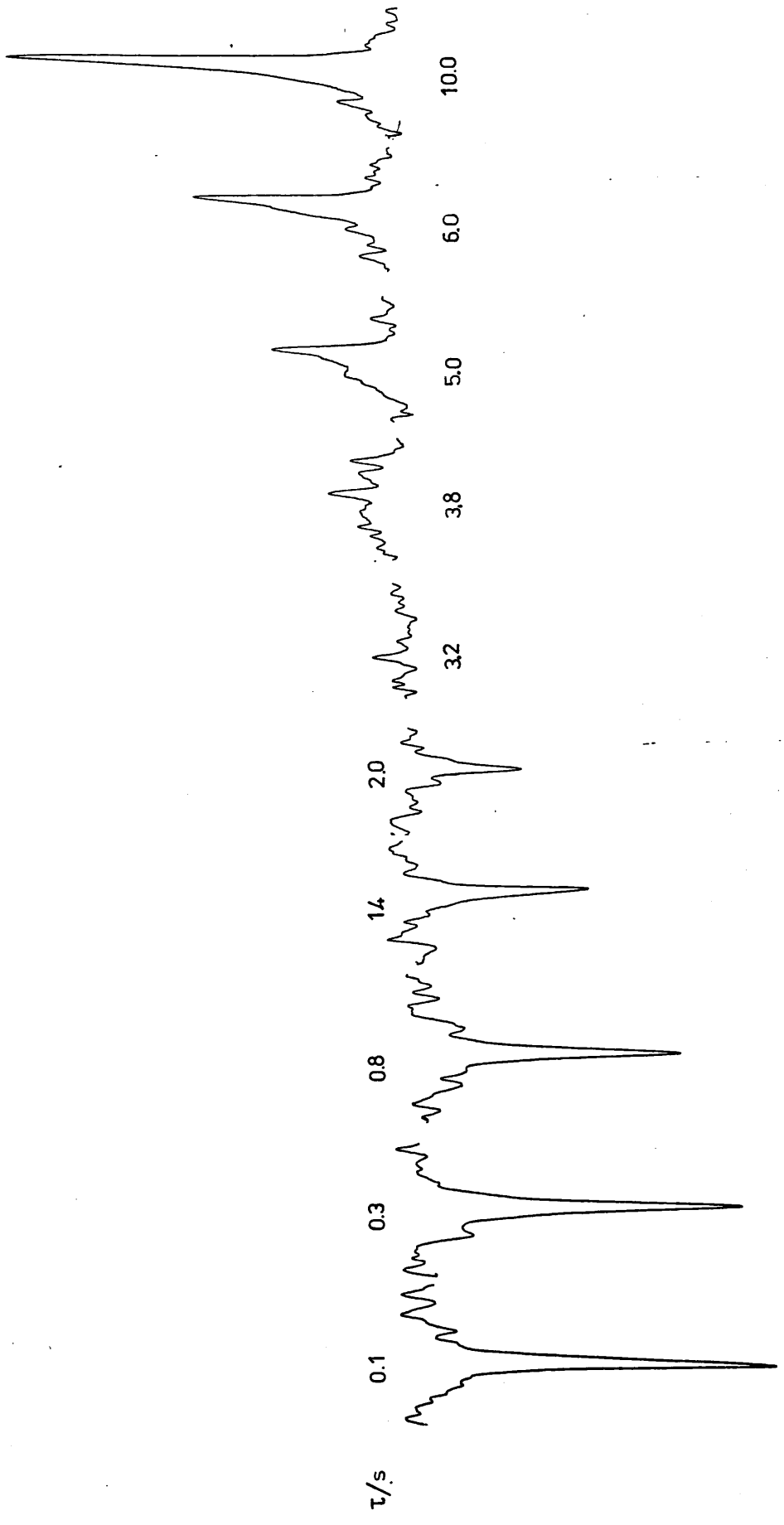
τ/s
0.1
0.3
0.8
1.4
2.0
3.2
3.8
5.0
6.0
10.0

Figure 1b

NOE determination for nPr_3SnCl (neat) at 299.3°K

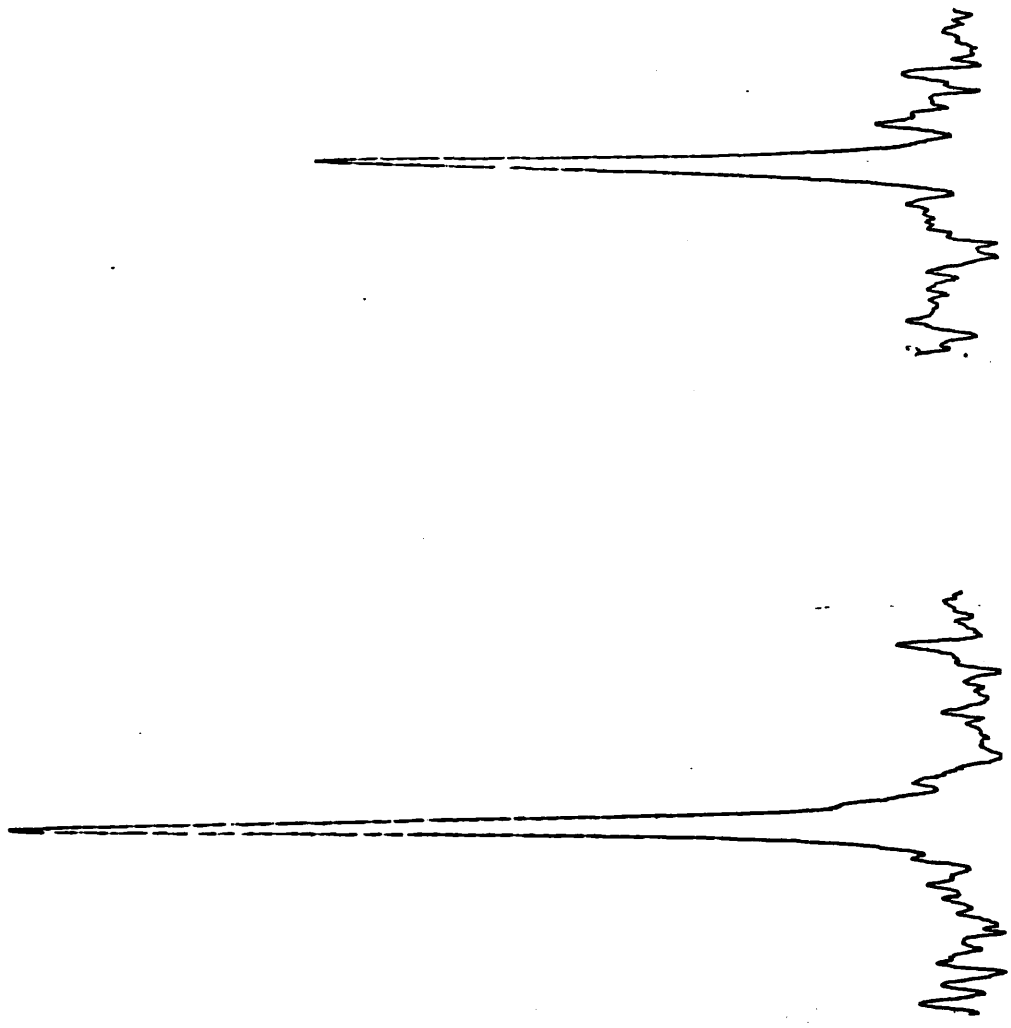

T_1 and NOE data for neat nBu_3SnCl. All measurements at 22.37 MHz using spectrometer described in Chapter 3.

Table 2

Temp/K	R_1^{Tot}/s^{-1}
250.7	0.77
257.7	0.53
262.9	0.44
300.3	0.17
319.3	0.16
338.0	0.17
370.7	0.21
381.5	0.26
390.4	0.27
410.4	0.37

Table 2a

Temp/K	η
253.5	-1.33
266.5	-1.26
276.6	-1.16
285.0	-1.09
300.4	-0.84
317.2	-0.50
330.6	-0.30
341.8	-0.15
348.0	-0.23
368.3	-0.32
394.5	0.00

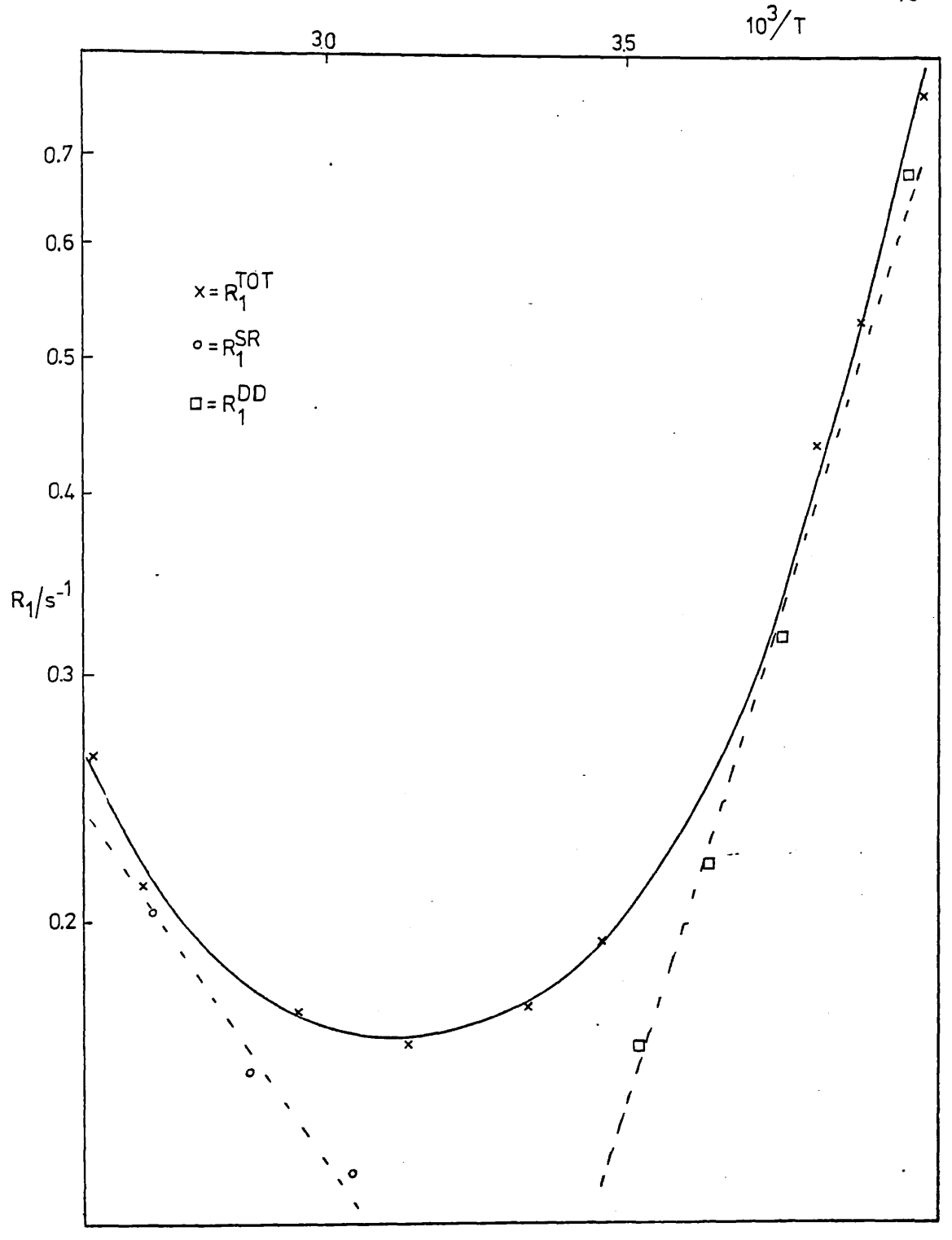

Figure 2

Arrhenius plot of data in Tables 2 and 2a for nBu_3SnCl

T_1 and NOE data for neat Sn_2Me_6. All measurements at 22.37 MHz using spectrometer described in Chapter 3.

Table 3

Temp/K	R_1^{Tot}/s^{-1}
331.5	0.79
341.4	0.78
347.3	0.91
356.0	1.01
366.0	1.12
388.0	1.54
403.0	1.79

Table 3a

Temp/K	η
303.0	-0.13
329.7	-0.05
341.8	-0.05
368.3	0.00

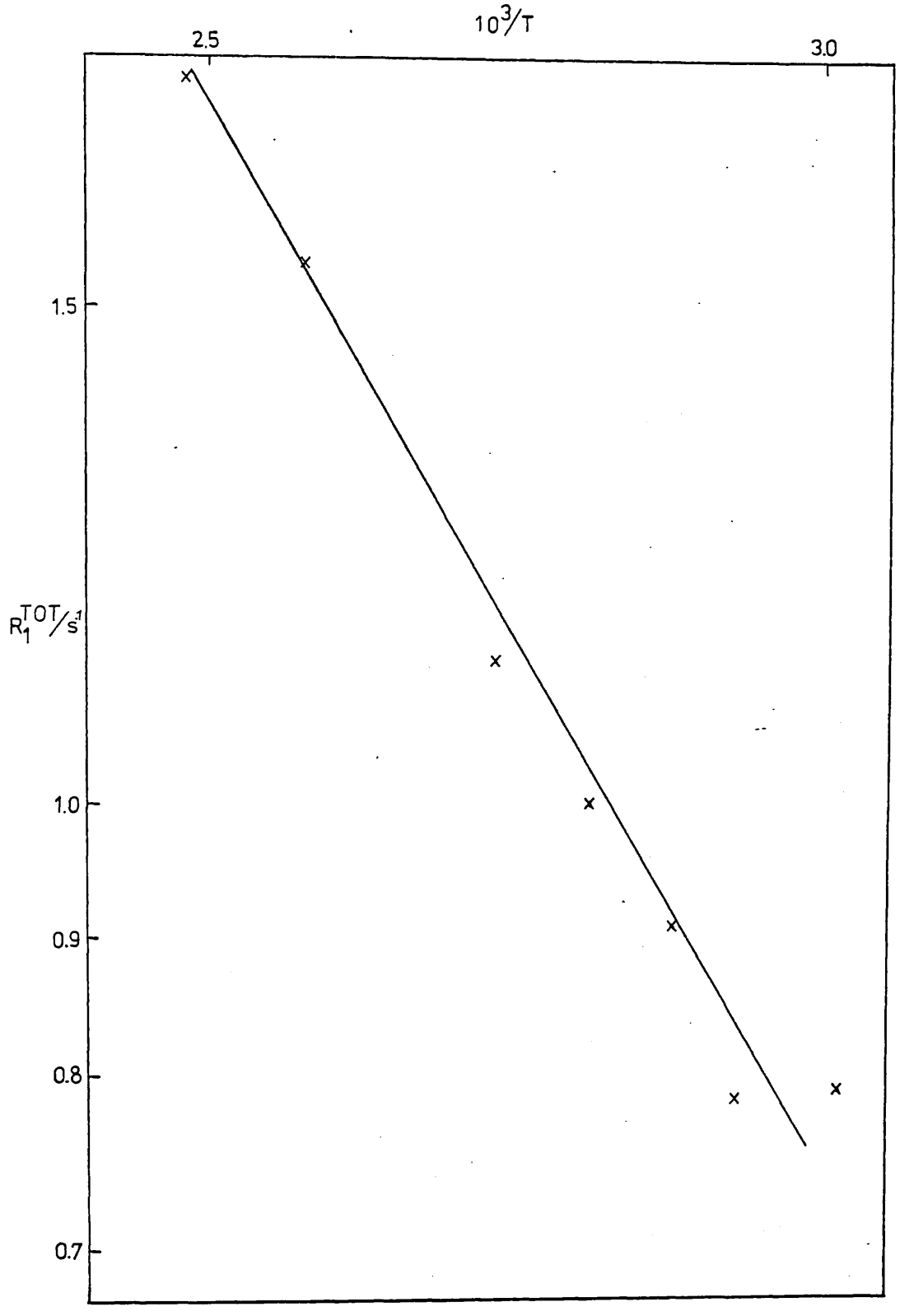

Figure 3

Arrhenius plot of data in Tables 3 and 3a for Sn_2Me_6

T_1 and NOE data for neat $nBu_2Sn(OAc)_2$. All measurements at 22.37 MHz using spectrometer described in Chapter 3.

Table 4

Temp/K	R_1^{Tot}/s^{-1}
280.0	3.12
299.8	1.19
312.7	0.70
319.3	0.50
325.8	0.37
337.5	0.39
350.3	0.32
372.0	0.28
402.0	0.27

Table 4a

Temp/K	η
276.6	-0.35
284.3	-0.34
300.7	-0.33
317.2	-0.33
348.0	-0.39
368.3	-0.30

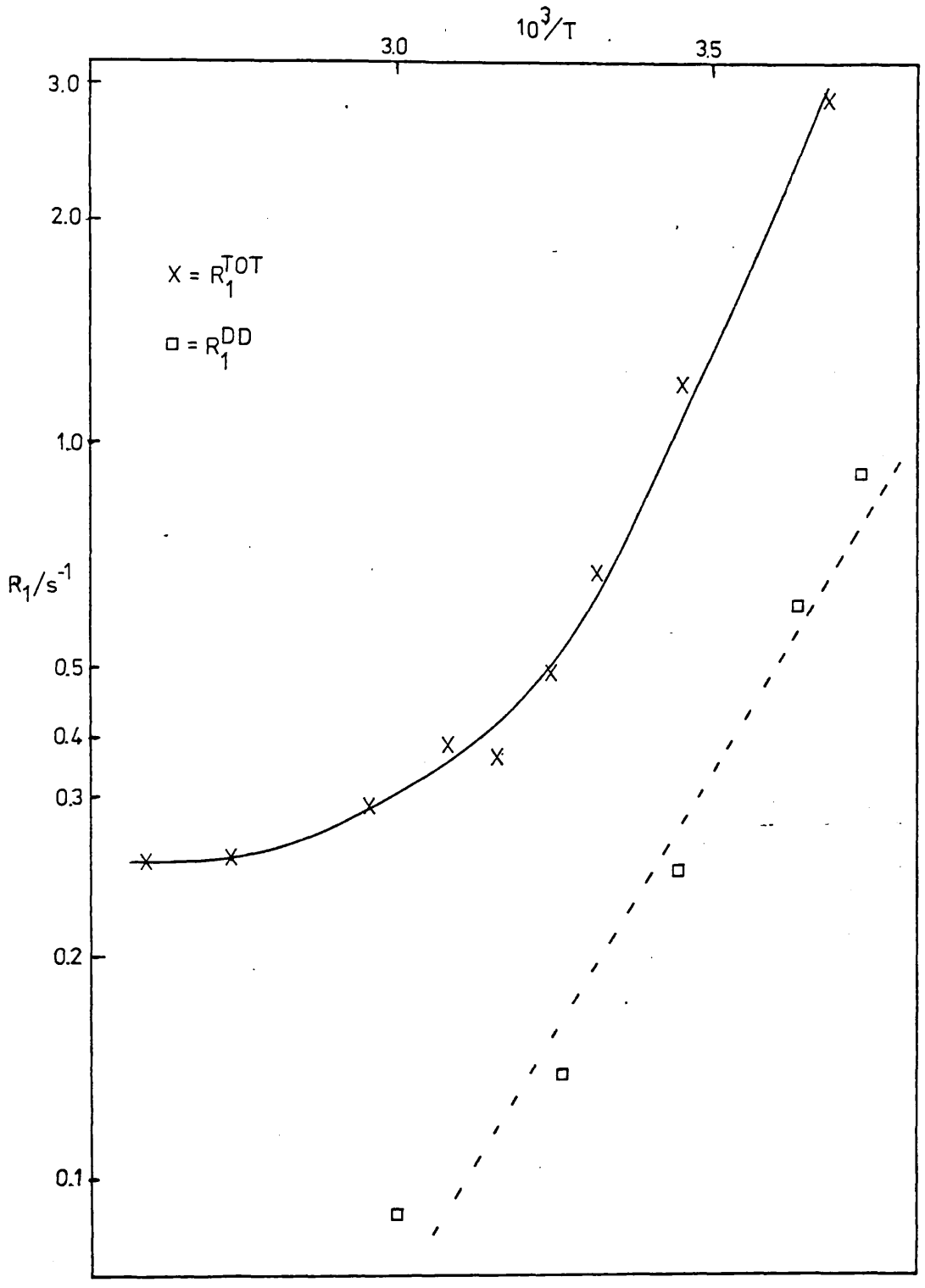

Figure 4

Arrhenius plot of data in Tables 4 and 4a for $nBu_2Sn(OAc)_2$

Table 5

^{119}Sn T_1 and NOE data at 307°K. Samples were run as the neat materials at 22.37 MHz unless otherwise indicated.

Molecule	R_1^{Tot}	η	R_1^{DD}/s^{-1}	R_1^{other}/s^{-1}
nPr_4Sn	0.210	-0.37	0.058	0.150
nPr_3SnCl	0.209	-0.28	0.044	0.165
nBu_4Sn*	0.159	-0.86	0.102	0.146
nBu_3SnCl	0.172	-0.68	0.087	0.085
nBu_3SnH*	0.215	-0.43	0.069	0.146

* Run at 37.29 MHz

stringent matching of time scales which allows the scalar coupling mechanism to contribute to R_1 is absent unless ^{127}I is present (see Chapter 2 section 2D).

Scalar relaxation of the second kind does however contribute to R_2 since a zero frequency term exists in the expression for R_2^{SC} that is absent in the R_1^{SC} expression. The reader is referred to reference 15 for a more detailed discussion of this point for the case of the ^{119}Sn nucleus. Hexamethylditin presents the only example reported here where the relaxation is spin-rotation dominated over the entire temperature range of study. A striking feature of the data presented here and that of Puskar et al[1] is that the ^{119}Sn relaxation times are somewhat short. These may be compared to the ^{29}Si relaxation times in related compounds[7,9,10] which are much longer. The longest ^{119}Sn T_1 measured is about 6 seconds yet the shortest ^{29}Si T_1 is about 20 seconds. A simple comparison of the relative importance of the dipolar mechanism for ^{13}C, ^{29}Si and ^{119}Sn nuclei can be obtained from equation 1.

$$R_1^{DD} = \frac{\gamma_X^2 \gamma_H^2 \hbar^2 \tau_c}{r_{X-H}^6} \quad \ldots \quad 1$$

where γ_X is the magnetogyric ratio of ^{13}C, ^{29}Si, ^{119}Sn

r_{X-H}^6 is the relevant internuclear distance

R_1^{DD}, γ_H, $\hbar$, τ_c have their usual meanings.

Table 6 shows this comparison for equal numbers of directly attached protons. The correlation time is assumed to be constant. On this

Table 6

Comparison of the relative effectiveness of a directly bound proton to X in providing dipolar relaxation

X	$\gamma_X/10^7$ rad $T^{-1}s^{-1}$	r_{X-H}/pm	Relative effectiveness
^{13}C	6.726	109	1.0
^{29}Si	-5.314	148	0.09
^{119}Sn	-9.971	170	0.15

basis then it might be expected that ^{119}Sn relaxation times should be a factor of about 1.5 to 2.0 shorter than for ^{29}Si. In fact it is quite common to observe ^{119}Sn T_1 values that are 5 to 10 times shorter than in homologous ^{29}Si compounds. This is exemplified by comparison of the dipolar rate of ^{119}Sn in Ph_3SnH to the dipolar rate of ^{29}Si in Ph_3SiH,[7] the tin rate being about eight times faster. The simplest and most obvious way of explaining this discrepancy is that the dipolar mechanism is much more efficient in the case of the tin containing molecule because it is not so efficiently averaged by fast motion. In other words the correlation times for the tin containing molecules are expected to be longer than those for the silicon molecules.

A practical consequence of increasing NOE values at low temperatures is that no T_1 values could be measured for nBu_3SnCl and nPr_3SnCl over the temperature range where the signal intensity is severely reduced (ie when η approaches - 1.0). In the former case the intensity recovered sufficiently at low temperatures to enable T_1 measurements whereas in the latter case the sample froze prematurely.

In order to calculate correlation times from the derived dipolar rates the distance between the nucleus concerned and the relevant protons must be known. In the case of the hydrides it may be thought that it is safe to assume that the dipolar contribution is from the hydride proton only. This point is discussed in more detail later in this chapter. In the case of organo tin (or organosilicon) molecules where the metal nucleus does not have any directly bound protons the internuclear distance of interest is much harder to define. Consider the molecules nPr_3SnCl and nBu_3SnCl. From figures 1 and 2 it can be seen that there are significant dipole—dipole contributions to the relaxation rate which can only arise from the protons on the alkyl

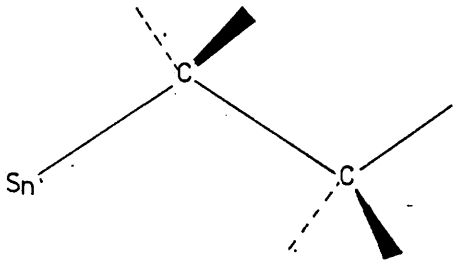

Figure 5

Table 7

Relative dipolar contributions from protons on n-alkyl groups

	r_{X-H}/pm	Relative effectiveness
Directly bound	170	1.00
α protons	275	0.056
β protons	325	0.021

chains. Since it is generally agreed that the intermolecular dipolar contributions to this are small this must be an intramolecular effect. At first sight it might be thought that only the protons on the α carbons will contribute to the relaxation rate because the r^{-6} dependence of R_1^{DD} will make the contributions from the protons on the carbons too small. In fact if a fixed zig-zag orientation of the alkyl groups is assumed as in figure 5, then the distance from the tin nucleus to the α protons can be calculated to be 275 pm, in agreement with Wallach's[8] value. The distance to the β protons is found to be 325 pm. Using equation 1 we may calculate the relative contributions of the α and β protons compared to a hydride proton directly bound to tin (see Table 7). Although the contribution from a remote proton seems insignificant compared to a hydride proton it is not insignificant when multiplied by the number of such protons especially in the monohydrides considered here.

From Table 7 it can be seen that the β protons are about 33% as effective in relaxing tin as the α protons. This contribution is significant and must consequently be included when correlation times are calculated. To do so requires that the r^{-6} term in equation 1 be replaced by $\sum_N r_i^{-6}$ where the r_i's are the relevant internuclear distances and N the number of contributing protons.

Part II

Discussion of ^{119}Sn Relaxation Data for nPr_3SnCl, nBu_3SnCl, nPr_4Sn and nBu_4Sn

Discussion of ^{119}Sn Relaxation Data for nPr_3SnCl, nBu_3SnCl, nPr_4Sn and nBu_4Sn.

Table 8 shows the effective correlation times derived from the ^{119}Sn relaxation data for the molecules nPr_3SnCl, $n\text{-}Bu_3SnCl$, nPr_4Sn and nBu_4Sn. Before any comment is passed on these values the difficulty of interpreting such data should be pointed out. In calculating τ_c^{eff} the inevitably crude assumption of overall isotropic tumbling has had to be made which may not be true for the tin chloride molecules. More significantly two different types of protons contribute to the dipolar relaxation of tin and these are the protons of the α and β methylenes of the alkyl groups. The effective correlation time derived from the tin data then is for motion perpendicular to the tin-remote α proton vector and tin-remote β proton vector (see figure 6). The correlation time for these vectors will be the same only if overall tumbling is isotropic and if the alkyl groups are rigid. Since the ^{13}C relaxation data for these molecules indicates that segmental motion is taking place along the alkyl chains (see Chapter 5) then the rigid model for such molecules must be a poor one. However since no other model exists for treating such data we are forced to adopt the rigid model. In so doing the derived correlation times become somewhat "fuzzy" on account of the segmental motion. Furthermore the distance of the β protons from the tin nucleus have been calculated assuming a fixed zig-zag orientation. If this is not the case the values of τ_c^{eff} will become even more imprecise. However for such closely related molecules as nPr_3SnCl and nBu_3SnCl even though the vectors that τ_c^{eff} describes are not exactly defined they are likely to be very similar in both molecules and can therefore be compared directly with some degree of confidence.

Table 8

Effective correlation times derived from the ^{119}Sn relaxation data in Table 5

Molecule	$\bar{I}$/g.cm^2 * (10^{40})	τ_c^{eff}/ps
nPr_4Sn	2274	30
nBu_4Sn	4267	51
nPr_3SnCl	1914	29
nBu_3SnCl	3355	58

* $\bar{I}$ calculated using Fortran IV program in appendix B.

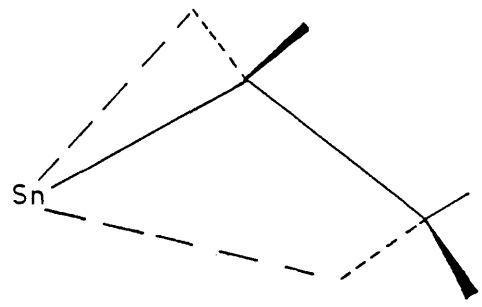

Figure 6

Showing the relevant Sn-remote proton vectors for n-alkyl tin chlorides assuming a fixed zig-zag orientation of the alkyl chains.

From Table 8 it can be seen that the τ_c^{eff} for nPr_3SnCl and nBu_3SnCl are 30 ps and 58 ps respectively. As expected the smaller molecule has the shorter correlation time because it can rotate more easily. This is due to fewer "solvent" molecules having to be swept out of the way for the rotation to occur. Also the molecular moment of inertia [$\bar{I} = 1/3(I_{xx} + I_{yy} + I_{zz})$] is smaller for nPr_3SnCl than for nBu_3BnCl (see Table 8) so that the inertial effect is less (see Chapter 5, section 2B). In fact the ratio of the correlation times for the two molecules is approximately the same as the ratio of the molecular moments of inertia. This gives us some confidence in comparing effective correlation times (τ_c^{eff}) of molecules where the vectors described by τ_c^{eff} are not fixed. Note also that the NOE is smaller for nPr_3SnCl than for nBu_3SnCl. This is due to the more efficient averaging of the dipolar relaxation mechanism by faster reorientation. As expected for a molecule which rotates relatively fast nPr_3SnCl has a larger spin-rotation contribution to the total relaxation rate than does nBu_3SnCl.

The effective correlation times derived from the ^{119}Sn data of nPr_4Sn and nBu_4Sn are also shown in Table 8 for comparison. Note the similarity in the values of τ_c^{eff} for the chlorides compared to the analogous tetraalkyl tin compounds. This observation could be taken as evidence suggesting that the overall tumbling characteristics of the tri n-alkyl tin chlorides considered here are quite close to isotropic. The mass of the chlorine nucleus is quite similar to that of the n-propyl group so that substituting one n-propyl group by chlorine apparently has little effect on the motion of the molecule.

The molecular moments of inertia of these molecules give more insight into the rationale of the values of τ_c^{eff}. Table 8 includes the moments of inertia of the molecules discussed and a rough correlation between τ_c^{eff} and $\bar{I}$ is apparent across the four molecules. This correlation is much better when the two types of molecules are considered separately. That is the ratio of $\bar{I}$ for the molecules nPr_4Sn and nBu_4Sn reflects the ratio of the correlation times of the two molecules. As stated above this is also the case for the two chloride molecules. That the relationship is not so good when dealing with molecules of different symmetry is not unexpected since the vectors to which the correlation times relate are not the same. This strong dependence of τ_c^{eff} on $\bar{I}$ for molecules of the same symmetry which becomes weaker when comparing τ_c^{eff} for molecules of different symmetry (in this case Td and C_{3v}) suggests that in the former case it is the increase in the inertial effect that dominates the value of τ_c^{eff} whereas in the latter case, although the inertial effect is still present the frictional effect plays a more significant role in determining τ_c^{eff}.

Interestingly the increase in τ_c^{eff} for the tin-remote proton vector in going from nPr_3SnCl to nBu_3SnCl is paralleled by the τ_c^{eff} values deduced for the α-C-H vector of the alkyl group (see Chapter 5, section 2C). The α methylene groups are the most restricted of the groups in the alkyl chains resulting from the anchoring effect of the massive tin nucleus.

Part III

The ^{119}Sn Spin-Lattice Relaxation Data for nBu_3SnH

Section 1

Introduction

Measurement of the spin-lattice relaxation time of ^{119}Sn and the appropriate NOE in organo tin hydrides in principle enables one to characterise the motion perpendicular to the tin-proton bond. The large one bond tin-proton coupling constant ($^{1}J_{^{119}Sn-H} = 1500 - 2000$ Hz) presents formidable problems in achieving a single line resonance to facilitate measurement of a spin-lattice relaxation time of ^{119}Sn. However if enough decoupling power is available ($\gamma B_2 > J_{^{119}Sn-H}$) then the recovery of the ^{119}Sn magnetisation is exponential and T_1 can be calculated using the usual $-\ln(M_\infty - M_\tau)$ vs τ plot. In this study in fact $\gamma B_2/2\pi$ was about 5 kHz.

The advantage of studying the stannanes arises because of the fixed tin-proton bond whose motion is characteristic of the overall molecular motion. Characterising the motion of this bond consequently enables the correlation time for molecular reorientation perpendicular to the symmetry axis to be determined. This is in contrast to the tetraalkyl tin molecules discussed above where no such vector exists. The chlorides are more amenable to similar investigations since the chlorine quadrupole coupling constant can be measured by nuclear quadrupole resonance (NQR) spectroscopy and this value in conjunction with chlorine T_1 data would enable an effective correlation time to be calculated for the tin-chloride bond.

A

Discussion

Table 9 shows the T_1 and NOE factors of ^{119}Sn in nBu_3SnH (at 307°K and 37.29 MHz) and for ^{29}Si in nBu_3SiH (at 308°K).[10]

Table 9

Comparison of the metal spin-lattice relaxation data of the molecules nBu$_3$XH (X = ^{119}Sn, ^{29}Si)

Molecule	R_1^{Tot}/s^{-1}	η	R_1^{DD}/s^{-1}	R_1^{SR}/s^{-1}	τ_c^{eff}/ps
nBu$_3$SnH	0.2146	-0.43	0.0689	0.1457	16-21
*nBu$_3$SiH	0.0310	-2.34	0.0287	0.0023	11-13

* Data taken from reference 10.

From the T_1 data for the tetra-alkyl tins and tri n-alkyl tin chlorides presented in Part II of this chapter it has been shown that the remote protons on the α and β methylene groups are able to contribute significantly to the dipole-dipole relaxation rate. In a molecule where a directly bound proton is attached to tin as well as three n-alkyl groups, some estimate of the relative contribution to the dipolar rate from the different protons is required. From Table 7 it can be seen that a single proton on an α methylene group is approximately 6% as effective in relaxing ^{119}Sn via the dipole-dipole mechanism as a proton directly attached to tin. This is merely a result of the r^{-6} dependence of this mechanism. Of course in nBu_3SnH there are a total of six α methylene protons so that the relative effectiveness rises from 5.5% to 33% assuming no internal rotation. This source of dipolar relaxation cannot be ignored when calculating τ_c^{eff} for the tin-proton vector. However from the ^{13}C spin-lattice relaxation data of nBu_3SnH (see Chapter 5, section 2C) it is apparent that segmental motion occurs along the alkyl chains. As usual any motion will tend to average the dipole-dipole mechanism reducing its effectiveness as a relaxation mechanism. The figure of 33% therefore is the maximum contribution to R_1^{DD} from the α protons. For this reason Table 9 shows a range of τ_c^{eff} calculated with and without this contribution. No doubt the actual value of τ_c^{eff} is somewhere between the two extremes. The actual values of τ_c^{eff} calculated for the two molecules are surprisingly similar although they do reflect the general trend that in analogous tin and silicon containing molecules, the organo tin molecule reorients more slowly.

Use of the measured NOE factors for ^{119}Sn and ^{29}Si show the contribution of other mechanisms to the total relaxation rate. For

the molecules nBu_3SnH and nBu_3SiH these "other mechanisms" can only be the spin-rotation mechanism. From Table 9 it can be seen that the spin-rotation contribution to the ^{119}Sn relaxation rate is much larger than that for ^{29}Si. This is expected and can be accounted for by the larger spin-rotation constant of ^{119}Sn which, although not measured in nBu_3SnH is anticipated to be larger than nBu_3SiH due to the larger chemical shift range of the ^{119}Sn nucleus compared to ^{29}Si.

Part IV

The ^{119}Sn Relaxation Data for $nBu_2Sn(OAc)_2$

Section 1

Discussion

The ^{119}Sn relaxation behaviour of $nBu_2Sn(OAc)_2$ exhibits some interesting characteristics. Tables 4 and 4a and figure 4 summarise the data at 22.37 MHz. We now present the variable field studies in Table 10.

From the Arrhenius plot at 22.37 MHz shown in figure 4 two main features stand out. Firstly the temperature dependence of the total relaxation rate is somewhat curious in that it is approximately linear up to 330°K and then flattens out rather rapidly, a feature not observed for any other molecules in this work. Secondly the NOE factor (η) at 22.37 MHz remains approximately constant at about -0.3 over the whole temperature range of study. This feature suggests some other contributing mechanism with the same temperature dependence as the dipolar mechanism.

From Table 10 it can be seen that at both 300°K and 372°K the relaxation is more efficient at the higher field. Such a field dependence tends to implicate the chemical shift anisotropy mechanism. At 372°K the dipolar relaxation rate is almost identical at the two fields. This of course is as expected. The residual rate then is presumably due to the spin-rotation and some other field dependent mechanism. That spin-rotation is a contributing mechanism is apparent from the Arrhenius plot (see figure 4). The relaxation data at 300°K however does not yield the same dipolar rate at the two fields and from this aspect is inconsistent.

In fact the ratio of $R_{1(37.29)}^{other} / R_{1(22.37)}^{other}$ at 372°K is found to be 3.3 (see Table 10) whereas one would expect a ratio of 2.78 if

Table 10

Spin-Lattice Relaxation Data for $nBu_2Sn(OAc)_2$

Measurements at 22.37 MHz using spectrometer described in Chapter 3. Measurements at 37.29 MHz using Jeol FX100Q.

Temp/^oK	ν_o/MHz	R_1^{Tot}/s^{-1}	η	R_1^{DD}/s^{-1}	R_1^{other}/s^{-1}
372	22.37	0.279	-0.30	0.063	0.216
	37.29	0.776	-0.11	0.064	0.712
300	22.37	1.191	-0.29	0.286	0.905
	37.29	2.294	-0.21	0.359	1.935

this was due solely to the CSA mechanism. Obviously if R_1^{other} has a contribution from the spin-rotation mechanism this will be the same at both fields (at a given temperature) hence the ratio will increase still further.

A

Effect of Exchange on R_1

In Chapter 8 the temperature and concentration dependence of $nBu_2Sn(OAc)_2$ is discussed and a monomer-dimer equilibrium is postulated. This equilibrium is rapid and from equation 9 (see Chapter 1, section 2B) the exchange rate can be estimated to be $1 \times 10^5 s^{-1}$ (with $\delta_A - \delta_B$ = 1400 Hz and $W-W^* = 30$ Hz). Under such conditions of rapid exchange the observed relaxation time will be a weighted mean of the relaxation parameters at the two different sites. The recovery of the magnetisation is therefore exponential. Within the limits of the experiment this is observed. The effect of high and low frequencies on R_1 is discussed in Chapter 2, section 1A.

With the limited data available on this system to date the information leads to the suggestion that $nBu_2Sn(OAc)_2$ may in fact have a contribution from the CSA mechanism to the total relaxation rate. That the data is not entirely consistent may be due to the complications of the equilibrium. Further work is required and detailed temperature dependent relaxation studies at a number of fields are suggested.

Part V

The ^{119}Sn Relaxation Data for Sn_2Me_6

Discussion of the Spin-Lattice Relaxation for Sn_2Me_6

Table 3 shows the ^{119}Sn spin lattice relaxation data for neat hexamethyl-di-tin. Figure 3 shows a graphical plot of these data and includes the ^{119}Sn data for Me_4Sn extracted from reference 1. Table 11 and figure 8 show the ^{13}C relaxation data.

From figure 3 it can be seen that the relaxation of ^{119}Sn in Sn_2Me_6 is almost completely dominated by the spin-rotation mechanism. This observation is notably different to the tin relaxation behaviour of the tri-n alkyl tin chlorides and the tetraalkyl tins. These molecules have significant dipolar contributions to the tin from the methylene groups on the alkyl chains. The three methyl groups on each tin nucleus in Sn_2Me_6 might be expected to provide a significant dipolar contribution to the relaxation of tin. However this is not so due to the efficient averaging of the dipolar mechanism that occurs for such rapidly rotating methyl groups. Although no NOE data are available for these methyl groups figure 8 indicates a rather broad minimum in the Arrhenius plot indicating approximately equal contributions to the measured relaxation rate R_1 from the dipole-dipole and spin-rotation mechanisms. This is in agreement with the work of Lippma et al[1] on Me_4Sn (see figure 8). From the ^{13}C T_1 data then a correlation time (τ_c^{eff}) of 0.6 ps can be estimated for the C-H vector of the methyl groups of Sn_2Me_6. A value of τ_c^{eff} for the same vector in $SnMe_4$ can be extracted from reference 1 and is found to be 0.5 ps. Harris and Kimber[9] have observed the ^{29}Si and ^{13}C spin-lattice relaxation times and NOE factors in hexamethyl disilicon and reported a value of 1.0 ps for the correlation time for the C-H vector of the methyl groups.

Table 11

^{13}C spin-lattice relaxation data for Sn_2Me_6 at 22.63 MHz

Temp/K	R_1/s^{-1}
308	0.0730
318	0.0788
328	0.0822
333	0.0824

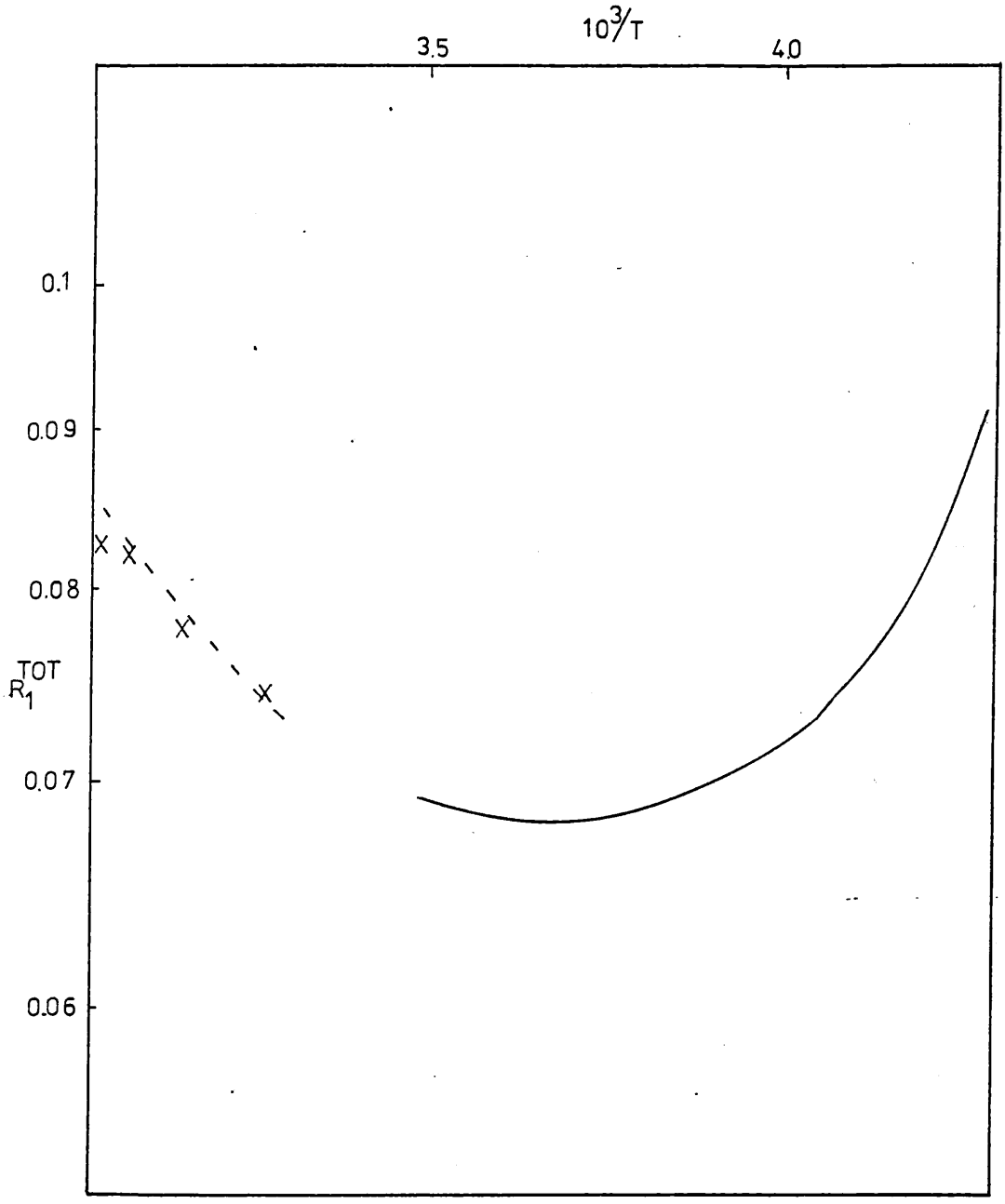

Figure 8

^{13}C T_1 data for neat Sn_2Me_6(——) at 22.63 MHz and neat $SnMe_4$(—). The latter are taken from reference 1.

As might be expected the methyl groups in all three molecules behave very similarly, having large contributions from the spin-internal rotation mechanism.

The maximum NOE factor measured for the ^{119}Sn nucleus in Sn_2Me_6 was -0.13 which corresponds to a 10% dipolar contribution to the measured total relaxation rate at 303 K. Data from reference 9 on the ^{29}Si relaxation time of Si_2Me_6 shows a T_1 of 45s and a NOE factor of -0.26 at 308 K. This also corresponds to a 10% dipolar contribution to R_1. Accurate NOE factors are notoriously difficult to measure and it is somewhat dangerous to calculate values of τ_c^{eff} when the measured NOE factors are effectively within the experimental error (generally assumed to be $\pm 5 - 10\%$). However it is informative to do so for these two closely related molecules since it does illustrate a general trend of ^{119}Sn relaxation times.

From the Arrhenius plot of the ^{119}Sn data (see figure 3) the dipolar relaxation rate at 308 K can be extrapolated to be $0.037s^{-1}$ giving a rate of $0.004s^{-1}$ per proton. The calculated τ_c^{eff} for the tin-remote proton vector is therefore 22 ps. This should be compared to 3 ps for the τ_c^{eff} of the hexamethyl disilicon molecule.

Molecules with the geometry of Sn_2Me_6 and Si_3Me_6 have the preferred axis of rotation through the metal-metal bond due to the inertial and frictional effects. Rotation perpendicular to this axis (end over end tumbling) is not preferred because two heavy nuclei (either ^{119}Sn or ^{29}Si) have to be moved off axis for such a rotation to occur. This inertial effect is more significant for the tin molecule on account of the large mass of tin. If τ_c^{eff} is dominated by rotation about the preferred axis the longer Sn-C bond compared to

Si–C (2.18×10^{-8} cm and 1.93×10^{-8} cm respectively) would cause a lengthening of τ_c^{eff} by increasing the volume required for the tin molecule to rotate. Consequently more "solvent" molecules would need to be swept out of the way making rotation about the preferred axis slower. Also the larger Sn–C bond length causes an increase in the moment of inertia about the main symmetry axis. The magnitudes of these effects do not however account for the large difference observed in τ_c^{eff}. This could be due to the errors in the small values of η measured.

Part VI

The Spin-Rotation Contribution to ^{119}Sn T_1 Values

Discussion

Spin-Rotation Relaxation

In general when dealing with small molecules and/or nuclei of large chemical shift range it is anticipated that the spin-rotation relaxation mechanism will be important. From the spin-lattice relaxation times and NOE data presented in this thesis for ^{119}Sn it is evident that spin-rotation is indeed important in relaxing the tin nucleus. Together with the dipole-dipole mechanism these are the two most important mechanisms when considering ^{119}Sn T_1 values. The apparent relation between the spin-rotation rate (R_1^{SR}) and the chemical shift arises because the chemical shift and the spin-rotation tensor components of a given molecule both depend on the electron distribution in a molecule. A distribution which leads to large chemical shifts also leads to large spin-rotation interactions.

In Table 12 it can be seen that as δ becomes more negative (ie σp increases) R_1^{SR} decreases. This is because the trace of the paramagnetic term of the shielding tensor becomes smaller with the upfield shift and consequently the spin-rotation constant (C_o) becomes smaller.[11] Also the angular momentum correlation time τ_ω decreases as the moment of inertia increases causing the spin-rotation interaction to become less effective thereby decreasing the spin-rotation relaxation rate.

Ramsey[12] and Flygare[13] have derived expressions relating the nuclear shielding constant σ_{av} to the spin rotation constant. Deverell[11]

$$\sigma_{av} = \frac{e^2}{3mc^2}\left\{\left\langle 0 \left| \sum_k r_k^{-1} \right| 0 \right\rangle - \sum_j \frac{z_j}{R_{ij}}\right\} + \left\{\frac{2\pi}{\hbar\gamma_I}\frac{M_p}{M_e} I C_o\right\} = \sigma'_d + \sigma'_p \qquad \ldots \quad 2$$

Table 12

^{119}Sn values of σ_p , $\bar{I}$ and R_1^{SR}

Compound		δ/ppm	σ'_p /ppm	$\bar{I}$/g cm^2 (10^{40})	$\sigma'^2_p/\bar{I}^{\frac{1}{2}}$	R_1^{SR}/s^{-1}
SnI_4	1	-1699	-1501	4270[b]	3.4	0.10
$SnBr_4$	2	-775	-2425	2140[b]	12.7	0.14
$SnCl_4$	3	-148	-3052	854[b]	31.9	0.63
Cl_3SnMe	4	15	-3215	720[b]	38.5	0.50
Me_2SnCl_2	5	130	-3330	602[b]	45.2	1.00
Me_3SnCl	6	150	-3350	503[b]	50.0	1.51
$SnMe_4$	7	0	-3200[a]	344[b]	55.2	1.67
$SnEt_4$	8	-1.4	-3199	978	32.7	0.56[c]
$SnPr_4$	9	-17	-3183	2274	21.2	0.15[c]
$Sn(nBu)_4$[d]	10	-12	-3188	4267	15.6	0.06
nPr_3SnCl[d]	11	140	-3340	1914	25.5	0.17
nBu_3SnCl[d]	12	143	-3343	3355	19.3	0.09
nBu_3SnH[d]	13	-95	-3105	3027	17.5	0.15
Ph_3SnH[d]	14	-148	-3052	3492	15.8	0.03

(a) σ_p obtained from reference 2. All other σ'_p values obtained from differences between experimental σ'_p ($SnMe_4$) and chemical shift differences relative to $^{119}SnMe_4$.

(b) Reference 16.

(c) Reference 1.

(d) $\bar{I}$, σ'_p and R_1^{SR} from this work.

$\bar{I}$ calculated using program in appendix B.

has argued that the first term $\sigma d'$ associated with a given nucleus i is constant from molecule to molecule and that the paramagnetic shielding σ_p' given by the second bracketed term is responsible for the observed differences in measured shifts. Thus $\sigma' p$ is directly related to the spin-rotation constant C_o and the molecular moment of inertia I.

For the central nucleus in a spherical top molecule the spin-rotation relaxation rate R_1^{SR} is given by[14,15]

$$R_1^{SR} = \frac{2IkT}{\hbar^2} (2\pi C_o^2) \tau_\omega \quad \ldots \quad 3$$

where the symbols all take their usual meanings.

Using the reduced correlation times $\tau_\omega^*, \tau_{\Theta,2}^*$ defined as

$$\tau_\omega^* = \left(\frac{kT}{I}\right)^{\frac{1}{2}} \tau_\omega \quad \ldots \quad 4$$

and

$$\tau_{\Theta,2}^* = \left(\frac{kT}{I}\right)^{\frac{1}{2}} \tau_\omega$$

then in the rotational diffusion limit

$$\tau_{\Theta}^*,2 \ \tau_\omega^* = 1/6$$

which is merely a restatement of the Hubbard relation.[14]

Combining equation 3 with the $\sigma' p$ term of equation 2 and τ_ω of equation 4 yields

$$R_1^{SR} = 2\gamma_I^2 \left(\frac{M_e}{M_p}\right)^2 (kT)^{\frac{1}{2}} \tau_\omega^* \frac{(\sigma_p')^2}{I^{\frac{1}{2}}} \propto \tau_\omega^* \frac{(\sigma_p')^2}{I^{\frac{1}{2}}} \quad \ldots \quad 5$$

In general τ_ω^* can only be obtained if C_o is known. From work by Sharp[4] and Lassigne and Wells[2,3] τ_ω^* can be taken as roughly constant. For instance Sharp[4] has shown that for neat $SnCl_4$ at 198°K $\tau_\omega^* = 0.048$ and for SnI_4 at 423°K $\tau_\omega^* = 0.134$. Lassigne and Wells[2,3] have found that for neat $SnMe_4$ at 300°K $\tau_\omega^* = 0.054$.

To test the validity of equation 5 requires an sbolute chemical shift scale. Lassigné and Wells[3] have evaluated C_o for $SnMe_4$ by temperature dependent relaxation studies on tetramethyl tin and its isotopic modifications $[(CH_3)_{4-n}Sn(CD_3)_n]$ yielding a value of $+17.7 \pm 2$ kHz for the spin rotation constant of ^{119}Sn. Use of this value for C_o in equation 2 yields a σ'_p for the tin-119 nucleus in $SnMe_4$ as -3200 ppm. This value agrees with the absolute chemical shift scale defined by the work of Sharp on the tin tetrahalides.[4]* Knowledge of σ'_p for $SnMe_4$ enables the calculation of σ'_p for all compounds with a known shift.

The measured ^{119}Sn chemical shifts, spin-rotation relaxation rates and moments of inertia for some organo tin molecules are shown in Table 12. Figure 9 shows a plot of $\sigma'^2_p/\bar{I}^{\frac{1}{2}}$ vs R_1^{SR}.

It can be seen from figure 9 that the dependence of R_1^{SR} on $\sigma'^2_p/\bar{I}^{\frac{1}{2}}$ is by no means exact. This is due to the somewhat gross approximations made (isotropic motion, rotational diffusion limit constant τ_ω). However the plot does correlate the spin-rotation relaxation behaviour with the chemical shifts to a first approximation. It also validates Deverell's relation between the spin-rotation constant and the paramagnetic shielding term for ^{119}Sn in a variety of compounds.

It should be noted that Table 12 and figure 9 include data from reference 1 on the tetraalkyl tin molecules. The line drawn by Lassigne and Wells[16] is also included. We have calculated the moments of inertia (see appendix B) of molecules studied in this work and also for the tetraalkyl tins of reference 1. Inclusion of this data in

* It should be noted that Sharp omitted the negative sign of the magnetogyric ratio of tin and consequently his values of σ'_p should be multiplied by -1.

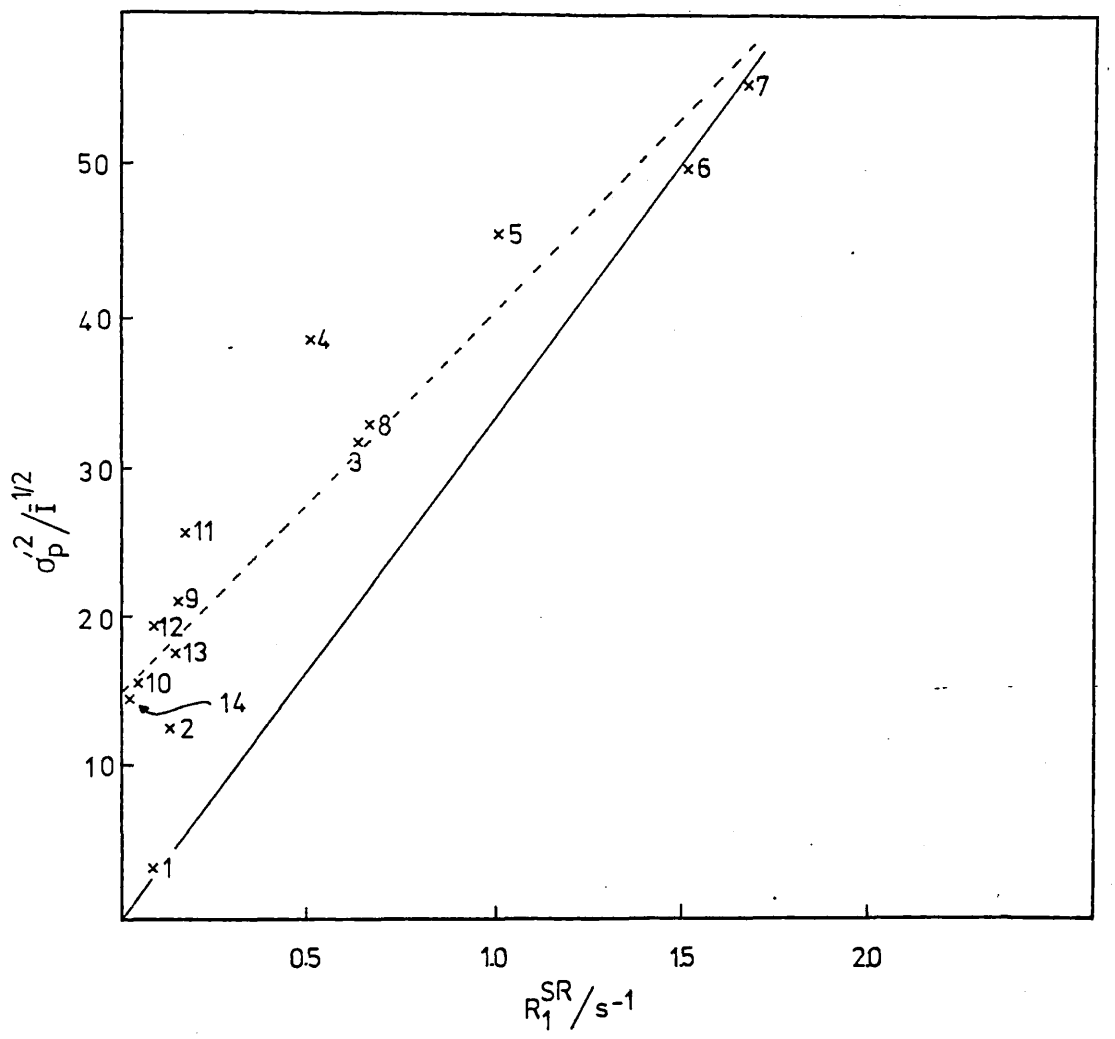

Figure 9

See Table 12 for molecules

figure 9 indicates a different line through the points which does not pass through the origin. This suggests a different shift zero although considering the assumptions made in the plot no further, more detailed comment is warranted.

Part VII

The Activation Energy

Section 1

Introduction

Whenever a rate constant (R) is measured over a range of temperature an energy of activation $\Delta H^{\neq}$ can be extracted from the gradient of a plot of lnR against the inverse temperature. This is the so-called Arrhenius plot.

Since the spin-lattice relaxation time, T_1 is merely the inverse of the relaxation rate R_1 (itself a first order rate constant) a plot of $\ln R_1$ vs $1/T$ yields the energy of activation for the process in question. It has been shown in Chapter 1 that for spin-lattice relaxation R_1 is directly proportional to an appropriate correlation time τ. An Arrhenius plot therefore yields an energy of activation for the reorientational correlation time τ_c or the angular momentum correlation time τ_j depending on the temperature dependence of the relaxation mechanism from which the correlation time has been derived.

A

Effect of Anisotropic Motion on $\Delta H^{\neq}$

It is a fact that molecular motion is rarely isotropic except in spherical top molecules. For molecules whose motion is anisotropic τ_c and τ_j can, in principle be separated into correlation times along the principle molecular axes. This requires a knowledge of the anisotropy of the molecular motion (see for instance Chapter 6). Assuming that $D_{||}$ and $D_{\perp}$ (the rotational diffusion constants parallel and perpendicular to the main symmetry axis respectively) can be determined from two sets of relaxation data, the individual temperature dependence of $D_{||}$ and $D_{\perp}$ can be determined.

A number of workers[17-21] have studied symmetric top molecules and determined $D_{||}$ and $D_{\perp}$ along with the associated activation energies. The general observation, as expected is that the faster diffusion rate (always $D_{||}$ in the molecules studied) has the lower activation energy.

Jonas[22] has studied the pressure dependence of $D_{||}$ and $D_{\perp}$ in liquid acetonitrile. A new activation parameter arises from such studies, namely the activation volume, $\Delta V^{\neq}$ which is interpreted in terms of the additional volume required for the molecules to rotate. Jonas found that for $D_{\perp}$, $\Delta V^{\neq}$ was 8.5 $cm^3 mol^{-1}$ and for $D_{||}$, $\Delta V^{\neq}$ was less than 3 $cm^3 mol^{-1}$. As expected then the extra volume required for rotation about the main symmetry axis is much less than for the perpendicular axis. This indicates that the same qualitative arguments can be used to interpret $\Delta V^{\neq}$ as are used for $\Delta H^{\neq}$.

If the motional anisotropy is unknown then $D_{||}$ and $D_{\perp}$ cannot be determined and obviously the measured activation energy relates to the effective correlation time τ_c^{eff}. The consequence of this is that the observed activation energy is some function of the activation energy of the different diffusion constants.

B

Results and Discussion

Table 12 shows the activation energy derived from the ^{119}Sn T_1 and NOE data for a number of molecules studied in this work. Note that for the two pairs of related molecules (nPr_3SnCl, nBu_3SnCl and Et_4Sn, nPr_4Sn) the smaller molecule always has the lower activation energy for τ_c or τ_j. This is as expected. For the two molecules nPr_3SnCl and nPr_4Sn it can be seen that the values of $\Delta H^{\neq}$ are

Table 12

Activation energies calculated from the Arrhenius plots of the ^{119}Sn T_1 data.

Molecule	$\Delta H_{\tau_c}^{\neq}$/kJmol^{-1}	$\Delta H_{\tau_j}^{\neq}$/kJ mol^{-1}
nPr_3SnCl	19 ± 2	-11 ± 1
nBu_3SnCl	22 ± 2	-14 ± 1
*Et_4Sn	10 ± 2	-11 ± 2
*nPr_4Sn	16 ± 2	-13 ± 2
Sn_2Me_6		-14 ± 1

* Data taken from reference 1.

remarkably similar. This reflects the almost identical values of τ_c^{eff} observed for these two molecules (see Table 8) and is presumably a consequence of the similarity of the moments of inertia and the frictional effect of the two molecules.

Part VIII

Microviscosity Theory

Calculation of Correlation Time for n-Bu_3SnCl

For small step diffusion we may use the hydrodynamic model first postulated by Debye[23] to calculate the correlation times τ_c associated with the symmetry axis of a symmetric top molecule using the formula

$$\tau_c = f \frac{4\pi\eta a^3}{3\,kT} \quad \ldots \quad 1$$

where η is the viscosity of the liquid, a is the radius of the molecular sphere. The microviscosity factor f was put forward by Gierer and Wirtz[24] when dealing with mixtures. It is defined as

$$f = \frac{6a_L}{a} + \frac{1}{[1 + (a_L/a)]^3}^{-1} \quad \ldots \quad 2$$

where a_L is the radius of a molecule in the surrounding medium. For a pure liquid $a = a_L$ and equation 2 reduces to

$$f = \frac{1}{6.125}$$

Obviously the calculated value of τ_c is most sensitive to the molecular radius a. For symmetric top molecules such as the ones studied in this work it is not immediately obvious to which axis a relates. We have therefore followed the method of Jonas et al[25] who calculated molecular volumes (i.e. $\frac{4}{3}\ a^3$) assuming hexagonal close packed spheres using equation 3

$$\frac{4}{3}\ a^3 = \frac{MW \times 0.74}{\rho \times N} \quad \ldots \quad 3$$

where MW = molecular weight, ρ = density (g cm^{-3}) N = Avagadro number and 0.74 is the efficiency of the packing arrangement. The molecular volume is in units of cm^3.

Use of equation 3 for nBu_3SnCl with MW = 319.5, ρ = 1.19 yields a value of 3.3×10^{-22} cm^3 for the molecular volume. Substituting this value into equation 1 with η = 7 cp (at 293 K) yields τ_c = 93 ps. From figure 2 a value of $R_1^{DD} = 0.13 s^{-1}$ can be extracted (at 293 K) which yields a value for τ_c^{eff} of 86 ps. Such good agreement is probably fortuitous bearing in mind that the vector to which the ^{119}Sn T_1 data relates is not the same as the one described by equation 1. However this could be taken as evidence for overall isotropic tumbling in this molecule.

It is interesting that using Jonas' method[25] to calculate the volume of the molecular sphere results in a value of τ_c intermediate between those taking the shortest and longest dimension of the molecule.

Part IX

Experimental and References

Experimental

All compounds were commercial samples obtained from Alpha Inorganics except for nBu_3SnH which was prepared according to the method outlined below. Purity was checked by IR and NMR (^1H, ^{13}C, and ^{119}Sn). Where available spectra were compared to those of authentic samples in the literature. All samples were degassed either by the freeze-pump-thaw method (5-10 cycles) or by bubbling oxygen free nitrogen for 10-15 minutes.

All relaxation measurements were carried out on neat samples unless otherwise indicated using the $(180 - \tau - 90 - 5T_1)_n$ pulse sequence. The delay between the pulse sequence was always adjusted to be at least five times the longest T_1 in any given sample. All NOE measurements had a delay of at least ten times the longest T_1. All T_1 measurements were under conditions of proton decoupling, the frequency of which was determined by experiment. Values of T_1 have an associated error of $\pm$ 5%.

The field frequency lock of the spectrometer was maintained by locking to a suitable resonance (either ^{19}F or ^2H) of a compound in a 5 mm tube, the sample being in the annular portion of the larger tube.

Preparation of nBu_3SnH

This compound was prepared in approximately 90% yield according to the method of Hayashi et al.[25]

Neat bis (tri-n-butyl) tin oxide (TBTO) (1 mole) was added dropwise via a dropping funnel to polymethylhydrosiloxane (PMHS, 2 moles) in a three necked round bottomed flask under an atmosphere of dry nitrogen. Evolution of heat occurred which subsided after 30 minutes. After this had subsided the dropping funnel was removed and a Claisen still head attached. A condenser and

collecting vessels were also attached. Vacuum distillation (6 mm Hg) afforded the pure nBu$_3$SnH.

References

1 Y.C. Puskar, T.A. Saluvere, E.T. Lippmaa, A.B. Pernin, V.S. Petrosyan, Doklady Akad. Nauk SSSR (1975) 220 112.

2 C.R.G. Lassigne, Ph.D Thesis Simon Fraser University 1975.

3 C.R.G. Lassigne, E.J. Wells, J. Magn. Resonance (1977) 26 55.

4 R.R. Sharp, J. Chem. Phys. (1972) 57 5321.

5 M.J. Ahmed, Ph.D Thesis London 1977.

6 T.N. Mitchell, J.C.S. Perkin II (1977) 1842.

7 R.K. Harris, B.J. Kimber, Advan. Mol. Relaxation Processes (1976) 8 23.

8 D. Wallach, J. Chem. Phys. (1967) 47 5258.

9 R.K. Harris, B.J. Kimber, J. Magn. Resonance (1975) 17 174.

10 R.K. Harris, B.J. Kimber, Advan. Mol. Relaxation Processes (1976) 8 15.

11 C.Deverell, Mol. Phys. (1970) 18 319.

12 N.F. Ramsey, Phys. Rev. (1950) 78 699.

13 W.H. Flygare, J. Chem. Phys. (1964) 41 793.

14 P.S. Hubbard, Phys. Rev. (1963) 131 1155.

15 R.E.D. McClung, J. Chem. Phys. (1969) 51 3842.

16 C.R.G. Lassigne, E.J. Wells, Can. J. Chem. (1977) 55 927.

17 T.T. Bopp, J. Chem. Phy. (1967) 47 3621.

18 D.E. Woessner, B.S. Snowden, E.T. Strom, Mol. Phys. (1968) 14 265.

19 J. Jonas, T.M. Digennaro, J. Chem. Phys. (1969) 50 2392.

20 W.T. Huntress, J. Phys. Chem. (1969) 73 103.

21 J.P. Kintzinger, J.M. Lehn, Mol. Phys. (1971) 22 273.

22 T.E. Bull, J. Jonas, J. Chem. Phys. (1970) 53 3315.

23 P. Debye, Polar Molecules (Dover, New York, 1945).

24 A. Gierer, K. Wirtz, Z. Naturforsch (1953) A8 532.

25 R.A. Assink, J. DeZwaan, J. Jonas, J. Chem. Phys. (1972) 56 4975.

26 K. Hayashi, J.Iyoda, I. Shiihara, J. Organometal. Chem. (1967) 10 81.

CHAPTER 5

^{13}C Spin-Lattice Relaxation in R_3SnX

(R = n-propyl, n-Butyl; X = H, Cl)

Section 1

Introduction to Segmental Motion

If a rigid model is assumed for a molecule whose overall tumbling is isotropic then obviously all derived correlation times are expected to be the same. In compounds with long alkyl chains differences in correlation times can be observed for different vectors in the molecule. Consequently a rigid molecule model cannot explain such behaviour and we are forced to invoke the concept of internal rotation about carbon-carbon bonds. This is sometimes termed segmental motion.

Such segmental motion was first postulated by Doddrell and Allerhand[1] who used the concept to explain the increasing ^{13}C relaxation times along the alkyl chain in n-decanol. The basis of the argument is that the hydrogen bonded hydroxyl group effectively anchors the $-CH_2OH$ end of the molecule while the hydrocarbon part of the molecule is relatively free. This results in the effective correlation time for rotation decreasing near the free end of the molecule leading to longer relaxation times for such carbons.

Chemical interactions such as hydrogen bonding are not a prerequisite for the observation of such segmental motion. The mass of a molecular fragment can be sufficient to anchor one part of the molecule thereby restricting motion near the fragment yet allowing the rest of the molecule to be relatively free.

Levy and coworkers[2] have used ^{13}C spin lattice relaxation times to monitor segmental motion along alkyl chains in n-alkyl amines and the corresponding n-alkyl ammonium salts. For the amines the T_1 values decrease as the size of the chain increases. Such behaviour is due to the slower overall reorientation which is expected as size and molecular weight

increases. For a given amine T_1 changes very little along the chain. This is due to the amino group being an inefficient anchor. Its mass after all is not very different to a terminal methyl group. For the amines with the larger aliphatic chains T_1 increases on moving away from the centre of the molecule. The reason for this observation is that the methylene groups near the centre of mass have restricted motion; this motion becomes progressively freer towards the ends of the chains. Lyerla[3] and Chachaty[4] have made similar observations on a number of substituted n-alkanes. The n-alkyl ammonium ions are found to have much shorter T_1 values compared to the parent amines, indicative of slower motion. This is due to the electrostatic solute ordering effects of the ammonium ion acting as a more efficient anchor than the amino group. The relaxation times of the carbons increase on moving along the alkyl chain away from the ionic part of the molecule. Levine et al[5] have observed similar behaviour in n-alkyl bromides although the effect there is due to the mass of the bromine nucleus.

For straight chain hydrocarbons large variations in ^{13}C spin-lattice relaxation times are not apparent.[6] It seems that internal motion only has a large effect on ^{13}C T_1 values when the overall reorientation of the molecule is restricted.[1] Levy et al[2] for instance have observed very short ^{13}C T_1 values in tri n-octyl amine [$T_1(C\alpha) = 0.24$ s] indicating slow overall molecular tumbling. The differences in T_1 of adjacent carbons in this molecule are large compared to n-octyl amine which has much longer relaxation times [$T_1(C\alpha) = 5.0$ s]. So the effect of slower overall reorientation is to decrease the observed relaxation time and to increase the effect of segmental motion.

Observation of ^{13}C spin-lattice relaxation times can also be used to monitor different solvation and aggregation effects of molecules in different solvents.[1, 7-11]

A

Spin-Lattice Relaxation of ^{13}C Nuclei

The relaxation of carbons with directly attached protons is normally dominated by the carbon-proton dipole-dipole mechanism (Chapter 2, section 2A). This is especially so for large molecules whose overall tumbling is expected to be slow. Equation 1 describes the dipolar

$$R_1^{DD} = \frac{1}{T_1^{DD}} = \frac{N\gamma_C^2\gamma_H^2\hbar^2}{r^6}\ \tau_c^{eff} \quad \ldots \quad 1$$

interaction where N is the number of directly attached protons, τ_c^{eff} is the effective correlation time for the C-H vector. The remaining symbols take their usual meanings.

If a rigid molecule is rotating isotropically then in the extreme narrowing limit τ_c^{eff} describes not only the reorientation of the particular C-H vector but also the overall molecular tumbling. In the presence of internal motions τ_c^{eff} is given by

$$\frac{1}{\tau_c^{eff}} = \frac{1}{\tau_R} + \frac{1}{\tau_G} \quad \ldots \quad 2$$

where τ_G is an effective correlation time for internal rotation and τ_R is the correlation time for overall reorientation. It is apparent from equation 2 that the shortest correlation time will always dominate τ_c^{eff} and the effect of τ_G increases as the overall motion becomes slower.

Section 2

Results and Discussion

In Tables 1 and 2 the ^{13}C T_1 data over a range of temperature, for the molecules nPr_3SnH and nBu_3SnH are presented. The data are summarised in figure 1. Figure 2 shows typical results for a

Table 1

^{13}C Spin-lattice relaxation data for nPr_3SnH (neat) at 22.63 MHz

	R_1/S^{-1}		
Temp/K	C_α	C_β	C_γ
273	0.215	0.199	0.237
283	0.190	0.180	0.166
293	0.136	0.149	0.114
307	0.107	0.097	0.097
318	0.097	0.098	0.088
333	0.079	0.076	0.081
353	0.060	0.068	0.061

Table 2

^{13}C Spin-lattice relaxation data for nBu_3SnH at 22.63 MHz

	R_1/S^{-1}			
Temp/K	C_α	C_β	C_γ	C_δ
233	1.969	1.949	1.648	1.337
243	1.518	1.359	1.271	0.864
253	1.189	1.125	0.838	0.718
263	0.973	0.646	0.599	0.492
273	0.527	0.441	0.380	0.295
293	0.300	0.259	0.219	0.238
307[a]	0.291	0.236	0.195	0.198
313	0.230	0.191	0.149	0.137
333	0.204	0.155	0.128	0.128
353	0.132	0.111	0.092	0.094
383	0.114	0.081	0.071	0.086

(a) Measured at 25.14 MHz

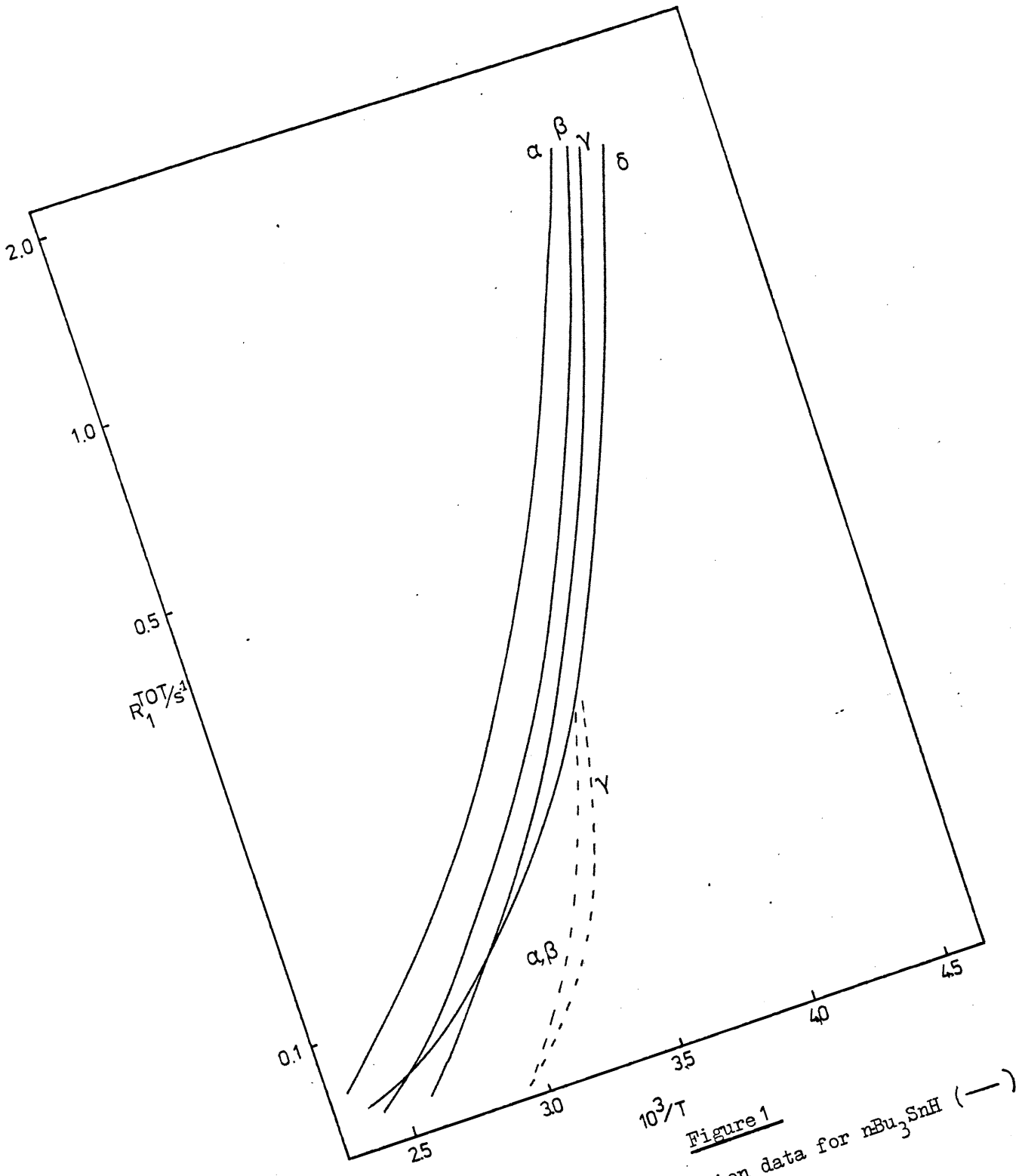

Figure 1

^{13}C Spin-lattice relaxation data for nBu_3SnH (—) and $n\text{-}Pr_3SnH$ (- - -) at 22.63 MHz

Figure 2

Results of $(180 - \tau - 90 - 5T_1)_n$ sequence for neat nBu_3SnCl at 25.14 MHz

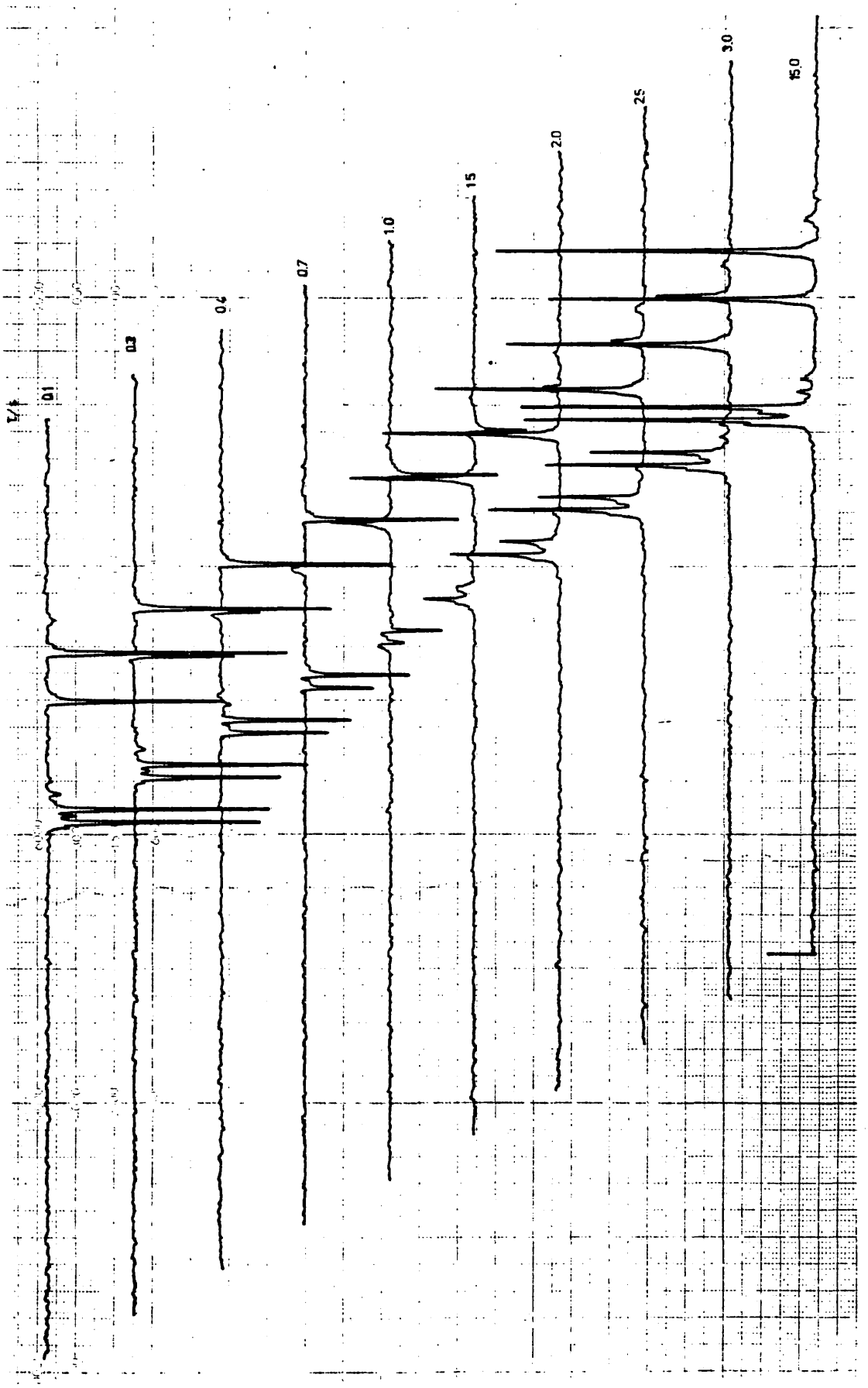
0.1
0.3
0.4
0.7
1.0
1.5
2.0
2.5
3.0
15.0

$(180 - \tau - 90 - 5T_1)_n$ sequence. Table 3 shows the relaxation data at 307° K for nPr_3SnH, nBu_3SnH, nPr_3SnCl and nBu_3SnCl

As expected for carbons with directly bound protons and in agreement with the work of Lippmaa et al[12] on tetraalkyl tins, the relaxation is dominated by the dipolar mechanism. The relaxation times for the methylene groups increase on moving away from the tin nucleus which is indicative of segmental motion. This is expected on account of the inertial effect of tin anchoring the methylene groups to different extents. Due to the inertial effect of the massive tin atom the overall tumbling of the organotin molecule is slow. This is indicated by the values of τ_c^{eff} derived from the ^{119}Sn relaxation data (see Chapter 4). The observed ^{13}C T_1 values for the trisubstituted organotin molecules reflect this fact and are themselves short. This data for nBu_3SnX (X = H,Cl) may be compared to that observed for the n-alkyl bromides.[5] For n-butyl bromide the ^{13}C T_1 values range from 11 to 16 seconds, which should be compared to the data presented in this work for nBu_3SnH of 3 to 5 seconds and for nBu_3SnCl of 1-3 seconds. For both tin containing molecules the T_1 values are much shorter. This is due to the tin restricting overall tumbling more than bromine and also because the organotin molecules are trisubstituted and therefore much bigger molecules. In fact the ^{13}C T_1 data for these molecules are similar to the longer chain n-alkyl bromide (number of carbons 7,8 or 9) since due to their size these molecules undergo much slower overall tumbling.

Both nPr_3SnCl and nBu_3SnCl show larger differences in T_1 values of adjacent methylene groups than do the analogous hydride molecules. This is due to the chlorine nucleus contributing significantly to the anchoring mass whereas the contribution of the hydride proton is insignificant.

Table 3

^{13}C T_1 and NOE data for the neat liquids shown at 25.14 MHz

No NOE data available for nPr_3SnH

Temp 307 K	C_α		C_β		C_γ		C_ω	
Molecule	R_1^{Tot}/s^{-1}	η	R_1^{Tot}/s^{-1}	η	R_1^{Tot}/s^{-1}	η	R_1^{Tot}/s^{-1}	η
nPr_3SnH[a]	0.107		0.097				0.097	
nBu_3SnH	0.291	1.62	0.236	1.99	0.195	1.66	0.198	1.61
nPr_3SnCl	0.361	1.89	0.276	2.00			0.256	1.87
nBu_3SnCl	0.885	1.90	0.547	2.0	0.433	2.0	0.294	1.88

(a) Measured at 22.63 MHz

The anchoring effect of the combined mass of tin and chlorine consequently restricts motion more effectively. This is in agreement with Levy's[2] observations on tri- and mono- n-octylamine that the effect of slower overall reorientation not only decreases T_1 but also makes the effects of differential motion along the chain more apparent.

From the work of Lippmaa et al[12] the segmental motion of the propyl chains in the appropriate tetraalkyl tins look very similar to the behaviour in the trisubstituted stannanes of this work. From equation 2 this indicates that the relaxation behaviour of the carbons is dominated by the fast internal motion of the chains rather than the overall tumbling of the molecule which is expected to be slow. In Chapter 4 the tin T_1 data of these molecules were presented and discussed. Although simplifying assumptions had to be made in order to interpret the data it was shown that the overall reorientation of the molecules as characterised by the tin T_1 data is indeed slow and consequently the internal motion is expected to dominate the carbon T_1 data.

A

The ω/α Ratio

The ratio of the spin-lattice relaxation time of the terminal methyl group and the T_1 of the α carbon can be taken as a measure of the degree of segmental motion in a chain. This is generally termed the ω/α ratio. For a rigid molecule undergoing overall isotropic reorientation this ratio is expected to be 2/3 since the methyl group contains three protons and the methylene group only two. The ratio 2/3 follows from equation 1. In the limit of very fast methyl rotation compared to the rotation of an α methylene group the ω/α ratio is given

by equation 3

$$\omega/\alpha = [\tfrac{1}{2}(3\cos^2\theta - 1)]^{-2} \quad \ldots \quad 3$$

where θ is the angle made by the C-H bond (in the methyl group) to the main symmetry axis.

For $\theta = 109.5^\circ$ $\omega/\alpha = 6$. Any motional restriction of the α methylene group will tend to increase this ratio still further. It has been stated above that as the overall reorientation becomes slower the segmental motion should become more apparent. Levy[2] has noted that all the T_1 values in the alkyl chain become shorter as the size and molecular weight of the molecule increase. A plot of molecular weight vs ω/α should give a positive gradient. Such a plot is shown in figure 3 for the molecules studied in this work and also includes data on nPr_4Sn extracted from reference 12. The behaviour is as anticipated and is due to a combination of factors.

i) increasing chain length makes overall reorientation more difficult since more "solvent" molecules have to be moved out of the way for a rotation to occur. This is generally termed the frictional effect

ii) increasing molecular weight also makes overall reorientation more difficult due to the inertial effect.

Since nPr_4Sn is a spherical top molecule its overall molecular tumbling is expected to be isotropic. For nPr_3SnX and nBu_3SnX (X=H,Cl) the overall tumbling is expected to be anisotropic and consequently should affect the carbon T_1 values along the chain in different ways. As the ω/α value for nPr_4Sn falls on the same curve as the trisubstituted compounds the segmental motion in the two types of molecules must be similar. This could be due to a number of factors.

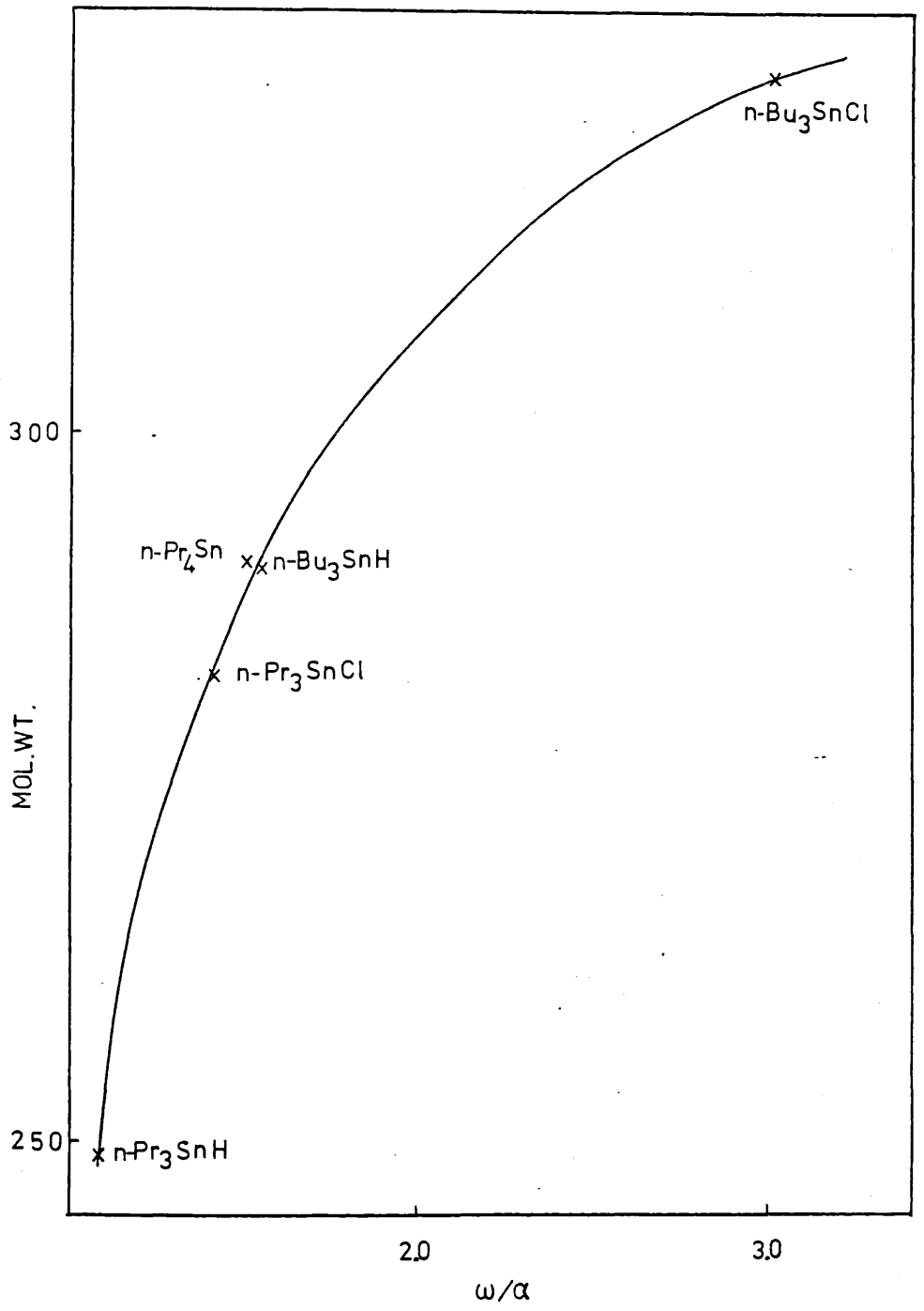

Figure 3

Ratio of T_1 for terminal methyl group to T_1 for αCH_2 as a function of molecular weight.

i) the overall tumbling is slow so that segmental motion dominates the ^{13}C T_1 values.

ii) the overall tumbling of the symmetric top molecules discussed here is close to isotropic.

The latter statement is substantiated by a plot of τ_c^{eff} vs ω/α (see Figure 4) where τ_c^{eff} has been calculated from the ^{119}Sn T_1 data. It is informative that the correlation does not fit the data for nBu_3SnH and may indicate that overall tumbling for this molecule is anisotropic. The tin hydride molecules are expected a priori to be the most anisotropic from the geometry and the relative mass of the substituents. The fact that the point for nBu_3SnH is significantly off the line appears to substantiate this.

B

Correlation Times

From Figures 1 and 2 and Table 3 the T_1 and NOE data at 307° K may be used to calculate the correlation times of the C-H vectors along the propyl and butyl chains. The correlation times derived from the ^{119}Sn data are also shown for comparison (Table 4).

As expected the correlation times for the C-H vectors decrease on moving away from the tin nucleus due to segmental motion. The α methylene groups exhibit the largest range of correlation times whilst the terminal methyl groups show the smallest as expected from the attenuation of the anchoring effect along the chain. Further the methyl groups undergo much freer rotation about the carbon-carbon bond since their rotation involves only one carbon-carbon bond rather than two.

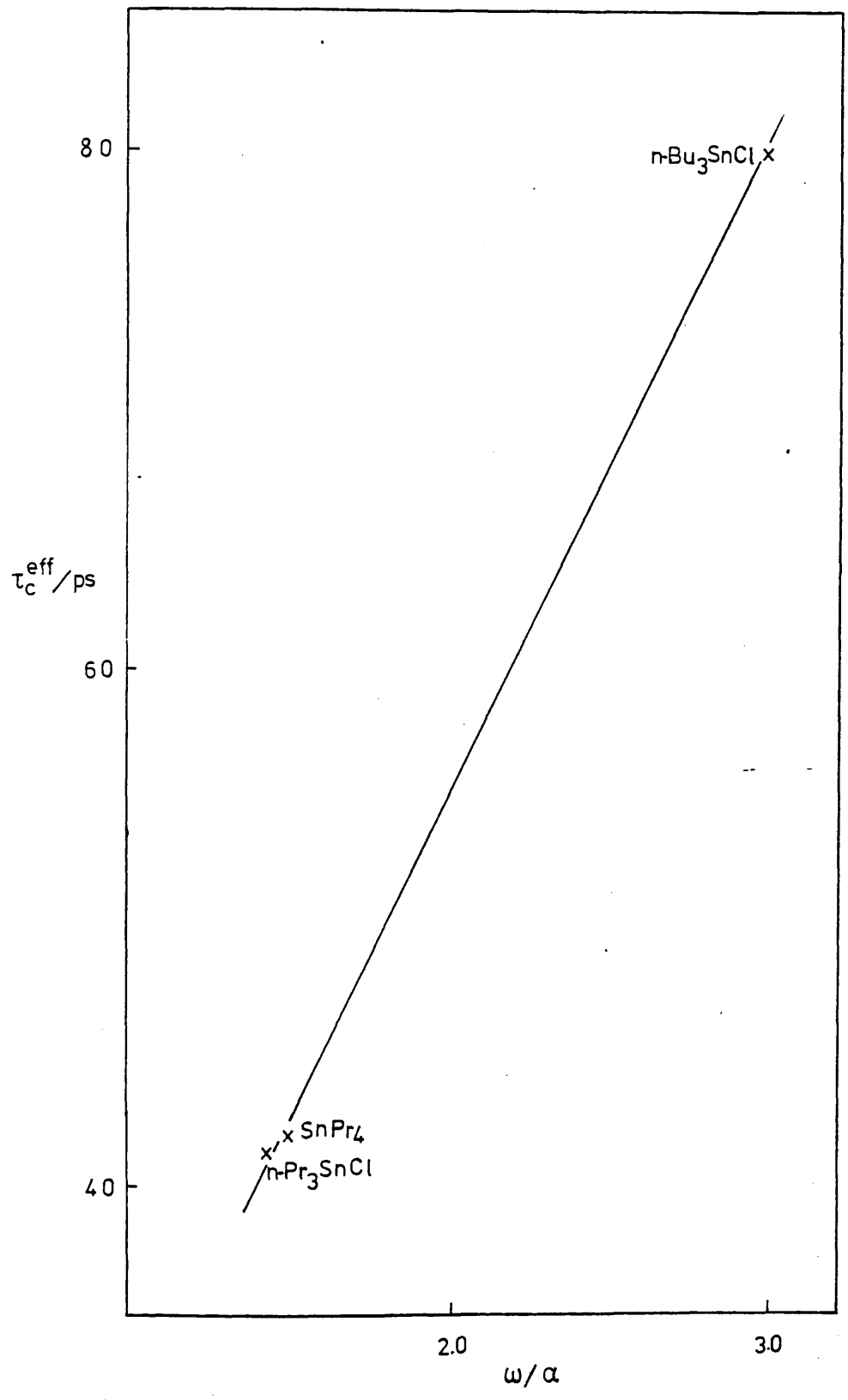

Figure 4

Table 4

Effective correlation times for C–H vectors in alkyl chains. Calculated from data in Table 3.

	$\tau_c^{*eff}(^{13}C)$/ps				$\tau_c^{*eff}(^{119}Sn)$ ps
Molecule	α	β	γ	δ	
nPr_3SnH	2.5	2.3	1.5		
nBu_3SnH	5.5	4.1	3.8	2.5	11–16
nPr_3SnCl	8.0	6.4	3.7		30
nBu_3SnCl	19.7	12.8	10.1	4.3	58

* Estimated average error in τ_c^{eff} approximately 5%.

C

The Activation Energy

Table 5 shows the mean activation energy ($\Delta H^{\ddagger}$) for the methylene groups in the molecules nPr_3SnH, nBu_3SnH, Et_4Sn and nPr_4Sn. A mean value of $\Delta H^{\ddagger}$ is quoted since, although it is expected that $\Delta H^{\ddagger}$ should decrease as the motion about the carbon-carbon bonds becomes freer, this is hidden by the experimental error. As was shown by the activation energies derived from the ^{119}Sn data in Chapter 4. Part VI the smaller molecule always has the lower activation energy and this is shown by the data here also. From the point of view of the activation energy, note how similar the values are for the trialkyl stannanes when compared to the tetraalkyl tins with one less carbon in the alkyl chain.

Section 3

The Quantitative Treatment of Segmental Motion

The difficulty of interpreting ^{13}C T_1 values in alkyl chains in a quantitative manner have already been pointed out. Levine et al[5] have developed a theory to interpret their ^{13}C T_1 values for n-alkanes and n-alkylbromides for which segmental motion is observed. The theory is based on three assumptions:-

i) that the chains are in the all trans configuration

ii) that the ratio of the diffusion coefficients about the molecular axes $[D_z/D_x(=D_y)]$ is given by the ratio of the moments of inertia $[(I_x=)I_y/I_z]$.

iii) that the molecules behave as an axially symmetric prolate ellipsoid.

Table 5

Activation energy for τ_c^{eff} calculated for the molecules indicated

Molecule	$\Delta H^{\neq}$ $\tau_c$eff/kJ mol^{-1}
nPr_3SnH	12.8 ± 1.0
nBu_3SnH	18.4 ± 1.0
Et_4Sn	12 ± 2
nPr_4Sn	19 ± 2

The main objection to this theory is the first assumption which for alkyl chains exhibiting segmental motion is not necessarily true. Since the second assumption is dependent on the fixed zig-zag conformation of the chains the general applicability of the treatment described by these authors must be in some doubt.

A

Libration Theory

Woessner has obtained expressions for the dipolar relaxation times of nuclei in spherical[13] and aspherical[14] rotors including the case where the internuclear vector of interest undergoes internal rotation about an axis fixed at an angle θ to the vector. Doddrell and coworkers[15] extended this theory to include the NOE. The basis of the theory assumes that the molecule undergoes overall isotropic tumbling described by a correlation time τ_R. The C–H vector of a protonated carbon can rotate at a value of θ to an axis fixed relative to the molecule. A C–H vector of length r can take up any direction within the cone defined by θ and its rotation is characterised by a correlation time τ_G. Woessner[13,14] has calculated the spectral densities $Jm(\omega)$ arising from such motion

$$Jm(\omega) = \frac{2}{r^6} f(\tau_R, \tau_G, \omega)$$

where w is the relevant angular frequency and m = 0,1,2

$$f(\tau_R, \tau_G, \omega) = A\frac{\tau_R}{1+\omega^2\tau_R^2} + B\frac{\tau_B}{1+\omega^2\tau_B^2} + C\frac{\tau_C}{1+\omega^2\tau_C^2}$$

where $$\frac{1}{\tau_B} = \frac{1}{\tau_R} + \frac{1}{\tau_G}$$

and $$\frac{1}{\tau_C} = \frac{1}{\tau_R} + \frac{2}{3\tau_G}$$

$$A = 1/4(3\cos^2\theta - 1)^2 \quad B = 3\sin^2\theta\cos^2\theta \quad C = 3/4\sin^4\theta$$

Using the notation of reference 15 we may write down the following expressions for R_1 R_2 and the NOE.

$$\frac{1}{T_1} = R_1 = K^2 \Omega \ /20$$

$$\frac{1}{T_2} = R_2 = K^2[\Omega + 4\ J_0(0) + 6\ J_1(\omega_H)]/40$$

$$NOE = 1 + \eta = 1 + [6J_2(\omega_H + \omega_C) - J_0(\omega_H - \omega_C)]\ \gamma_H/\gamma_C\ \Omega$$

where $K = \gamma_H\ \gamma_C \hbar$

$$\Omega = J_0(\omega_H - \omega_C) + 3\ J_1(\omega_C) + 6J_2(\omega_H + \omega_C)$$

These equations have been interpreted in terms of rotation about a carbon–carbon bond so that $\theta = 109.5^\circ$ for aliphatic C–H and 60° for an ortho or meta aromatic C–H vector.[15,18,19] Recently Howarth[20] has reinterpreted these equations arguing that θ is equally applicable to any random internal motion of a C–H vector confined to the cone defined by θ as could be caused by internal libration. Using this model then θ is interpreted as a mean librational angle and τ_G as a single correlation time which describe the random jumps of the C–H vector. Determination of the values of θ and τ_G requires the observation of field dependent dipolar relaxation times. Such field dependence is only observed for large molecules when the extreme narrowing condition is no longer valid. Since Howarth is dealing with large proteins the field dependence is expected enabling θ and τ_G to be fixed. Although no field dependence is observed for T_1^{DD} in this work due to the (relatively) small molecules studied, Howarth's theory is important in the interpretation of segmental motion to be included in the discussion here.

Using Howarth's theory then, segmental motion along alkyl side chains is interpreted in terms of the variation of the librational angle Θ. That is, the increase in ^{13}C T_1 values observed for methylene groups on moving away from the anchoring group is due to an increase in the angle Θ and not to an increase in the internal rotational correlation time τ_G. In fact Howarth's theory fits the field dependence of ^{13}C T_1's so far observed for proteins[16-18] using values of $\tau_G = 1 \times 10^{-11}$s and $\Theta = 20^\circ$ (0.35 rads) for the α carbon librations.

The dependence of T_1 on Θ can be represented by the formula

$$\frac{1}{T_\Theta} = (0.78 - \Theta)/0.43 \times T_{0.35} \quad \ldots \qquad 4$$

where Θ is in radians.

The formula is accurate to within 3% for $\Theta = 0.35$ to 0.7 rads.

If τ_G is assumed to be 1×10^{-11}s and $\Theta = 20^\circ$ for the α C-H libration for the molecules reported in this work then use of equation 4 and the data in Table 3 enables Θ to be calculated for the remaining C-H vectors. Table 6 summarises this data.

The values of Θ calculated for the molecules studied in this work exhibit similar behaviour in the increase of Θ on moving along the alkyl chain away from the heavy end of the molecule as reported by Howarth. This author reports an average increase in Θ of approximately 6° on moving away from the anchoring group.

Table 6

The librational angle Θ (in degrees) calculated using equation 4

	Θ		
Molecule	C_α	C_β	C_γ
nPr_3SnH	20	22	
nBu_3SnH	20	26	28
nPr_3SnCl	20	25	
nBu_3SnCl	20	29	32

Section 4

Experimental

The samples of nPr_3SnCl and nBu_3SnCl were commercial samples purchased from Cambrian Chemicals Ltd. Purity was checked by IR, ^1H, ^{13}C and ^{119}Sn NMR. The sample of nBu_3SnH was prepared according to the method outlined in the experimental section of Chapter 4. M.J. Ahmed kindly provided the sample of nPr_3SnH.

T_1 measurements were obtained using neat degassed samples on the Bruker HX90 Spectrometer (PCMU Harwell) at 22.63 MHz and at Jeol Ltd. Colindale on the Jeol FX100Q at 25.14 MHz. Both utilised the normal $180^\circ-\tau-90$ pulse sequence with proton noise decoupling. NOE measurements used the Jeol FX100Q.

References

1 D. Doddrell, A. Allerhand, J. Amer. Chem. Socs. (1971) 93 1558.

2 G.C. Levy, R.A. Komoroski, J.A. Halstead, J. Amer. Chem. Soc. (1974) 96 5456.

3 J.R. Lyerla Jr., H.M. McIntyre, D.A. Torchia, Macromolecules (1974) 11 7.

4 C. Chachaty, Z. Wolkowski, F. Piriou, G. Lukacs, J. Chem. Soc. Chem. Sommun. (1973) 951.

5 Y.K. Levine, N.J.M. Birdsall, A.G. Lee, J.C. Metcalf, P. Partington, G.C. Roberts, J. Chem. Phys. (1974) 60 2890.

6 R. Freeman, H.D.W. Hill, J. Chem. Phys. (1970) 53 4103.

7 G.C. Levy, J. Chem. Soc. Chem. Commun. (1972) 768.

8 G.C. Levy, Accounts Chem. Res. (1973) 6 161.

9 G.C. Levy, J.D. Gargioli, F.A.L. Anet, J. Amer. Chem. Soc. (1973) 95 1527.

10 G.C. Levy, J. Magn. Resonance, (1972) 8 122.

11 A. Allerhand, D. Doddrell, R. Komoroski, J. Chem. Phys. (1971) 55 189.

12 Yu. Kh. Puskar, T.A. Saluvere, E.T. Lippmaa, A.B. Permin, V.S. Petrosyan, Doklady Akademii Nauk SSR (1975) 220 112.

13 D.E. Woessner, J. Chem. Phys. (1962) 36 1.

14 D.E. Woessner, J. Chem. Phys. (1962) 37 647.

15 D. Doddrell, V. Glushko, A. Allerhand, J. Chem. Phys. (1972) 56 3683.

16 D.J. Wilbur, R.S. Norton, A.D. Clouse, R. Addleman, A. Allerhand, J. Amer. Chem. Soc. (1976) 98 8250.

17 M. Llinas, W. Meier, K. Wuthrich, Biochim. Biophys. Acta (1977) 492 1.

18 R.B. Visscher, F.R.N. Gurd, J. Biol. Chem. (1972) 247 3176.

19 D.J. Nelson, S.J. Oppella, O. Jardetzky, Biochem. (1976) 15 5552.

20 O. Howarth, J.C.S. Faraday II (1978) 74 1031.

CHAPTER 6

The Motional Anisotropy of Ph_3SnH

Section 1

Introduction

As has been shown in Chapters 4 and 5 the ^{119}Sn and ^{13}C T_1 and NOE data for the alkyl tin compounds are not easy to interpret due to segmental motion unless gross simplifying assumptions are made. Systems such as triphenyl stannane (Ph_3SnH) have a number of well-defined vectors making different angles to the main symmetry axis which can yield valuable information about the details of the motional behaviour of the molecule. The ^{119}Sn and ^{13}C T_1 and NOE data is therefore presented separately in this chapter.

A

Anisotropic Motion

Although the effect of molecular motion on relaxation times was discussed in chapter II only the case of isotropic reorientation was considered. The effects of anisotropy were not discussed. In fact the overall tumbling of small molecules is quite often anisotropic[1,2] and this makes dipolar relaxation rates difficult to interpret. If a preferred axis of rotation can be qualitatively predicted in the molecule from symmetry arguments T_1 data can yield quantitative information about internal motions as well as the overall tumbling of the molecule.

Levy et al[3] have observed that the T_1 for the para carbon in a number of monosubstituted benzenes is always shorter than T_1 for the meta or ortho carbons of the same phenyl ring. This is because in monosubstituted benzenes rotation about the C_2 molecular axis coincident with the C-X bond is preferred.

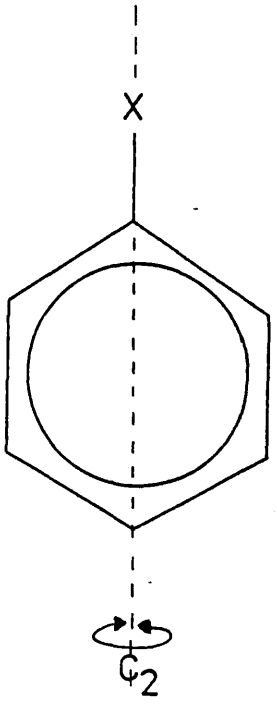

Two effects result from this:-

i) the moment of inertia about the C_2 axis is lower.

ii) fewer solvent molecules are disturbed by rotation about the C_2 axis. The first effect is termed the inertial effect and the second the frictional effect.

The degree of the anisotropy is principally determined by the size, polarity, bonding ability and symmetry of the X substituent.

The anisotropic motion affects the T_1 values for ring carbons aligned and not aligned with the preferred rotational axis (axes) in different ways. Rotation about the C_2 axis does not modulate the dipole-dipole interaction of the para ^{13}C and its attached proton and

consequently does not affect the relaxation of the carbon. The C_2 rotation does modulate the dipole-dipole interaction for the ortho and meta carbons since the C-H bonds make angles θ of 60 and 120° with the C_2 axis. This leads to motional averaging of the interaction and hence lengthens the T_1 values. In the limit of very fast (free) rotation about the C-X bond compared to rotation about any other axis, the T_1 values of the ortho and meta carbons should be increased by a factor given by equation 1

$$\chi = \frac{T_{1(o,m)}^{DD}}{T_{1(p)}^{DD}} = [\tfrac{1}{2}(3\cos^2\theta - 1)]^{-2} \quad \ldots \quad 1$$

which for 60 and 120° is 64. This ratio χ can thus be used as a measure of the motional anisotropy in monosubstituted benzenes and related molecules.

If the overall reorientation of the molecule is isotropic then the motion of the rotating phenyl groups can be described by a diffusion or a jump model.[4] It can be shown[3,5,6] that the T_1 ratio for the internal diffusion model is given by equation 2

$$\chi = 64/\left(1 + \frac{36}{1+\rho} + \frac{27}{1+4\rho}\right) \quad \ldots \quad 2$$

where $\rho = R_d/6D$ and Rd is the internal rotation diffusion constant. For the jump model

$$\chi = 64/\left(1 + \frac{63}{1+\sigma}\right) \quad \ldots \quad 3$$

where $\sigma = R_j/6D$ and R_j is a constant depending on the nature of the rotor and the jump rate. For both models D is the isotropic diffusion constant.

These functions are plotted in Figure 1. For a given ratio of χ, ρ and σ can be calculated. R_d and R_J can also be evaluated since D can be calculated from the correlation time τ_c^{iso} of the para carbon using equation 3a

$$D = \frac{1}{6\tau_c^{iso}} \qquad \ldots \qquad 3a$$

Section 2

Results and Discussion

The ^{119}Sn and ^{13}C T_1 and NOE data of Ph_3SnH are presented in Table 1. Figure 2 shows the results of the (180-τ-90) sequence for ^{119}Sn. Figure 2a shows the NOE. The T_1 ratio χ is 2.98 and from Figure 1, ρ and σ, the tumbling ratios are found to be 1.25 and 2.07 respectively (see Table 2). These should be compared to those found by Harris and Kimber[7] for triphenyl silane of ρ = 1.05 and σ = 1.78. Note that both the diffusion and the jump model show the tumbling ratio to be greatest for Ph_3SnH indicating that the rotation of the phenyl groups about the metal-carbon bond is less hindered for the tin case. Presumably the longer tin-carbon bond reduces the steric hindrance between the ortho protons.

Mislow et al[8-11] have found that a two ring flip occurs in trimesityl methane and similar systems. The effect of such motion on the relaxation of the carbon nuclei in Ph_3SnH has not been considered in this work since such a high degree of crowding at the ortho position is unlikely due to the absence of methyl groups at the ortho position as well as the longer tin-carbon bond.

If the overall tumbling of Ph_3SnH is indeed isotropic then the correlation times τ_c^{iso} derived from the para carbon T_1^{DD} and the tin

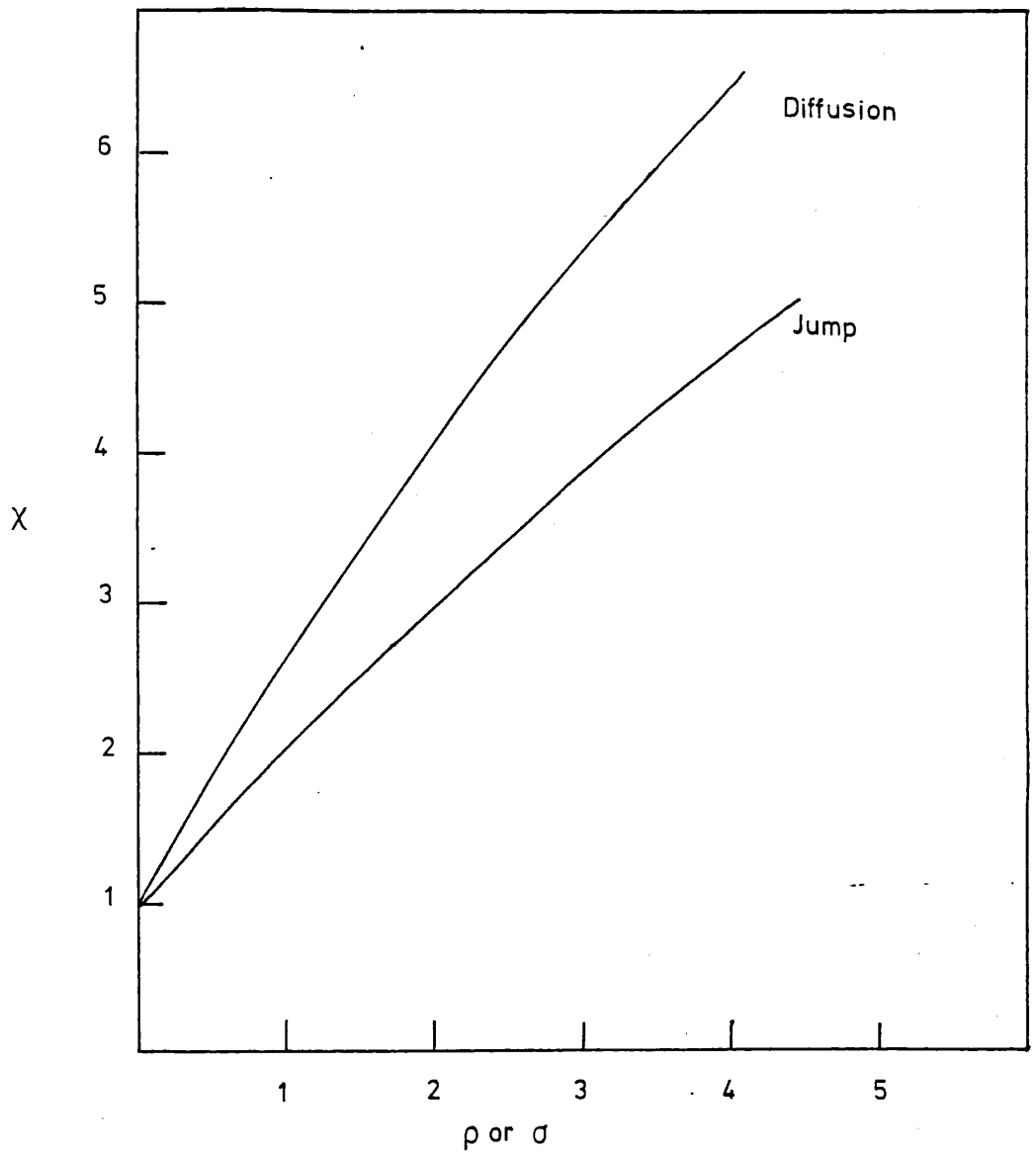

Figure 1

Plot of χ vs tumbling ratio ρ or σ

Table 1

^{13}C, ^{119}Sn and ^{29}Si spin-lattice relaxation data

		T_1/S			η					
Molecule	χ	C_o	C_m	C_p	C_o	C_m	C_p		T_1/S	η
Ph_3SnH*	2.99	0.468	0.543	0.168	1.80	1.71	1.75	^{119}Sn	1.514	-1.21
Ph_3SiH+	2.70	2.7	2.5	1.0	1.98	1.90	2.06	^{29}Si	12.0	-2.41

* 50% v/v in toluene d_8, at 303°K

\+ Saturated solution in benzene d_6. Unspecified temperature. Assumed ambient.

Figure 2

Inversion recovery sequence for ^{119}Sn in Ph_3SnH at 37.29 MHz.

Temperature was 303° K. T_1 = 1.51 s

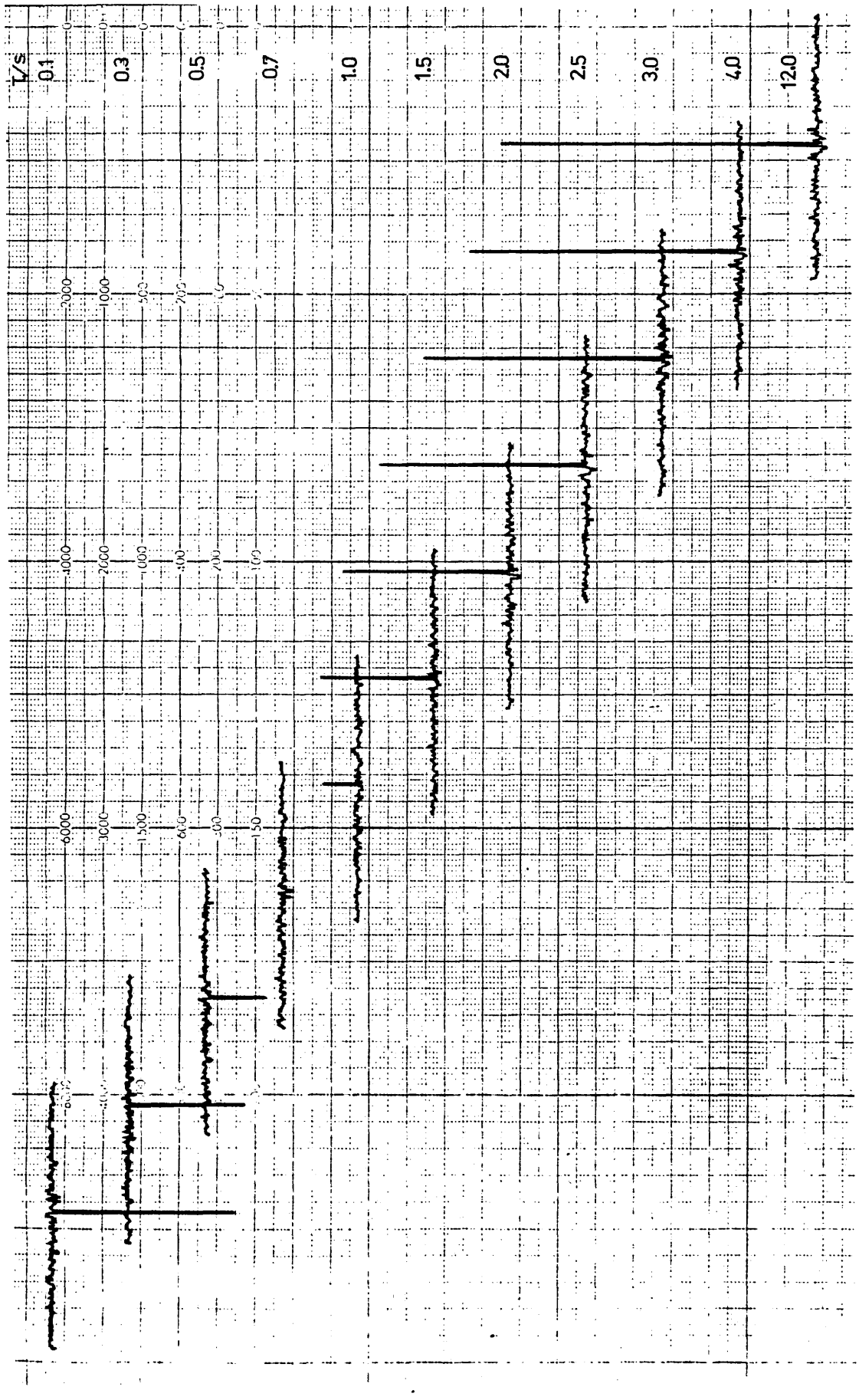
T/s
0.1
0.3
0.5
0.7
1.0
1.5
2.0
2.5
3.0
4.0
12.0

Figure 2a

^{119}Sn NOE determination for Ph_3SnH at 303°K

$\eta = -121$

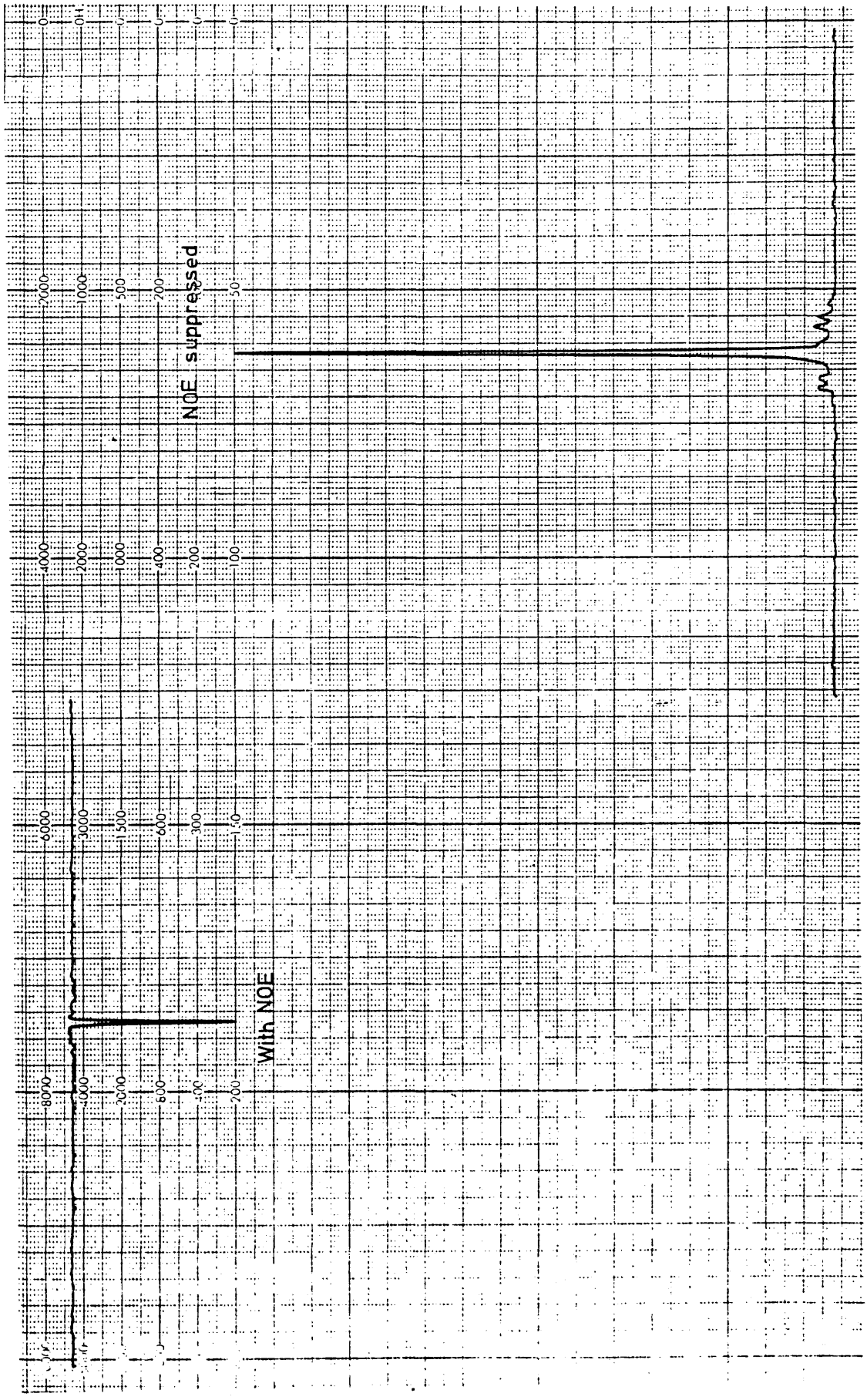
NOE suppressed
With NOE

Table 2

Tumbling ratio (ρ or σ) derived from χ using Figure 1

Temp: 303°K	$T_1^{DD}(C_{O,m})$ /s^{-1}	$T_1^{DD}(C_p)$ /s	χ	ρ	σ	τ_c /ps	D/ns^{-1}	R_a/ns^{-1}	R_j/ns^{-1}
Ph_3SnH	0.572	0.192	2.98	1.25	2.07	243	0.69	5.1	8.5
Ph_3SiH*	2.7	1.0	2.7	1.05	1.7	46.6	3.58	22.6	38.1

* from ref. 7.

T_1^{DD} should be the same. This isotropic correlation time may be calculated from equation 9 given in Chapter 2, section 2A.

$$\frac{1}{T_1^{DD}} = \frac{\gamma_X^2 \gamma_H^2}{r^6} \hbar^2 \tau_c^{iso}$$

where the symbols take their usual meanings. What is found, in fact is that τ_c^{iso} for the tin proton vector is 182 $\pm$ 10 ps and for the para carbon-proton vector 243 $\pm$ 10 ps. This indicates that the overall tumbling is anisotropic. This may be tested assuming the molecule acts as a symmetric top.

Using the expressions derived by Woessner et al[5,6] Harris and Kimber[7] have derived an expression for the T_1^{DD} ratio of the para carbon and the metal nucleus X in terms of the ratio of the diffusion constants parallel ($D_{||}$) and perpendicular ($D_\perp$) to the C_3 symmetry axis. This is given in equation 4

$$\frac{T_1^{DD}(C_p)}{T_1^{DD}(X)} = \frac{N}{\left[\frac{(1-3\cos^2\theta)^2}{6} + \frac{3\sin^2 2\theta}{\left(\frac{D_{||}}{D_\perp}\right) + 5} + \frac{3\sin^4\theta}{4\left(\frac{D_{||}}{D_\perp}\right) + 2}\right]} \quad \ldots 4$$

where $N = \frac{2}{3}\left(\frac{r_{C-H}}{r_{X-H}}\right)^6 \left(\frac{\gamma_X}{\gamma_C}\right)^2$

θ is the angle the vector of interest makes with the C_3 axis. For the para carbon this is 109.5°.

Equation 4 is plotted for X = ^{119}Sn (r_{X-H} = 1.7 x 10^{-8} cm, γ = -9.971 x 10^3 $G^{-1}s^{-1}$) in Figure 3. From Table 3 the T_1^{DD} ratio is seen to be 0.1145 which corresponds to $D_{||}/D_\perp$ of 0.49. The diffusion constant perpendicular to the C_3 axis can be calculated from equation 3 and is found to be 0.92 x 10^9 s^{-1}, thus $D_{||}$ is calculated to be 0.45 x $10^9 s^{-1}$. This indicates that tumbling perpendicular to the C_3 axis is preferred to tumbling about the axis. This is in

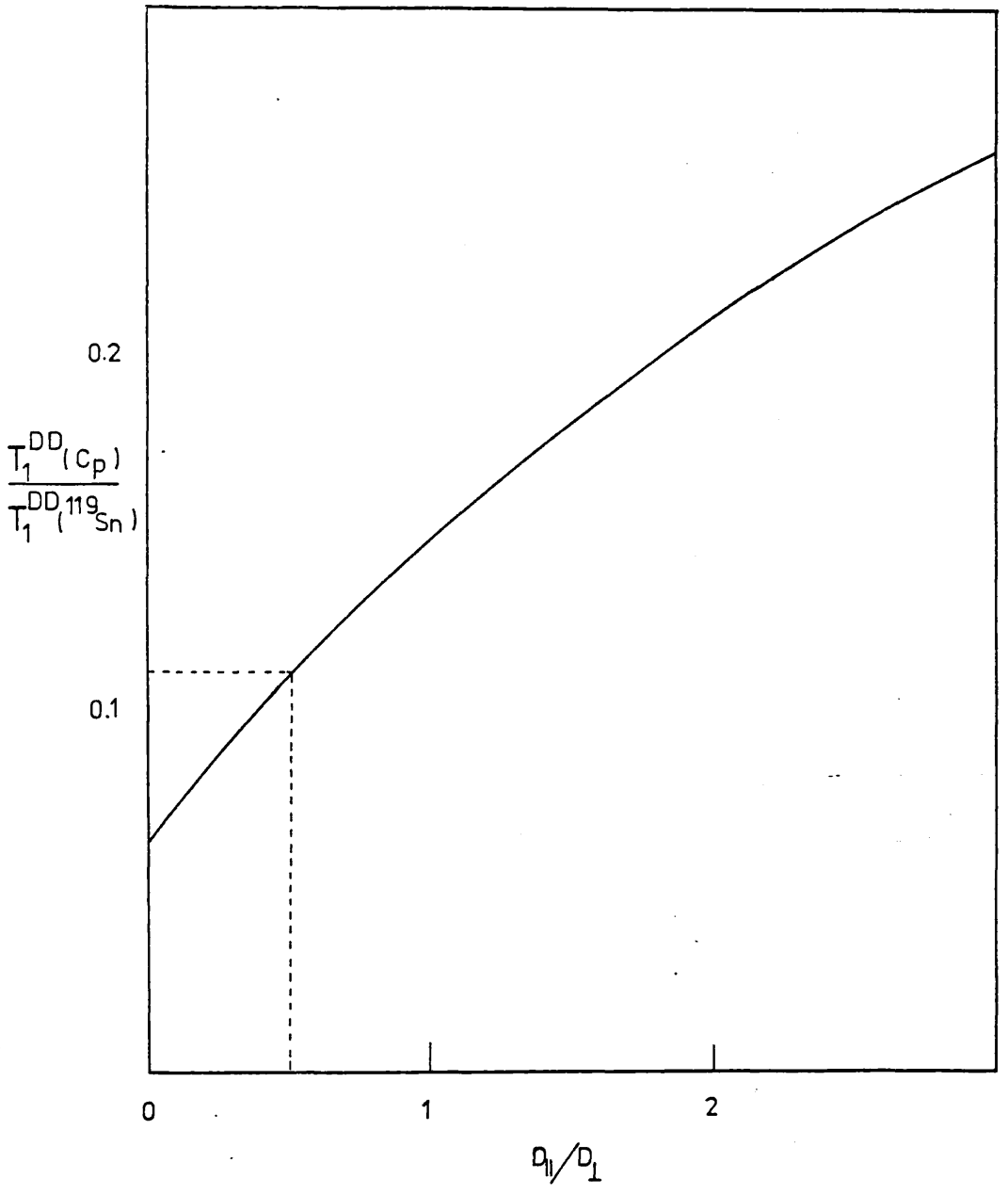

Figure 3

Ratio of diffusion constants estimated from the ^{119}Sn and ^{13}C T_1^{DD} values

Table 3

$D_{\perp}$ and $D_{\parallel}$ for the molecules Ph_3SnH and Ph_3SiH

	T_1^{DD}/s		$\frac{T_1^{DD}(C_p)}{T_1^{DD}(X)}$	$\frac{D_{\parallel}}{D_{\perp}}$	$D_{\perp}/ns^{-1}$	$D_{\parallel}/ns^{-1}$
	X	$C(_p)$				
$X = {}^{119}Sn$	1.677	0.192	0.1145	0.49	0.92	0.45
$X = {}^{29}Si$ *	12.5	1.0	0.08	0.6	4.46	2.68

* From reference 7.

agreement with the observations of Harris and Kimber[7] for Ph_3SiH (Table 3). Note the similarity in $D_{11}/D_{\perp}$ for the two molecules. These results are not expected since if the molecule is not distorted in any way then it is anticipated that motion about the C_3 axis would be preferred due to the inertial effect since tin or silicon need not be moved off axis. The authors interpret their observations for Ph_3SiH by invoking a squat shape to the molecule presumably resulting in a decrease of the $\angle HSiC$ angle giving the molecule a propeller like appearance. No reasons are given for this although steric crowding of the ortho protons could account for the effect.

An alternative explanation is that the frictional plus the inertial effect of the three phenyl groups when rotation about the C_3 axis occurs is larger than the inertial effect of moving the heavier metal nucleus off axis plus the frictional effect of the two phenyl rings when the molecule (rather than a phenyl ring) rotates about a tin carbon bond (Figure 4). This implies that the inertial plus frictional effect of the phenyl rings is greater than the inertial effect of the metal nucleus and considering the geometry and size of the phenyl rings this is not totally unexpected.

No comment has yet been made about any dipolar contribution to tin from the ortho protons of the phenyl groups. The distance between tin and the ortho protons is calculated to be 317 pm. Consequently the maximum dipolar contribution these six protons can provide is a factor of 40 down* compared to a single hydride proton. In view of the fact that the phenyl groups are rotating this contribution is further reduced so that when calculating correlation times only small errors are introduced by assuming that the NOE arises solely from the dipolar contribution of the hydride proton.

* Calculated from equation 9, Chapter 2.

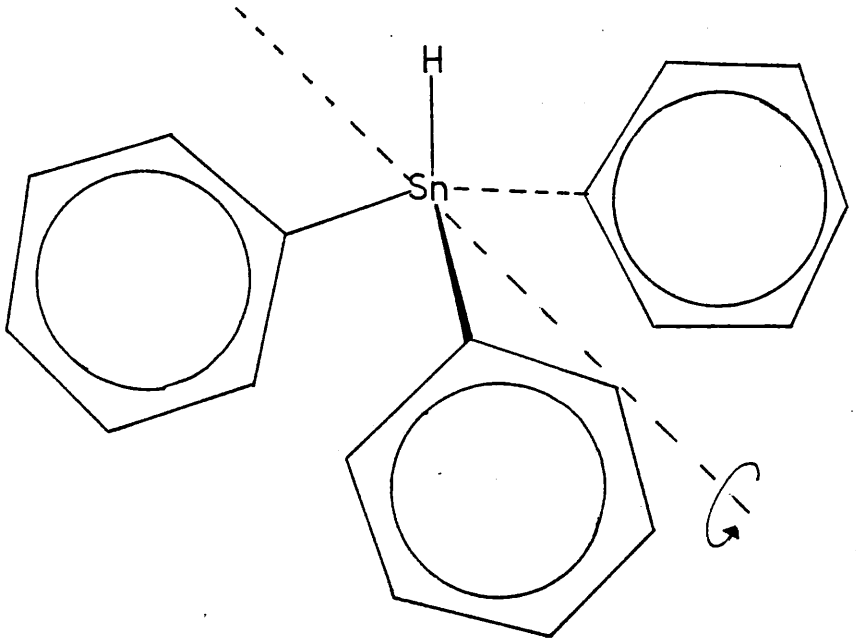

Figure 4

A

Correlation Times

The comment was made in Chapter 5 about the length of ^{119}Sn correlation times compared to the values in analogous ^{29}Si compounds. In the molecules discussed there the relevant vectors are somewhat ill-defined due to segmental motion of the alkyl chains and the assumption that a fixed zig-zag orientation exists. These uncertainties do not exist in molecules such as Ph_3XH (X = ^{13}C, ^{29}Si, ^{119}Sn) since the X-H vector is fixed.

It has been shown in this chapter that the value of τ_c for motion about the Sn-H and Si-H bonds are 182 ps and 37 ps respectively. Smith et al[12] have measured the deuterium spin-lattice relaxation time in Ph_3C D observing a value of 0.11s. Assuming the quadrupole coupling constant for deuterium in an sp^3 hybridised C-D bond to be 175 kHz yields a value for τ_c of 20 ps. Plotting τ_c (which for these molecules is 1/6 $D_\perp$) vs molecular weight (see Figure 5) clearly illustrates the dependence of τ_c on molecular weight for this series. It further illustrates the point that although the carbon and silicon analogues are quite similar from the point of view of τ_c the ^{119}Sn analogue exhibits a markedly different value of τ_c.

Section 3

Experimental

The ^{13}C and ^{119}Sn spin lattice relaxation times and NOE factors were measured using a Jeol FX 100 at 37.29 MHz fitted with multinuclear accessories. The ^{13}C spectra were run under conditions of proton noise decoupling. The one bond tin proton coupling constant (1934 Hz)

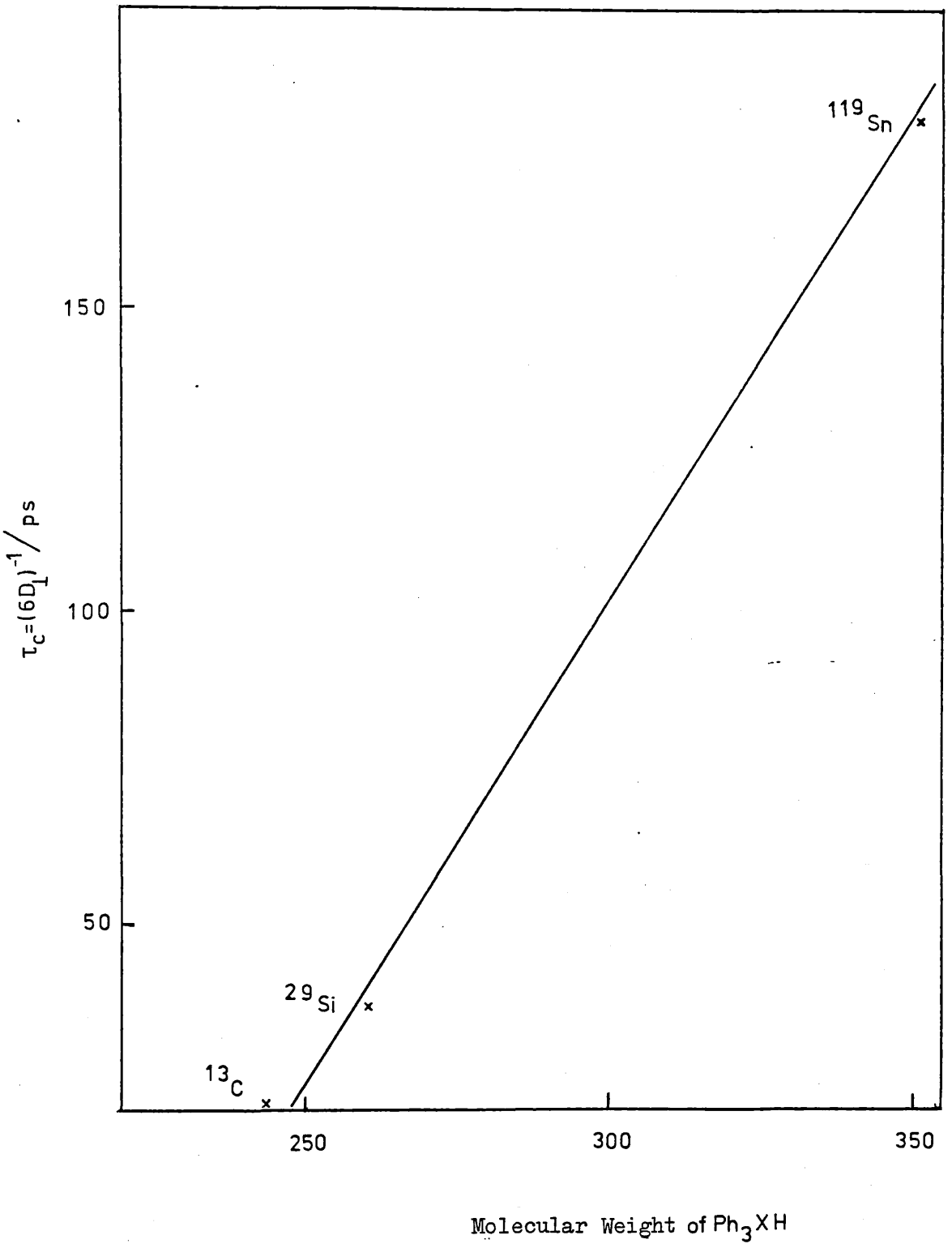
150
100
50
$\tau_c=(6D_1)^{-1}$/ps
^{119}Sn
^{29}Si
^{13}C
250
300
350
Molecular Weight of Ph_3XH

Figure 5

could only be decoupled using continuous wave irradiation in the vicinity of the hydride feature. The field frequency lock was maintained by locking to the methyl region of the solvent.

The sample of Ph_3SnH was purchased from Cambrian Chemicals. Proton and ^{13}C NMR spectra showed no impurities and the sample was used without further purification. The sample was made up in toluene d_8 50% v/v.

The author is indebted to Dr P. Beynon of Jeol Ltd. for these measurements.

References

1 W.T. Huntress Jr. J. Chem. Phys. (1968) 48 3524.

2 D.E. Woessner, J. Chem. Phys. (1965) 42 1855.

3 G.C. Levy, J.D. Cargioli, F.A.L. Anet, J. Amer. Chem. Soc. (1973) 95 1527.

4 N. Bloembergen, Phys. Rev. (1956) 109 1542.

5 D.E. Woessner, J. Chem. Phys. (1962) 36 1.

6 D.E. Woessner, B.S. Snowden, G.H. Meyer, J. Chem. Phys. (1969) 50 719.

7 R.K. Harris, B.J. Kimber, Advan. Mol. Relaxation Processes, (1976), 8 23.

8 J.D. Andose, K. Mislow, J. Amer. Chem. Soc. (1974) 96 2168.

9 R.J. Boettcher, D. Gust, K. Mislow, J. Amer. Chem. Soc. (1973) 95 7157.

10 P. Finocchiaro, D. Gust, K. Mislow, J. Amer. Chem. Soc. (1974) 96 2165.

11 P. Finocchiaro, D. Gust, K. Mislow, J. Amer. Chem. Soc. (1974) 96 2176.

12 H.H. Mantsch, H. Saito, L.C. Leitch, I.C.P. Smith, J. Amer. Chem. Soc. (1974) 96 256.

CHAPTER 7

Spin-Lattice Relaxation of ^2H in neat nBu_3SnD.

Section 1

Introduction

Deuterium is an attractive nucleus to study from the standpoint of spin-lattice relaxation time measurement since the quadrupole relaxation mechanism dominates the observed values of T_1. Consequently there is no need to separate different contributing mechanisms or indeed to degass the sample.[1,2] Furthermore the processes that give rise to quadrupolar relaxation are entirely intramolecular and thus measurement of T_1's of quadrupolar nuclei yield reorientational correlation times (τ_c).

Due to the low magnetogyric ratio of ^2H ($\gamma_{1_H} / \gamma_{2_H} = 6.14$) and its low natural abundance its sensitivity to NMR detection compared to ^1H is 1.5×10^{-6}. This has limited NMR studies of ^2H at natural abundance. Smith et al[1] have shown the ^2H spectrum of H_2O in a 12 mm tube at 2.1T at natural abundance, the spectrum being clearly observable after one pulse. However, the ease of deuteration at least of relatively small molecules has resulted in most ^2H NMR studies utilising near 100% ^2H enrichment.

A

Deuterium T_1 Measurement

For mobile liquids where the condition of extreme narrowing holds $T_1^Q = T_2^Q$ and therefore the quadrupole spin-lattice relaxation time T_1^Q can be simply estimated by measurement of the ^2H linewidth at half height ($\Delta\nu_{1/2}$);

$$\Delta\nu_{1/2} = \frac{1}{\pi T_2^*} = \frac{1}{\pi T_2^Q} + \delta\nu_{\frac{1}{2}}$$

where $\delta\nu_{\frac{1}{2}}$ is the line broadening due to inhomogeneity of the static field. This method is quite acceptable for resonances of large linewidths since the contribution of $\delta\nu_{\frac{1}{2}}$ will be small compared to the natural linewidth ($\frac{1}{\pi T_2^Q}$). However for narrow lines (long T_2^Q) the linewidth will be dominated by $\delta\nu_{\frac{1}{2}}$ and estimation of the quadrupole spin-lattice relaxation time by this method is subject to large errors. Obviously the best method for the determination of T_1^Q is by direct measurement. With CW spectrometers the adiabatic rapid passage experiment is used[2-6] and with pulse spectrometers the inversion recovery technique ($180^\circ - \tau - 90^\circ$).[7-9] The latter is obviously more convenient when magnetically inequivalent deuterons appears in the spectrum since all the T_1 values in a sample may be determined simultaneously.

B

The Quadrupole Coupling Constant

It has been shown in Chapter 1 that in the extreme narrowing limit the following equation is valid

$$\frac{1}{T_1^Q} = \frac{1}{T_2^Q} = \frac{3}{40}\,\frac{2I+3}{I^2(2I-1)}\left(\frac{1+\eta^2}{3}\right)\left(\frac{e^2Qq}{\hbar}\right)^2 \tau_c \qquad \ldots 1$$

the asymmetry factor η is normally taken as zero for ^2H. It can be seen then that T_1^Q depends on the value of QCC and τ_c . Knowledge of one of these quantities enables the other to be calculated if T_1^Q is known.

C

Results and Discussion

Table 1 shows the ^{2}H T_1 values over a range of temperature for neat nBu_3SnD. The data are summarised in Figure 1. Figure 2 shows typical results from an inversion recovery sequence. The temperature dependence is as expected for the quadrupole relaxation mechanism and the energy of activation is calculated to be 16.0 kJ mol^{-1}.

D

Motion of the Sn-^{1}H and Sn-^{2}H bonds

The motional behaviour of the Sn-^{2}H and Sn-^{1}H bonds are expected to be identical with the proviso that small changes may arise due to the larger mass ^{2}H compared to ^{1}H. However although such changes in mass and consequently moments of inertia may be important in methyl groups[10] the small fractional increase of these parameters on deuterating nBu_3SnH will be insignificant. For the purposes of this discussion therefore the motion of the two vectors is taken to be identical.

From the ^{119}Sn T_1 and NOE data of nBu_3SnH presented in Chapter 4 a value of τ_c^{eff} of 11-16 ps was derived for the Sn-H vector at 307°K. The range in τ_c^{eff} arises from the uncertainty of the dipolar contribution of the α methylene protons to the observed ^{119}Sn T_1 value. From Figure 1 the ^{2}H relaxation rate at 307 K is estimated to be 1.56 s^{-1}. Using a mean value for τ_c^{eff} of 13.5 ps and R_1^{Q} = 1.56 s^{-1} equation 1 may be used to estimate the ^{2}H quadrupole coupling constant in the Sn-D bond yielding a value of 88 $\pm$ 10 kHz. This value compares reasonably well with that estimated by Ahmed[11] in the molecule

Table 1

Spin-lattice relaxation time of ^{2}H in neat nBu_3SnD

T/K	T_1^Q/S
258	0.18
268	0.26
278	0.33
288	0.44
299	0.62
311	0.70
324	0.96
336	1.09
356	1.35

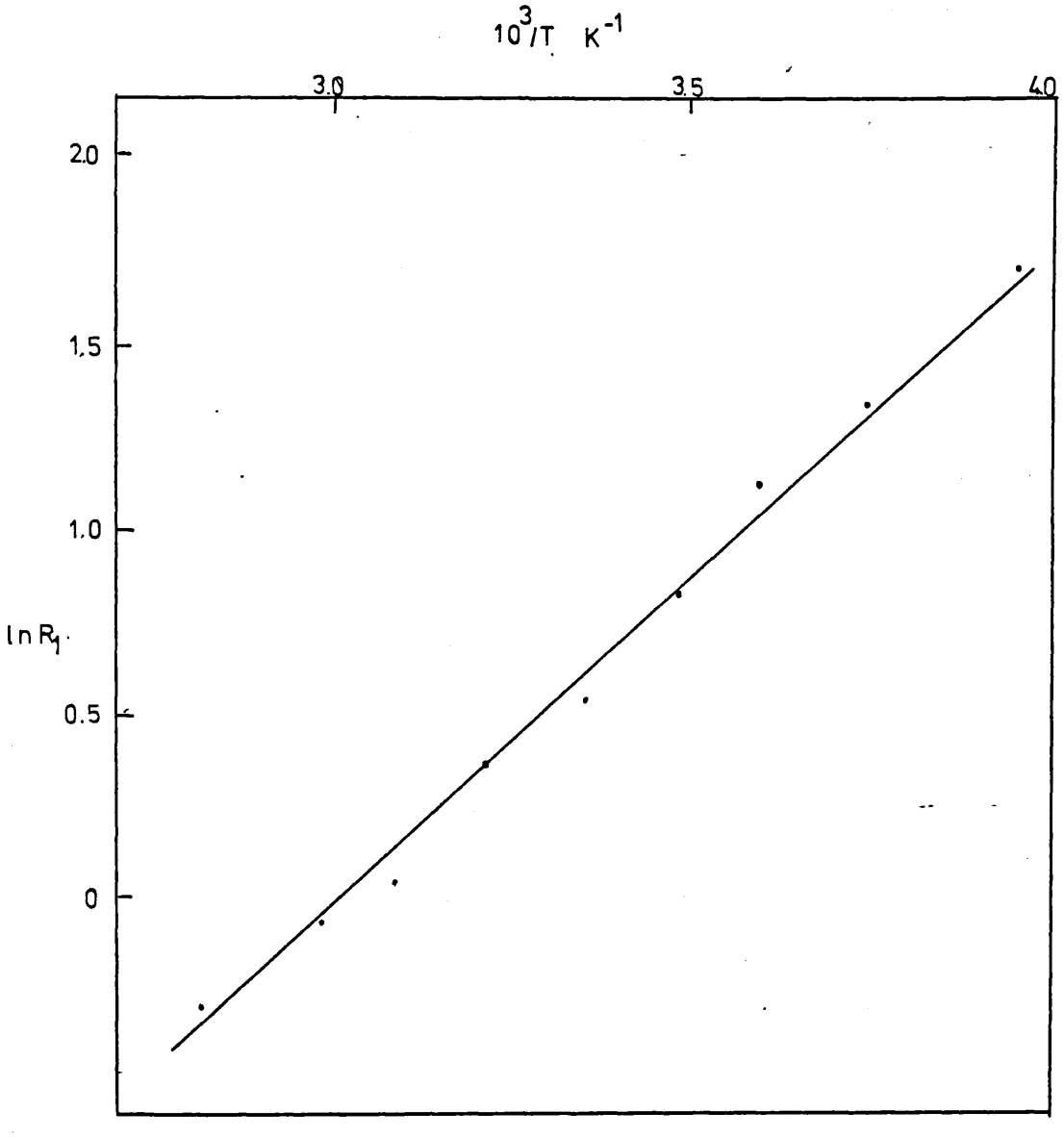

Figure 1

Graphical plot of the data in Table 1

Figure 2

Typical results of inversion recovery sequence for ^{2}H in nBu_3SnD at 323.8°K

Each spectrum results from 20 transients.

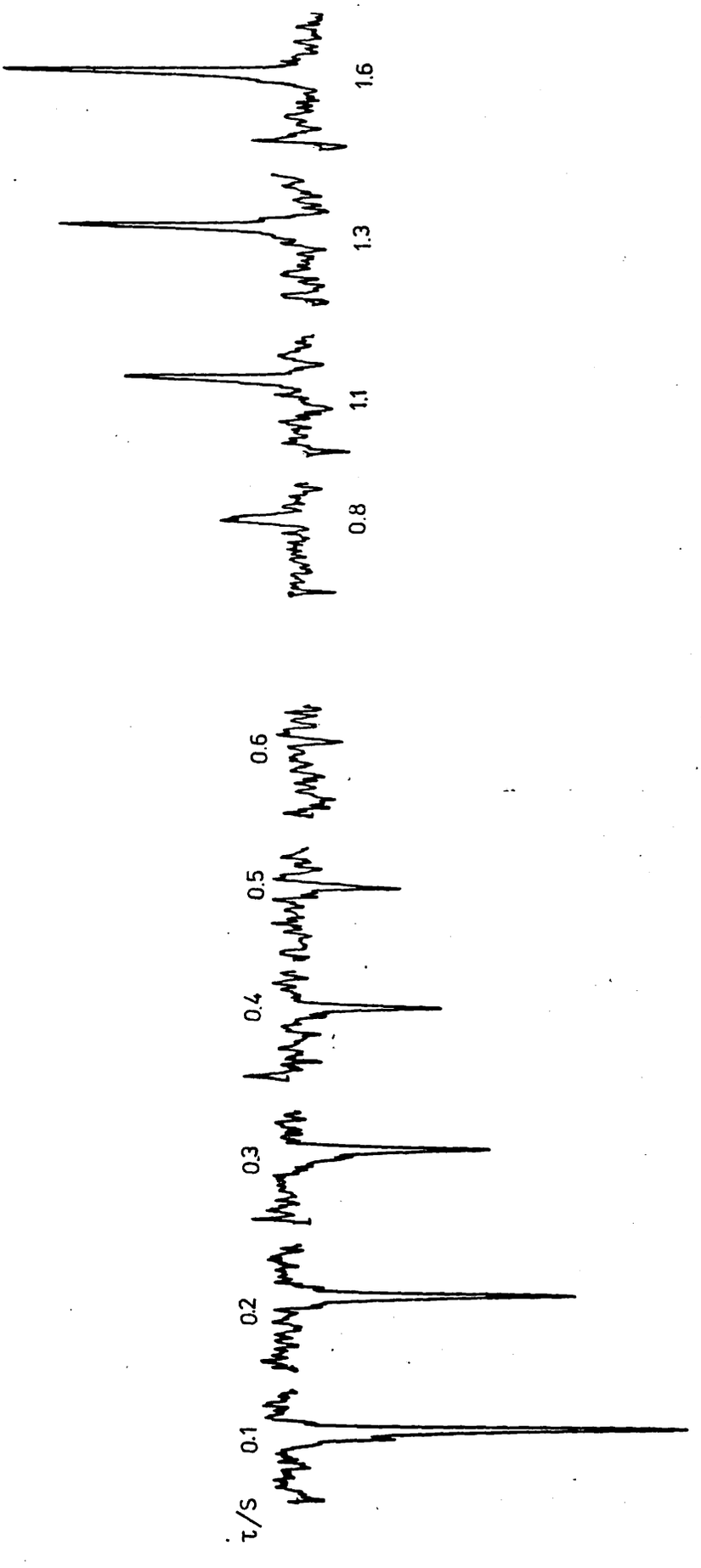
τ/s
0.1
0.2
0.3
0.4
0.5
0.6
0.8
1.1
1.3
1.6

Ph_2SnHD of 121.5 kHz. Fung et al[12] have reported a value for the QCC of deuterium in $PhSiD_3$ using liquid crystal solvents of 91 ± 2 kHz. In a sp^3 hybridised C–D bond the value of QCC is expected to be approximately 170 kHz.[1]

E

Experimental

The sample of nBu_3SnD was purchased from Cambrian Chemicals Ltd. and used without further purification. Spectra were obtained and T_1 values measured using the pulse spectrometer system described in Chapter 3 at 9.203 MHz. The 90° pulse length was 95 μs. The inversion recovery technique was used for the T_1 measurements. The field-frequency lock was maintained using a ^1H resonance of a suitable material (DMSO or acetone) in the annular portion of a 12 mm OD tube, the neat liquid sample being in a 5 mm OD tube placed centrally in the larger tube.

References

1 H.H. Mantsch, H. Saito, I.C.P. Smith, Progress in NMR Spect. (1977) 11 211.

2 J.A. Glasel, J. Amer. Chem. Soc. (1969) 4569.

3 A. Abragam, The Principles of Nuclear Magnetism, Clarendon Press, 1961.

4 J.A. Glasel, J. Sci. Instr. (1953) 1 963.

5 R.G. Parker, J. Jonas, Rev. Sci. Instr. (1970) 41 319.

6 R.A. Assink, J. Jonas, J. Chem. Phys. (1970) 53 1710.

7 R.L. Vold, J.S. Waugh, M.P. Klein, D.E. Phelps, J. Chem. Phys. (1968) 48 3831.

8 R. Freeman, H.D. Hill, J. Chem. Phys. (1971) 54 3367.

9 T.C. Farrar, E.D. Becker, Pulse and Fourier Transform NMR Academic Press, 1971.

10 J.P. Jacobsen, K. Schaumburg, J. Magn. Resonance (1977), 28 191.

11 M.J. Ahmed, Ph.D Thesis University of London, 1977.

12 B.M. Fung, I.Y. Wei, J. Amer. Chem. Soc. (1970) 92 1497.

CHAPTER 8

The Dependence of the ^{119}Sn Chemical Shift in $nBu_2Sn(OAc)_2$ on Temperature and Concentration

Section 1A

Complex Formation

A number of workers[1,2,3] have observed that an increase in the coordination number of tin from four to five or six results in ^{119}Sn chemical shifts that are to high field relative to the four coordinate parent compound.

Hunter and Reeves[2] showed that the shifts of trimethyl tin chloride and bromide were essentially invariant in non coordinating solvents at different concentrations. This indicates that complexing between the solvent and the tin compound does not occur and also that the tin compound does not auto associate. Tupciauskas[4] has studied this system in more detail.

Polar coordinating solvents such as acetone and pyridine can produce large variations in the ^{119}Sn chemical shifts which are both temperature and concentration dependent. The addition of pyridine to trimethyl tin chloride in carbon tetrachloride[5] shows a change in shift from 159 to -9 ppm as the mole ratio of Me_3SnCl:pyridine is increased from 1:0 to 1:12. This has been interpreted as due to the formation of a 1:1 pentacoordinate trigonal bipyramidal adduct of type A.

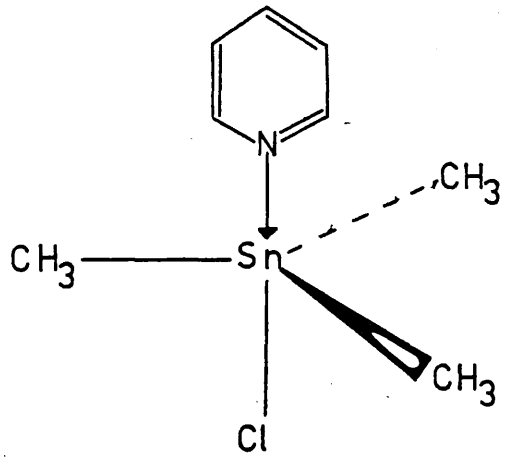

A

The complex is known to dissociate in non polar solvents,[6] the observed ^{119}Sn chemical shift presumably being the weighted mean of the free and complexed Me_3SnCl and therefore a reflection of the degree of dissociation of the complex.

A number of authors [3,7-18] have studied the methyl and ethyl tin halides in a variety of complexing solvents. Torocheshnikov et al[10] have studied the ^{119}Sn chemical shifts of trimethyl and triethyl tin chloride as a function of temperature and concentration in a number of solvents. They calculated equilibrium constants at various temperatures using an equation first derived by Hunter and Reeves,[2] and using the Van t'Hoff equation derived the molar enthalpy for the formation of the complexes. Their results are close to those calculated by Bolles and Drago[7] using thermochemical methods.

B

Auto-association

In the preceding section the discussion has been limited to organotin complexes of various coordinating solvents. A variety of organotin compounds can increase their coordination number by forming inter- or intramolecular bonds via functional groups on the molecule itself. This kind of autoassociation also results in a high field shift of the ^{119}Sn NMR signal as occurs for complex formation.

McFarlane and Wood[19] have observed the ^{119}Sn chemical shift of trimethyl tin formate at various concentrations in chloroform noting a large change in chemical shift to low field on dilution (150 ppm). This was attributed to the formation of oligomers or polymers of type B .

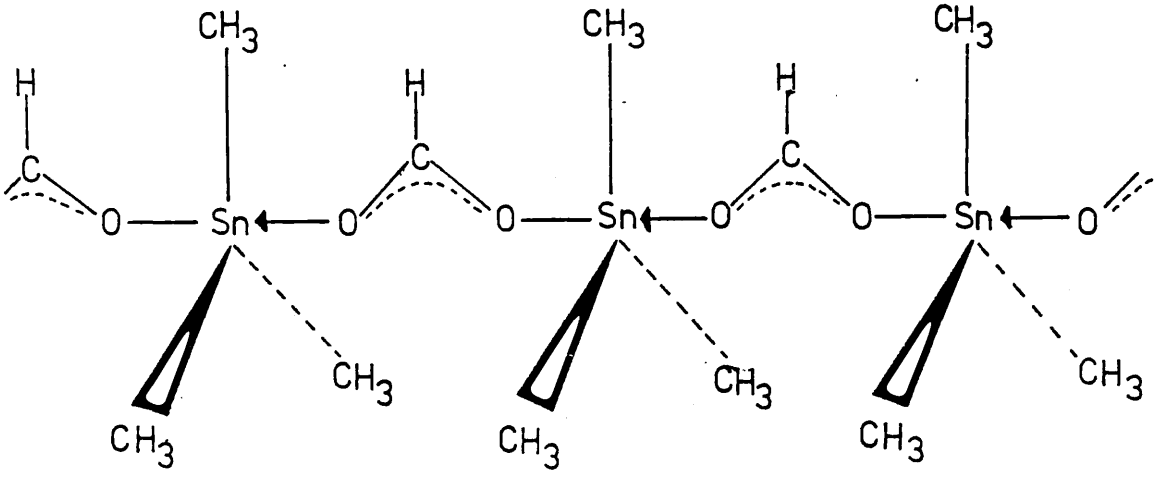

B

Such species are known to exist in the solid state but are not proven in the liquid state. Other examples of such self associated polymeric species are trimethyl tin hydroxide and trimethyl tin isothiocyanate in the solid state.[20,21]

It has been suggested that di n-butyl dimethoxide, di n-butyl di n-propoxide and di n-butyl di butoxy tin exist as dimers in the pure liquid state[22,23] with structures of type C .

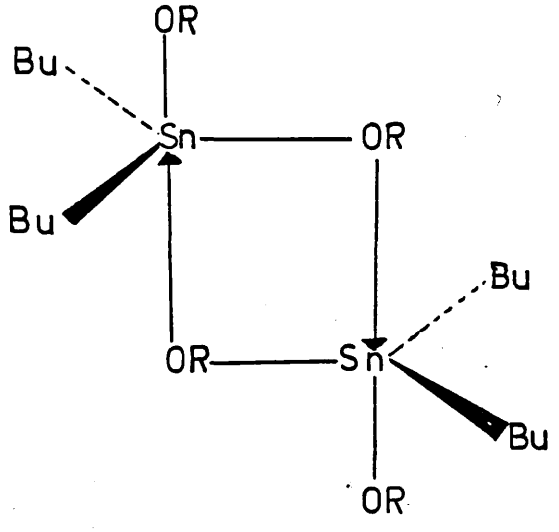

C

Replacement of the alkoxide groups by weaker bridging groups such as thioalkoxides results in the ^{119}Sn chemical shift appearing to low field compared to the shifts of the alkoxide analogues. This is indicative of the decreased tendency to dimerisation.[24]

Smith et al[25] have observed the variation of the chemical shift of some di butyl tin dialkoxides as a function of concentration and temperature and evaluated equilibrium constants. More recently Kennedy[26] has determined the molar enthalpies of association for a number of methyl and butyl tin alkoxides.

A number of authors[27-30] have measured the ^{119}Sn chemical shifts in a series of functionally disubstituted distannoxanes ($XR_2SnOSnR_xX$) and a dimer of type D is postulated.

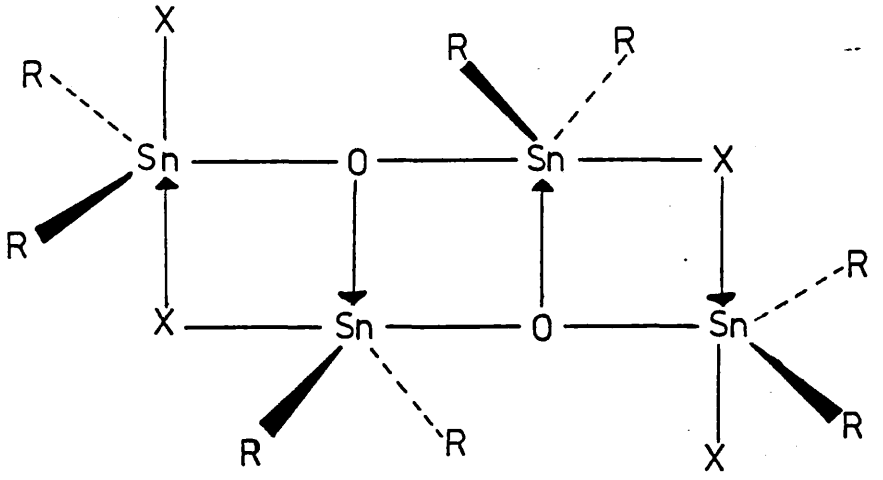

D

It is worth mentioning here a practical aspect of the data analysis. In the case of complex formation a shift for the unassociated species can normally be obtained by merely dissolving the organotin compound in a non-polar solvent, and a ^{119}Sn chemical shift can be observed for the

complexed species by dissolving the complex in the appropriate donor solvent. Knowing both chemical shifts makes the analysis of the data quite simple. In the case of auto-associated species the sample may contain an equilibrium mixture of associated and unassociated species, so unless the kinetics of the exchange are slow compared to the chemical shift difference or the equilibrium strongly favours one or other species, neither shift of pure species will be known.

C

Origin of the High Field Shift

The origin of the high field shift which results when tin increases its coordination number, although qualitatively useful is not well understood. However it is instructive to consider the possibilities of its origins to serve as a basis for discussion.

In chapter 1 sect. 3 the paramagnetic term (σp) was said to dominate the shielding of tin. The contribution to σp by the 5d orbitals was ignored since in most tetrahedral molecules these would be uninvolved in the bonding. It is tempting therefore to attribute the observed behaviour as due to the occupancy of the 5d orbitals. Unfortunately it is unclear why this should be so. All of the organotin molecules showing this shift have groups which can take part in π bonding with the tin atom. Consequently, it has been suggested[31] that the effect may arise from a reduction in the d electron inbalance on the tin atom as a result of placing electron density in all of the tin d orbitals. Also rehybridisation occurs as a result of the increase in coordination number and this may decrease the p electron imbalance.

The increase of electron density on the tin atom as a result of donation from the ligand may increase the dimagnetic contribution although this effect would be small compared to the paramagnetic contribution.

Section 2A

Results and Discussion

Tables 1 - 4 show the variation of the observed ^{119}Sn chemical shift of di n-butyl tin diacetate [$nBu_2Sn(OAc)_2$] with temperature at various concentrations in toluene. Figure 1 summarises this data.

Observation of only one reversibly temperature dependent signal is indicative of an equilibrium occurring. The temperature dependence is similar at all concentrations and its occurrence in the neat sample suggests that the equilibrium is between a self associated and non associated species. Toluene is regarded as a non complexing solvent and should not take part in the equilibrium other than as a diluent. Absence of any severe line broadening and other signals is indicative of fast exchange (this chapter sect. 2), and is confirmed by the proton and ^{13}C data (Table 5). These spectra are temperature independent over a wide temperature range except for some broadening in the proton spectrum of the neat liquid at low temperatures due to increased viscosity. On the basis of osmometry at low concentrations Maeda and Okawara[32] suggest that $nBu_2Sn(OAc)_2$ is intramolecularly associated and exists as the hexacoordinated monomer II. Infra red spectra show two vibrational bands at 1600 - 1610 cm^{-1} and 1370 - 1380 cm^{-1} which these authors assign to the carbonyl in the unassociated and asymmetrically associated species II respectively.

Table 1

C = 1.852 mol l^{-1}	
Temp/K	δ_{OBS}/ppm
280.0	-169.1
291.5	-165.8
299.8	-163.6
300.7	-163.6
312.7	-161.0
319.3	-159.8
325.8	-158.4
331.1	-157.9
337.5	-157.1
350.3	-155.5
371.5	-153.2
380.1	-152.5
380.1	-152.5
394.4	-151.3
402.0	-150.9
421.0	-149.5

Table 2

C = 1.205 mol l^{-1}	
Temp/K	δ_{OBS}/ppm
230.7	-182.1
238.4	-179.0
251.1	-172.8
263.0	-168.8
291.0	-161.4
300.1	-159.7
315.0	-157.6
322.8	-156.7
334.3	-155.0
343.5	-154.2
358.0	-153.0

Table 3

C = 0.849 mol l^{-1}	
Temp/K	δ_{OBS}/ppm
217.2	-185.1
230.7	-177.0
238.4	-173.4
251.1	-168.4
263.0	-164.8
291.0	-159.0
300.1	-157.6
315.0	-155.9
322.8	-155.2
334.3	-153.9
343.5	-153.4
358.0	-153.2

Table 4

C = 0.443 mol l^{-1}	
Temp/K	δ_{OBS}/ppm
217.7	-175.9
235.9	-167.6
252.0	-163.0
277.1	-158.4
283.1	-156.7
299.8	-155.5
312.4	-154.6
322.1	-153.8
332.8	-153.1
341.2	-152.4
351.9	-151.9

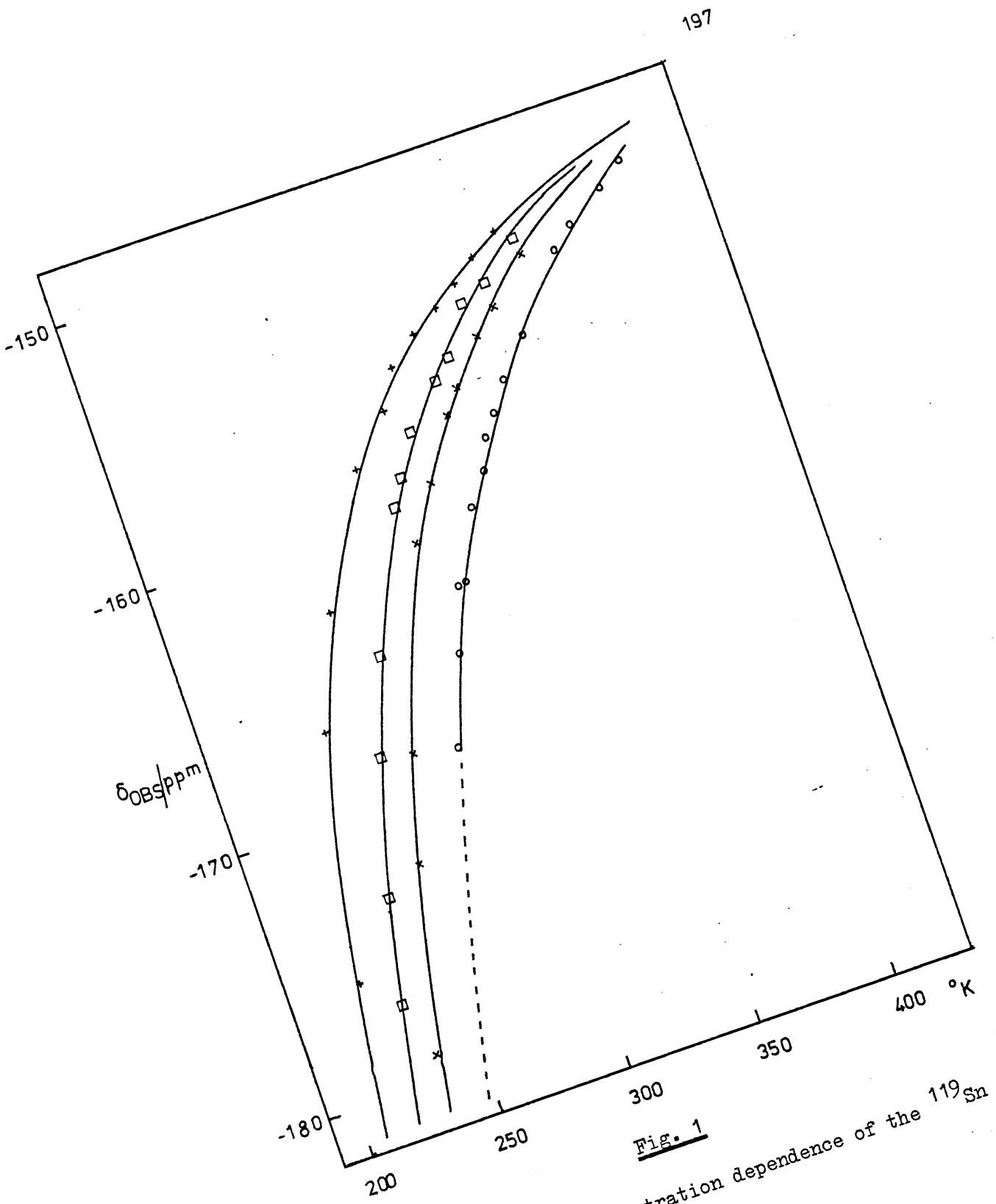

Fig. 1

Temperature and concentration dependence of the ^{119}Sn chemical shift of $nBu_2Sn(OAc)_2$

- ○ 1.852 mol l^{-1}
- × 1.205 " "
- □ 0.849 " "
- \+ 0.443 " "

Table 5

Conc/mol l^{-1}	Temp/K	$\delta_{^{13}C}$/ppm
1.852	306	180.9
	356	180.7
	406	180.7
0.443	310	180.6
	370	180.7

Variation of ^{13}C chemical shift of C=O resonance in $nBu_2Sn(OAc)_2$ with Temperature and Concentration

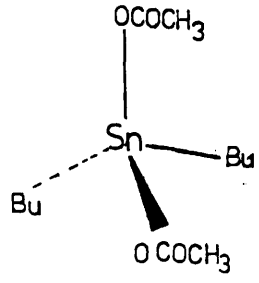

I

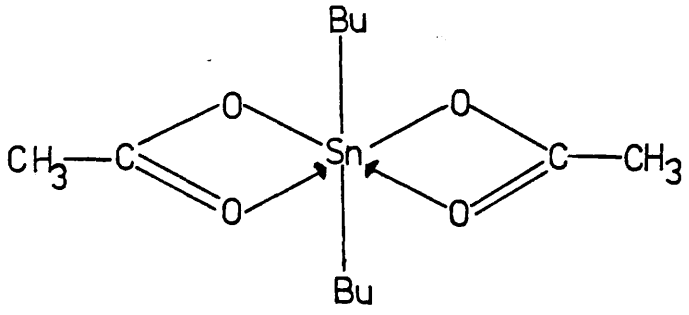

II

In the neat liquid a band at 1565 cm^{-1} appears which also appears in the infra red spectrum of trialkyltin acetates[33,34] where acetoxy groups are known to form the bridge between two tin atoms also suggesting an inter molecular association for $nBu_2Sn(OAc)_2$. Mitchell[35] has studied the tin carbon coupling constants in a variety of organo tin compounds and concludes that the one bond tin carbon coupling constant $^1J_{Sn-C}$ is indicative of the hybridisation state and coordination number of the tin atom. From the observed coupling constant of 630 Hz he concludes that $nBu_2Sn(OAc)_2$ can exist as the dimeric structure III.

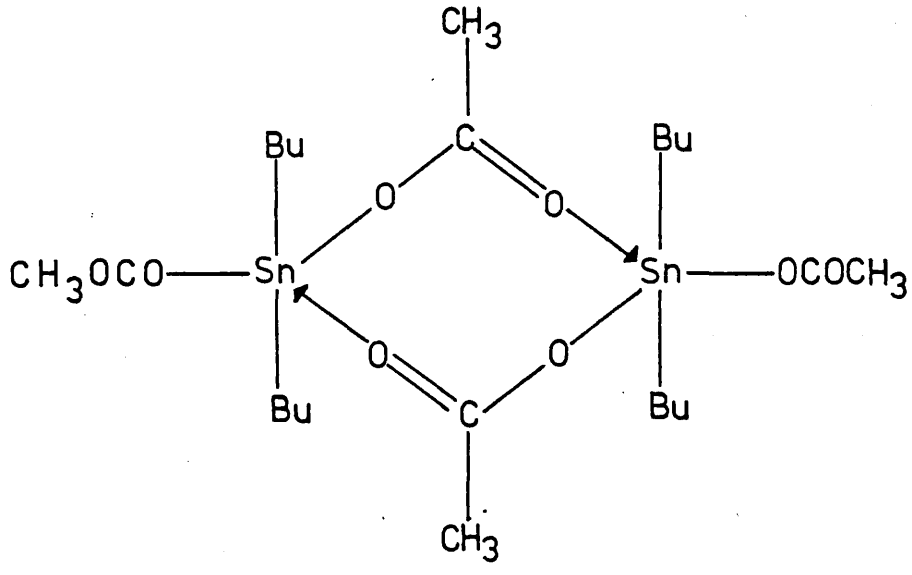

III

The ^{13}C chemical shift of the carbonyl resonance in the neat liquid has been observed to be 181 ppm[35] in agreement with our measurement of 180.6 ppm (Table 5). We have extended this to dilute solutions in toluene and over a temperature range (Table 5), and within the limits of the experiment have found the shift to be constant, as are the shifts of the remaining carbons in the molecule. This is in agreement with Mitchell's conclusion and with our ^{119}Sn shift observations that the exchange is rapid, leading to equivalence of the bridging and non-bridging carbonyls. Mossbauer data has been interpreted[36] as indicating a distorted octahedral structure II. Such a small distortion as claimed by these authors is unlikely to lead to a 300 Hz decrease in $^{1}J_{(C-Sn)}$ of $nBu_2Sn(OAc)_2$ compound to the one bond tin carbon coupling constant in the known regular octahedral structure of $Bu_2Sn(AcAc)_2$. To be fair to these authors they make no claims as to the structure of the molecule in the liquid state and considering the dangers of such extrapolation this is understandable. Furthermore, the observed concentration dependence of the ^{119}Sn chemical shift (Fig 1) reported in this work indicates that any association is intermolecular since an intramolecular association would be unaffected by dilution.

Considering the available data[32-39] in the literature and the data presented in this work it is likely that at the concentrations studied here the equilibrium is between monomeric $nBu_2Sn(OAc)_2$ and the dimeric species III. The data will be analysed in these terms,

bearing in mind that at very low concentrations type II associated monomers may exist. The ^{119}Sn chemical shift data will be analysed since the ^{13}C and ^{1}H data are invariant to changes in temperature and concentration.

The equilibrium may be written as the dissociation of the dimer thus:

$$\text{Dimer} \leftrightharpoons \text{Monomer} + \text{Monomer}$$

$$(1-\alpha)C \qquad \alpha C \qquad \alpha C \qquad \text{At equilibrium}$$

where α is the degree of dissociation and C the initial concentration of dimer, assuming no dissociation.

The equilibrium constant K may be written as

$$K = \frac{4\alpha^2C^2}{(1-\alpha)C} = \frac{4\alpha^2C}{(1-\alpha)} \qquad \ldots\ldots \quad 1$$

The equilibrium may be interpreted in terms of the tin nucleus being able to occupy one of two sites; either in the unassociated monomer or in the autoassociated dimer. Rapid exchange between these two sites occurs and an average ^{119}Sn signal is observed. Consequently the observed chemical shift, δ_{OBS} is a weighted mean of the shift of the pure monomer, δ_M and the shift of the pure dimer δ_D. So the observed chemical shift is given by:-

$$\delta_{OBS} = \frac{(1-\alpha)\ \delta_D + 2\alpha\delta_M}{1+\alpha} \qquad \ldots\ldots \quad 2$$

Equation 2 describes the behaviour of the observed shift as a function of the degree of dissociation, α. The pure monomer shift and pure dimer shift are expected to be constant. Obviously α varies in accordance with the equilibrium constant K, which is in turn related to

changes in temperature by ΔH^o (in this case the molar enthalpy of dissociation) in accordance with the Van t'Hoff equation.
So equation 2 describes a sigmoid curve with two limiting shifts δ_D and δ_M (see Figure 2). For a given pair of limiting shifts the details of the curve will depend on the thermodynamics of the equilibrium specifically the equilibrium constant and ΔH^o, the enthalpy change.

As has been shown above the two limiting shifts will only be observed if α can take the values from 0 to 1. If the equilibrium favours one species (ie if K is large or small) then only a portion of the curve will be observed. The rate of change of the observed shift with temperature will depend primarily on ΔH^o, a small value of ΔH^o indicating a small fractional change in K for a given temperature change and a large ΔH value a large change in K. These two situations are indicated by the dashed and solid lines respectively in Fig. 2.

From Fig. 1 it is apparent that only the high temperature limiting shift is observed indicating that the equilibrium constant is large and that ΔH^o is relatively small.

The limiting shift in Fig. 1 can be extrapolated to be -148 ppm. This is taken as the shift of the pure unassociated species since high temperature will tend to dissociate the dimer. Also the observed shift tends to be less negative on dilution which is expected to favour the dissociated species (see sections B&C).

It is apparent from equation 2 that for a given observed chemical shift at differing concentrations, since δ_D and δ_M are constant α must also be constant. It follows from equation 1 therefore that for a given shift the equilibrium constant is proportional to the concentration.

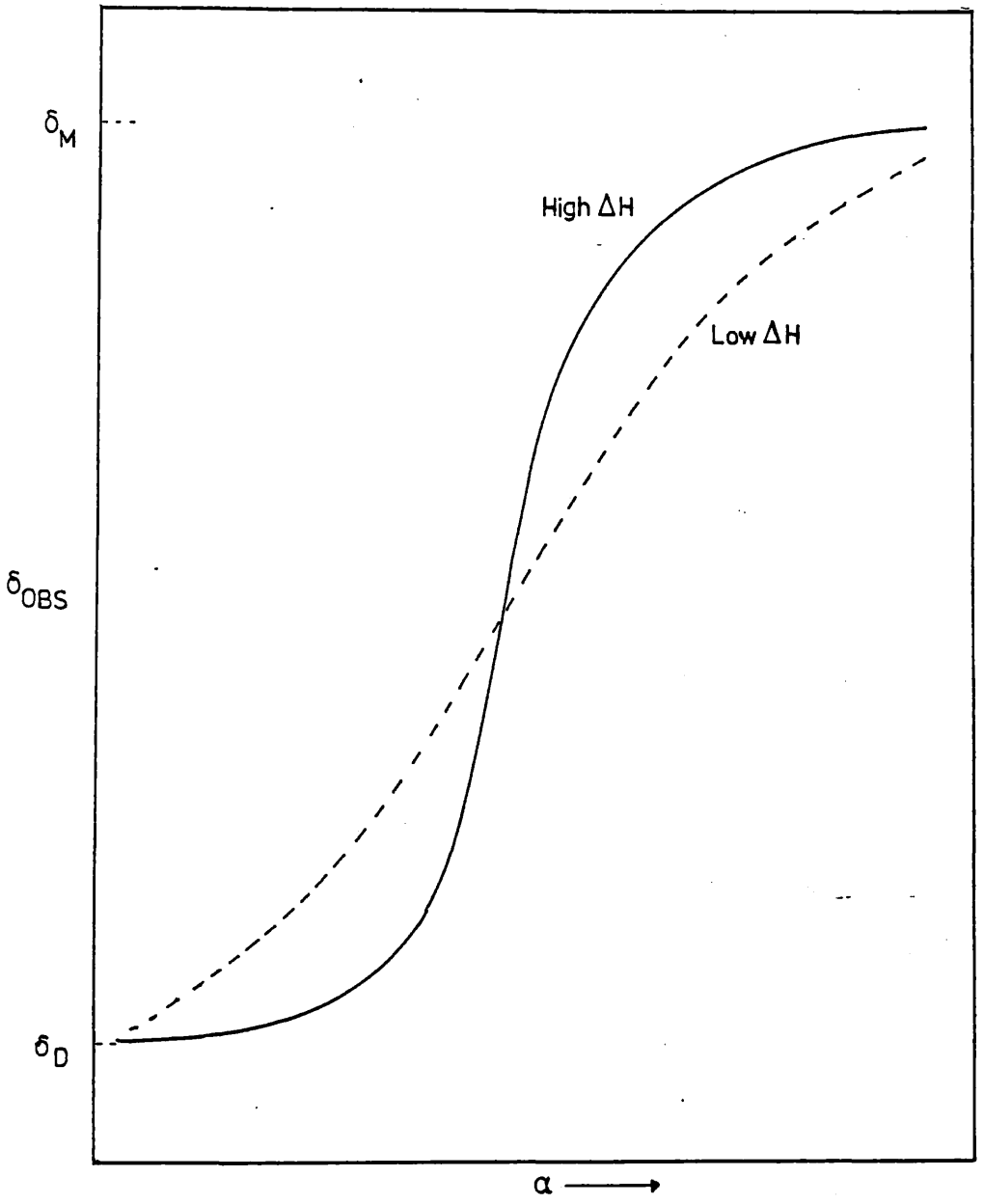

Figure 2

The variation of the observed chemical shift (δ_{OBS}) with the degree of dissociation (α).

Therefore from Fig. 1 we may choose a shift, δ_{OBS} and read off the temperature axis the temperature at which each of the four concentrations have the same δ_{OBS} and α. At each of these temperatures, therefore equation 3 holds and consequently a plot of lnC vs.1/Temperature will yield the molar enthalpy for the dissociation of the dimer. Table 6 shows some values of temperature for various observed shifts interpolated from Fig. 1. Figure 3 summarises these. Note that good straight lines result for these plots giving an average $\Delta H^{o} = +18.15 \pm 0.76$ KJ mol^{-1}.

Knowledge of ΔH and δ_M facilitates the estimation of K and δ_D by the following method.

It has been shown in section 1 of this chapter that the ^{119}Sn chemical shift moves to high field when the coordination number of tin increases from four to five or six. It has also been shown, albeit tentatively that $nBu_2Sn(OAc)_2$ exists in solution as an equilibrium mixture of four coordinate monomers and five coordinate dimers thus enabling an estimate of δ_D to be made, insofar as it will be to high field relative to the monomers (see section 1C). If an estimate of δ_D is made which is 100 ppm upfield from δ_M then simple rearrangement of equation 2 yields α for a given δ_{OBS}. Using equation 1 enables K to be calculated for different concentrations. For a given temperature K must be the same at all concentrations, and consequently any variation in K must be due to a wrong choice of δ_D. A simple program was written (see appendix 1) to vary δ_D and calculate equilibrium constants at the different concentrations studied in this work. Errors in K for given temperatures were estimated. The minimum error was chosen and the δ_D associated with it taken as the

Table 6

δ_{OBS}/ppm	−158	−160	−162	−164	−166	−168
Conc/mol l^{-1}	Temperature/K					
1.852	332	320	308.5	299	290	283
1.205	313	300	289	280	272	264
0.849	297	288	278	269	260.5	254
0.443	280	267	257	247	240	234
ΔH°/kJmol^{-1}	21.13	19.33	18.50	17.04	16.64	16.28

ΔH mean = 18.15 $\pm$ 0.76 kJ mol^{-1}

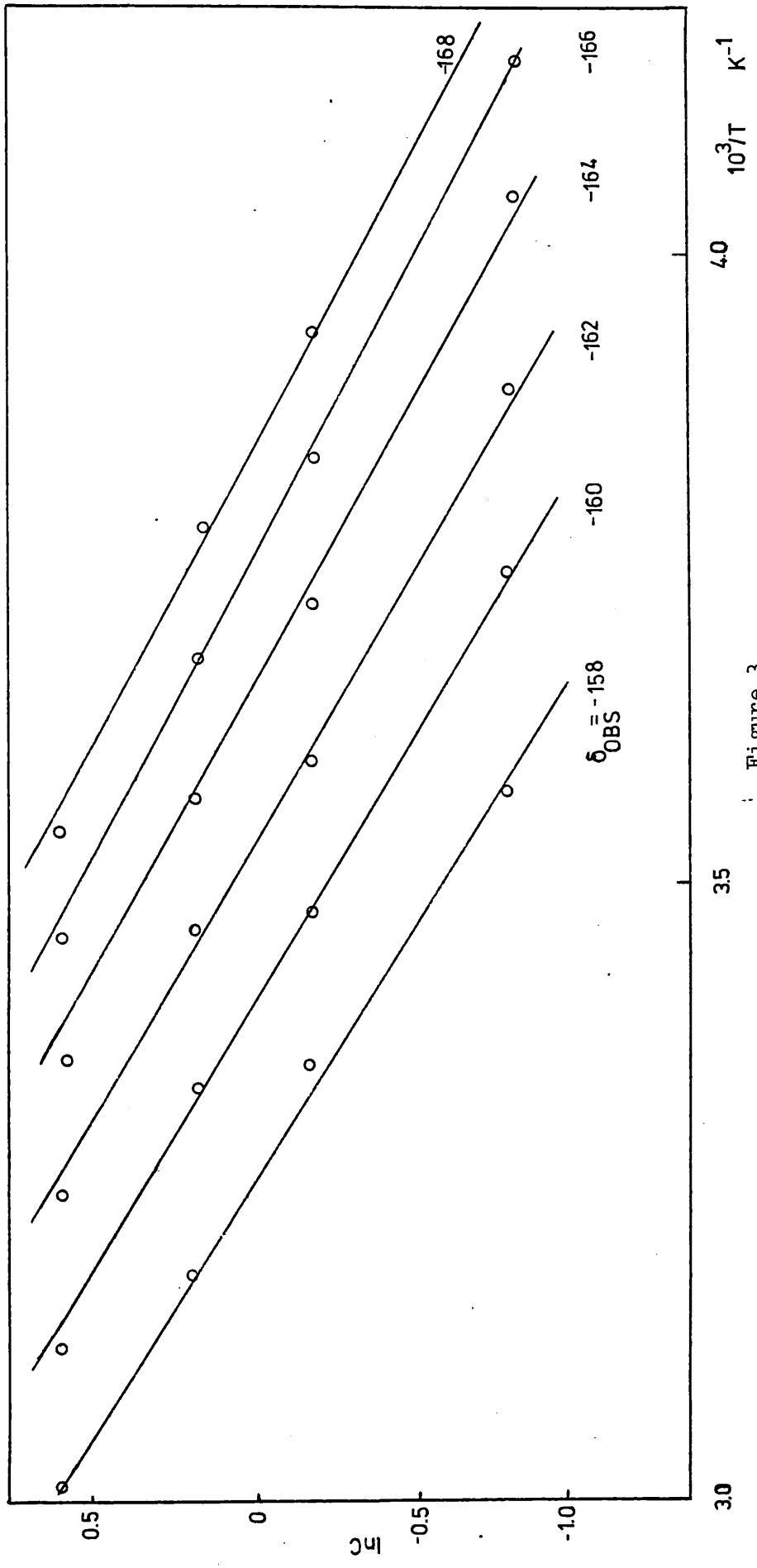
0.5
0
-0.5
-1.0
$\bar{\delta}_C$
3.0
3.5
4.0
$10^3/T$ K^{-1}
$\delta_{OBS} \equiv -158$
-160
-162
-164
-166
-168

Figure 3

shift of the dimer. Figure 4 shows a typical error curve. It should be noted that values of δ_D that are obviously wrong give very large errors. From this analysis the best value of δ_D is calculated to be -210.0 ppm.

The analysis was carried out over the temperature range 293 - 213 K where the change in δ_{OBS} is greatest and where the procedure should be most sensitive to changes in δ_D. In practice the program indicated a number of different values for δ_D which varied in a non-systematic manner with temperature (see Table 7). The mean value of -210 ppm was taken as the true value. The mean equilibrium constants (K_{mean}) calculated between 293-313 K are tabulated in Table 7 and a plot of ln K_{mean} vs 1/Temp. shown in Fig. 5. The molar enthalpy change, ΔH calculated from this plot is $+18.05 \pm 0.73$ kJ mol^{-1} which is in excellent agreement with the value derived from the plot of lnC vs 1/Temp. (Fig. 3).

Knowledge of δ_D, δ_M and K facilitates the calculation of δ_{OBS} for any temperature and concentration. Figure 6 shows the experimental points and the lines predicted from the calculated parameters. For the three strongest concentrations the calculated lines agree very well with the experimental data and only show significant variation for the neat solution at high temperature. This is to be expected since under such conditions the dimer is almost completely dissociated and δ_{OBS} is consequently insensitive to changes in the equilibrium constant. Changing δ_D by $\pm$ 10 ppm significantly alters the calculated lines indicating the sensitivity of δ_{OBS} to the value of δ_D.

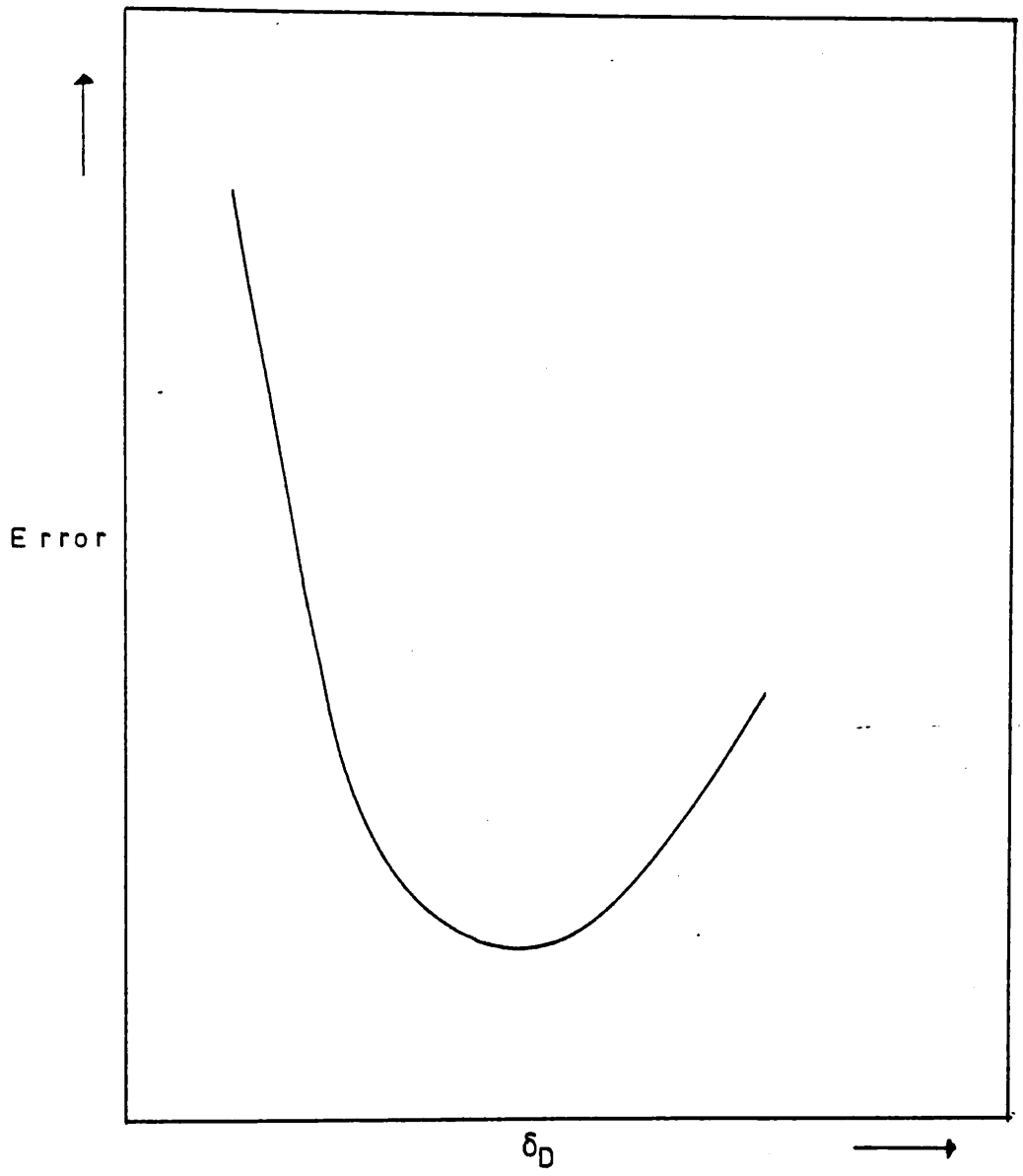

Figure 4

Table 7

Temp/K	Calculated δ_D/ppm	K_{mean}/mol^{-1}
293	-212.0	5.4694
297	-211.5	6.0731
301	-216.0	6.6815
305	-205.0	7.1123
309	-207.0	8.1281
313	-208.0	8.8015

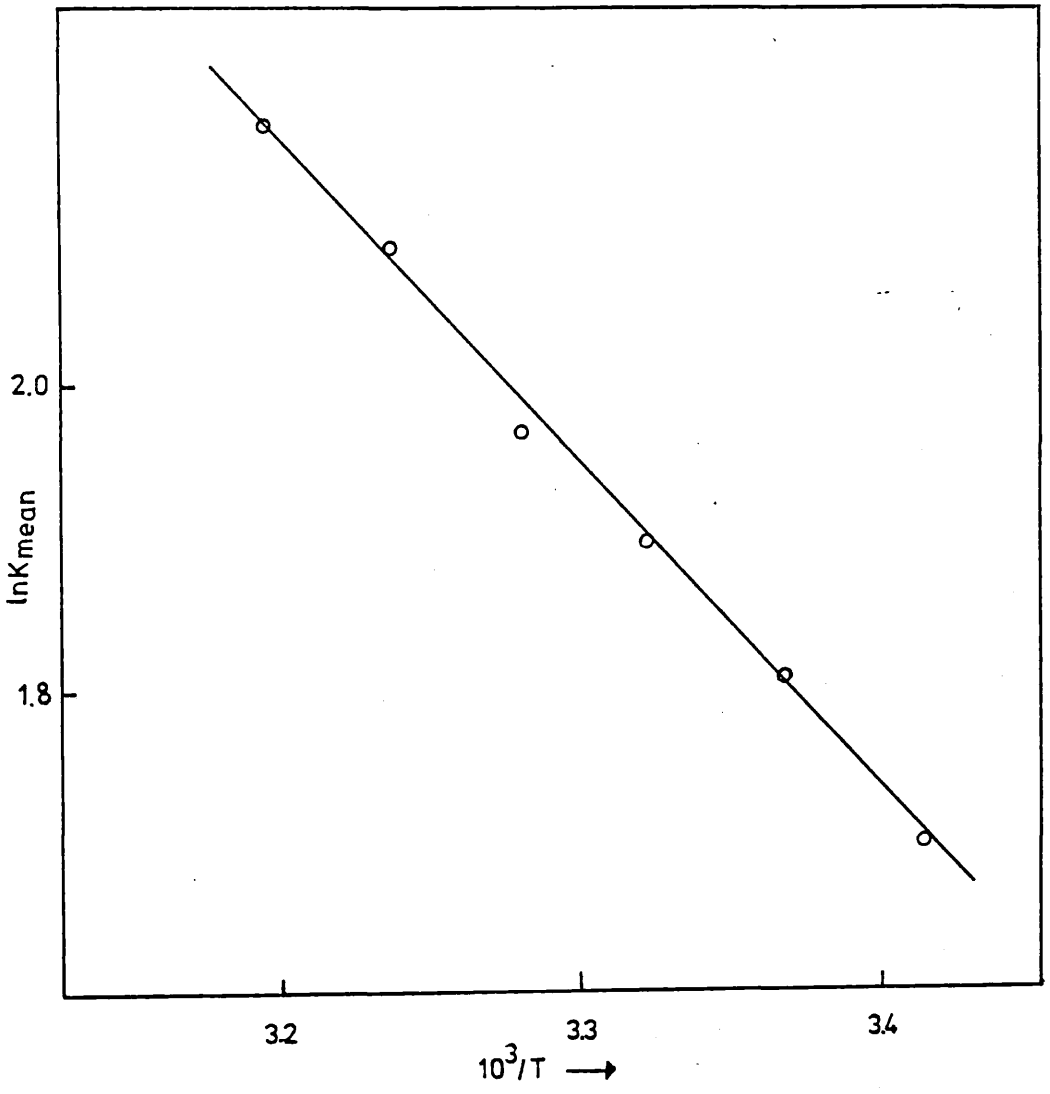

Figure 5

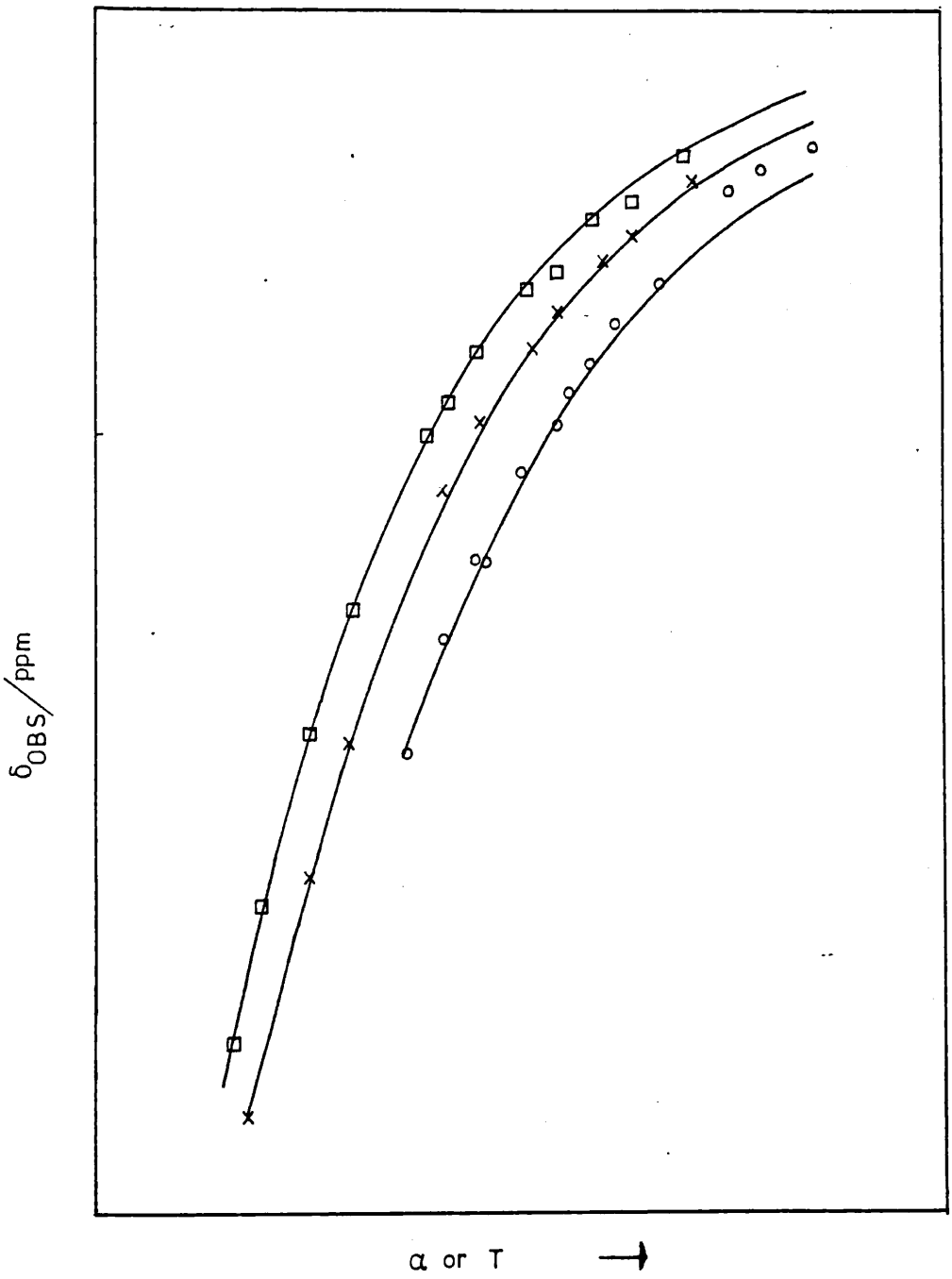

Figure 6

—— Calculated lines using $\delta_M = -148_{ppm}$ and $\delta_D = -210$ ppm

o, x, □ Experimental points. Key as in Fig. 1

The data for the weakest concentration $nBu_2Sn(OAc)_2$ could not be fitted to the parameters used above. It is possible that at these dilutions a more complicated equilibrium occurs involving intramolecular hexacoordinated species of type II as indicated by Maeda and Okawara[32] as well as the intermolecular dimer III. No further attempt was made to fit these data.

The value of ΔH^o for the dissociation of the di n-butyl tin diacetate dimer is somewhat small compared to the values calculated by Kennedy et al for various alkoxides where bridging occurs via the oxygen. Typical values of ΔH^o for the dialkoxides are approximately 60-70 kJ mol^{-1}. Our value of ΔH^o for the dissociation of the diacetate is 18 kJ mol^{-1}. This can be attributed to two factors:

(i) the oxygen atom of an alkoxy group is a stronger electron donor than an oxygen atom of a carbonyl and hence forms a stronger intermolecular bond to tin.

(ii) the stereochemistry about the carbon atom of the carbonyl group in the diacetate is such that overlap of the p orbitals of the oxygen with the d orbitals of tin is not as favourable as the overlap occurring when the alkoxy oxygen takes part in the intermolecular bond.

The two factors above conspire to reduce the strength of the intermolecular bonds of the dimer in $nBu_2Sn(OAc)_2$ compared to the dialkoxides thereby reducing ΔH^o. Furthermore the plots of observed ^{119}Sn chemical shifts vs temperature for the alkyl tin alkoxides[6] indicate that they exist almost totally as dimers at temperatures where the diacetate is still significantly dissociated.

B

Conclusion

Di n-butyl tin diacetate exists in solutions of concentration 1.852 to 0.849 mol l^{-1} as an equilibrium mixture of four coordinated monomers (I) and pentacoordinated dimers (III). Intramolecular hexacoordinated monomers (II) may take part in the equilibrium at lower concentrations. The equilibrium constant at 298°K is found to be 6.2 mol l^{-1} and ΔH^{o}= 18.1 kJ mol^{-1}.

C

Advantage of Pulse FT compared to INDOR

The investigation described in this chapter demonstrates the suitability of direct pulse FT observation of ^{119}Sn signals. All previous work on similar systems utilises the INDOR method to detect the resonances (see reference 6 for instance). This requires well resolved ^{119}Sn satellites in the proton spectrum to yield accurate tin chemical shifts. For organo tin molecules containing n-butyl groups the satellites tend to be broad due to the complexity of the butyl proton resonances. Tin -119 chemical shifts derived from such experiments are estimated to be accurate to $\pm$ 3 ppm.[6] The use of direct observation by the pulse method and proton noise decoupling increases the accuracy to $\pm$ 0.1 ppm irrespective of the organic groups bound to the tin atom. Only severe line broadening of the ^{119}Sn resonance will significantly affect this value. Although the INDOR method utilises the sensitivity of the proton to detect ^{119}Sn signals, signal averaging and proton noise decoupling in the pulse FT mode overcome the sensitivity problem of observing ^{119}Sn signals directly. Consequently direct observation by pulse FT yields more

accurate ^{119}Sn chemical shift data in a shorter time. If the variation of observed chemical shifts is small, as in this study this increased accuracy could be crucial as to whether or not a meaningful analysis of the data can be carried out.

Experimental

The sample of di n-butyl tin diacetate was purchased from Cambrian Chemicals. Proton and ^{13}C NMR spectra showed no impurities and the infra red spectrum was identical to an authentic spectrum. The sample was used without further purification.

The ^{119}Sn spectra were recorded in pulse mode using the spectrometer described in chapter 3 under conditions of proton noise decoupling. The NMR sample tubes were 12 mm O.D. and the field-frequency lock maintained using perdeutero acetone or dimethyl sulphoxide in a 5 mm tube inserted in the larger tube (see Figure 7).

The temperature of the probe was controlled using the Varian unit V6040 and was measured using a Comark electronic thermocouple in a 12 mm tube. Good thermal contact was ensured by the use of oil (see Figure 8). Approximately thirty minutes were required for the temperature to stabilise and the same waiting period was used on introducing the sample to the probe prior to a shift measurement. Monitoring the shift served as a final check that the temperature was stable.

The shifts are estimated to be accurate to better than $\pm$ 0.1 ppm and the temperature maintained to within $\pm$ 0.3 K.

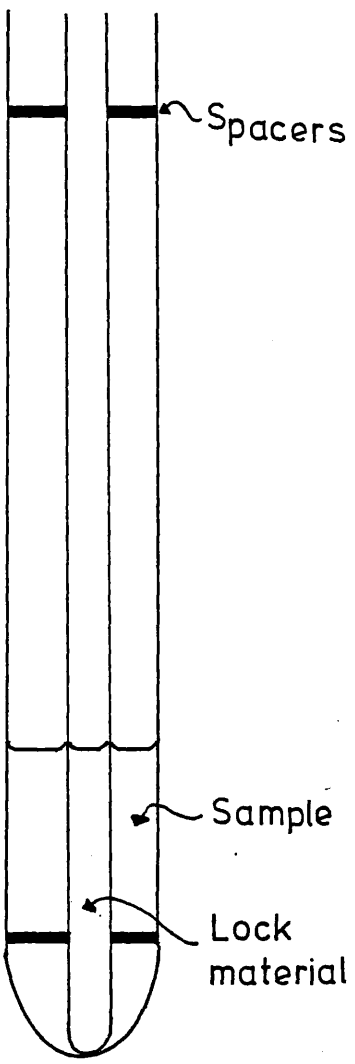

Figure 7

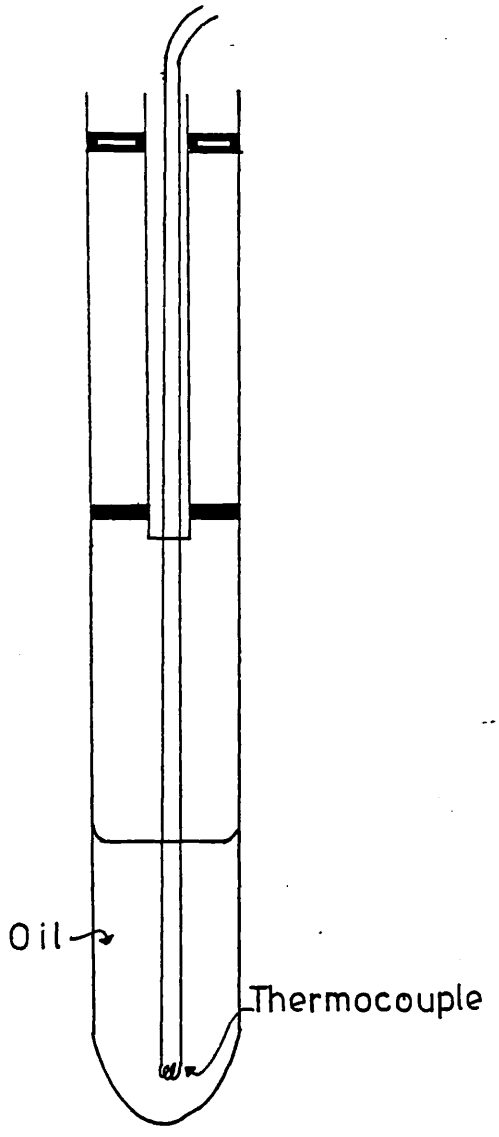

Figure 8

References

1 J.J. Burke, P.C. Lauterbur, J. Amer. Chem. Soc. (1961) 83 326.

2 B.K. Hunter, L.W. Reeves, Can. J. Chem. (1968) 46 1399.

3 A.G. Davies, P.G. Harrison, J.D. Kennedy, T.N. Mitchell, R.J. Puddephatt, W. McFarlane, J. Chem. Soc. C (1969) 1136.

4 A.P. Tupciauskas, Cand. Diss. Moscow State University, 1972.

5 L. Smith, Ph.D Thesis, University of London, 1972.

6 E.V. van den Berghe, G.P. van der Kelen, J. Organometal. Chem. (1968) 11 479.

7 T.F. Bolles, R.S. Drago, J. Amer. Chem. Soc. (1966) 88 1392.

8 W.D. Honnick, M.C. Hughes, C.D. Schaeffer, J.J. Zuckerman, Inorg. Chem. (1976) 15 1391.

9 E.V. van den Berghe, G.P. van der Kelen, L. Verdonck, J. Organometal. Chem. (1969) 16 497.

10 V.N. Torocheshnikov, A.P. Tupciauskas, N.M. Sergeyev, Yu. A. Astynyuk, J. Organometal. Chem. (1972) 35 C25.

11 V.S. Petrosyan, N.S. Yashina, O.A. Reutov, J. Organometal. Chem. (1973) 52 315.

12 V.S. Petrosyan, N.S. Yashina, O.A. Reutov, J. Organometal. Chem. (1973) 52 321.

13 V.S. Petrosyan, N.S. Yashina, O.A. Reutov, J. Organometal. Chem. (1973) 52 333.

14 D.W. Thompson, J.F. Lefelhocz, J. Organometal. Chem. (1973) 47 103.

15 Matsubayash, Okunaka, Tanaka, J. Organometal Chem. (1973) 56 215.

16 V.S. Petrosyan, N.S. Yashina, V.I. Bakhmutov, A.B. Permin, O.A. Reutov, J. Organometal. Chem. (1974) 72 71.

17 V.S. Petrosyan, O.A. Reutov, Pure Appl. Chem. (1974) 37 147.

18 D.P. Graddon, B.A. Rana, J. Organometal. Chem. (1976) 105 51.

19 W. McFarlane, R.J. Wood, J. Organometal. Chem. (1972) 40 C17

20 N. Kasai, K. Yasuda, R. Okawara, J. Organometal. Chem. (1965) 3 172.

21 R.A. Forder, G.M. Sheldrick, J. Organometal. Chem. (1970) 21 115.

22 J.C. Pommier, J. Valade, J. Organometal. Chem. (1968) 12 433.

23 J. Mendelsohn, J.C. Pommier, J. Valade, Compt. Rend. Ser. C. (1966) 263 921.

24 D. Sukhani, V.D. Gupta, R.C. Mehrotra, J. Organometal. Chem. (1967) 7 85.

25 P.J. Smith, R.F.M. White, L. Smith, J. Organometal. Chem. (1972) 40 341.

26 J.D. Kennedy, J. Chem. Soc. Perkin II (1977) 242.

27 D.L. Alleston, A.G. Davies, M. Hancock, R.F.M. White, J. Chem. Soc. (1963) 5469.

28 W.J. Considine, G.A. Baum, R.C. Jones, J. Organometal. Chem. (1965) 3 308.

29 T.N. Mitchell, Org. Magn. Res. (1976) 8 34.

30 A.G. Davies, L. Smith, P.J. Smith, W. McFarlane, J. Organometal. Chem. (1971) 29 245.

31 J.D. Kennedy, W. McFarlane, Revs. Si. Ge, Sn, Pb (1974) 1 235.

32 Y. Maeda, R. Okawara, J. Organometal. Chem. (1967) 10 247.

33 R. Okawara, D.E. Webster, E.G. Rochow, J. Amer. Chem. Soc. (1960) 82 3285.

34 M.J. Janssen, J.G.A. Luuten, G.J.M. van der Kerk, Rec. Trav. Chim. (1963) 82 90.

35 T.N. Mitchell, J. Organometal. (1973) 59 189.

36 A.G. Maddock, R.H. Platt, J. Chem. Soc.(A) (1971) 1191.

37 J.D. Kennedy, J. Chem. Soc. Perkin II (1977) 242.

38 J.D. Kennedy, W. McFarlane, P.J. Smith, R.F.M. White, L. Smith J. Chem. Soc. Perkin II (1973) 1785.

39 P.J. Smith, R.F.M. White, L. Smith, J. Organometal. Chem. (1972) 40 341.

CHAPTER 9

Concluding Remarks

Concluding Remarks

The most striking of the ^{119}Sn spin-lattice relaxation times has been their length and the large NOE associated with them. These characteristics have significant practical implications for obtaining Fourier ^{119}Sn NMR spectra. Obviously short T_1's are advantageous from the point of view of $(90-\tau)_n$ pulse experiments since the delay (τ) is kept short. However under conditions of proton decoupling the presence of large NOE factors which are typical for alkyl tin compounds (other than the smallest) reduces the intensity of the resonances negating the advantage of the relatively short T_1 values. Suppression of the NOE effect by the gated decoupling technique restores the intensities but a time penalty has to be paid since one needs to wait 10 T_1 in order to completely suppress the NOE. In practice, though if sensitivity is the objective the experiment can be run faster. A further complication arises when there is significant scalar relaxation as in alkyl tin halides. This reduces T_2 (not T_1) causing line broadening. The use of shiftless relaxation reagents has only recently begun to be investigated and such compounds will be welcomed by all involved in Fourier transform ^{119}Sn NMR. Such methods however are of limited use if relaxation behaviour is under investigation and the large NOE factors for ^{119}Sn are certainly a problem when measuring T_1's. The use of gated decoupling when measuring T_1's is not advised since the values thus obtained may not be characteristic of the true ^{119}Sn T_1. Unfortunately then the experimenter is faced with decreasing sensitivity as the NOE increases which results in the need for many free induction decays being accumulated in order to build up sufficient signal for spectra to be observed.

The spin-rotation relaxation mechanism is expected to be important in relaxing ^{119}Sn because of the large chemical shift range of this nucleus and this has been confirmed in a number of molecules in this work. The relationship between R_1^{SR} and the paramagnetic term (σp) of the screening constant has been demonstrated.

The motional behaviour of the organotin molecules studied in this work suggests that the overall motion is not too anisotropic even where the molecules are not spherical tops. Even for Ph_3SnH where the anisotropy is expected to be most marked the ratio of the diffusion constants $D_{\parallel} / D_{\perp}$ is found to be 0.49.

In the n-alkyl tin compounds studied the ^{13}C relaxation data indicates segmental motion with the inertial effect of the tin nucleus effectively anchoring the alkyl methylene groups differentially.

The values of the effective correlation times derived from the ^{119}Sn and α-^{13}C data are consistently different, the values calculated from the ^{13}C data being approximately three times faster. This is not surprising since the tin-remote α proton vector and the ^{13}C-H vector make different angles to the main symmetry axis. Also there is rotation about the tin-carbon bond which will reduce the correlation time for the ^{13}C-H vector. This is quite a useful aspect of the carbon relaxation data since it seems that τ_c^{eff} for the tin-remote proton vector can beestimated (albeit crudely) by measuring a ^{13}C T_1. For workers with access to a ^{13}C spectrometer without facilities for observing ^{119}Sn this could well be important.

Except for the investigation of Ph_3SnH the choice of molecules has been such that the vectors have been somewhat ill-defined and have consequently limited the detailed understanding of the motional behaviour

of these molecules. The overall impression from the available data is that the organotin molecules reorient somewhat slowly. As has been shown it is quite common to observe correlation times between 30 and 100 ps. This observation should be tempered with the fact that the vectors from which these correlation times have been derived are not fixed and must therefore be somewhat imprecise. However comparison with analogous carbon and silicon molecules (and therefore closely related vectors) reveals that the organotin molecules do indeed reorient comparatively slowly. This is attributable to the large inertial effect of tin. It is this slow reorientation of such organotin molecules that enables non-bonded protons to contribute significantly to the dipolar relaxation of ^{119}Sn.

APPENDIX A

T_1 and NOE data for ^{119}Sn and ^{13}C nuclei in

$n\text{-}Bu_3SnH$(neat)

^{13}C T_1 measured at PCMU on Bruker HX 90

^{119}Sn T_1 and NOE measured using JEOL FX100Q

T = 233 K	M_τ			
τ /S	α	β	γ	δ
2.2			57.0	57.5
1.9			56.0	
1.6				52.5
1.3	43.0	51.0	45.0	39.0
1.0	39.0	44.0	40.0	25.5
0.8	37.0	36.5	33.0	19.0
0.7	33.0	32.5	22.0	14.0
0.55	28.0	24.5	15.0	1.0
0.4	17.0	8.0	5.0	-8.0
0.3	9.0	-2.0	-3.0	-14.0
0.1	-18.0	-26.0	-33.0	-39.0
0.05	-28.0	-39.0	-34.0	-45.0
M_∞	50.0	59.5	60.0	64.0
T_1/S	0.51	0.51	0.61	0.75

T = 243 K	M_τ			
τ /S	α	β	γ	δ
2.2			59.0	48.0
1.9	49.0	51.0	46.5	39.0
1.6	48.0	50.0	45.0	35.0
1.3	46.0	43.0	36.0	22.0
1.0	35.0	30.0	25.0	16.0
0.7	30.0	18.0	12.0	0.0
0.4	7.0	-6.9	-11.0	-21.5
0.1	-28.0	-39.0	-42.0	-40.0
M_∞	51.0	61.0	69.0	64.0
T_1/S	0.66	0.74	0.79	1.16

T = 253 K	M_τ			
τ/S	α	β	γ	δ
3.0	50.5	57.5	52.0	51.0
2.6	51.5	55.5	50.5	46.0
2.2	44.0	50.5	48.0	35.5
1.8	43.0	43.0	38.0	31.0
1.4	37.0	33.5	20.5	18.0
1.0	24.5	12.0	9.0	0.0
0.6	6.0	-2.0	-9.5	-18.0
0.2	-21.5	-36.0	-38.0	-39.5
M_∞	54.0	62.0	63.5	65.0
T_1/S	0.84	0.89	1.19	1.39

T = 263 K	M_τ			
τ/S	α	β	γ	δ
3.6		53.5	49.0	45.5
3.1	46.5	49.0	42.6	34.3
2.6	41.0	41.0	33.6	28.2
2.1	41.0	33.0	30.0	22.2
1.6	31.0	24.0	20.0	6.5
1.1	14.8	11.0	0.0	-1.0
0.6	-1.0	-15.0	-17.0	-24.0
0.1	-40.5	-46.0	-45.0	-51.0
M_∞	51.0	64.5	61.0	63.3
T_1/S	1.03	1.55	1.67	2.03

T = 273 K	M_τ			
τ/S	α	β	γ	δ
5.1	53.0	56.0	44.0	45.0
4.4	40.0	44.5	34.0	28.0
3.7	39.5	43.8	35.0	25.0
3.0	35.5	33.0	27.0	23.7
2.3	29.0	25.0	19.0	10.5
1.6	1.8	5.5	0.0	0.0
0.9	0.0	-7.0	-12.5	-17.4
0.2	-26.0	-36.5	-35.5	-34.4
M_∞	57.0	65.7	47.0	64.0
T_1/S	1.90	2.27	2.63	3.39

T = 293 K	M_τ			
τ/S	α	β	γ	δ
7.0	39.3	46.0	35.0	34.5
6.0	38.5	41.0	32.6	31.5
5.0	37.0	38.0	28.0	25.0
4.0	26.5	28.0	22.0	16.0
3.0	16.5	9.0	7.5	6.0
2.0	8.5	0.0	-2.0	-9.5
1.0	-12.0	-21.0	-18.0	-25.0
M_∞	51.0	65.0	56.0	54.6
T_1/S	3.33	3.86	4.56	4.20

T = 313	M_τ			
τ/S	α	β	γ	δ
15.0	47.0	55.6	49.5	48.0
13.0	53.0	58.0	46.5	52.5
11.0	38.0	48.0	39.5	38.5
9.0	40.5	45.0	34.5	32.0
7.0	36.0	34.5	26.5	25.5
5.0	15.0	15.0	13.0	7.0
3.0	8.0	4.0	3.0	5.0
1.0	-19.5	-28.0	-29.5	-37.5
M_∞	54.0	64.0	60.0	65.0
T_1/S	4.36	5.24	6.73	7.32

T = 333	M_τ			
τ/S	α	β	γ	δ
10.8	39.5	40.0	33.0	33.0
9.6	42.0	36.5	31.5	30.0
8.4	35.0	28.0	23.5	21.0
7.2	29.5	24.0	17.0	15.5
6.0	22.0	18.5	10.5	9.5
4.8	15.0	5.0	-1.0	-1.0
3.6	5.5	-4.0	-10.5	-12.0
2.4	-6.0	-16.0	-21.4	-20.0
M_∞	52.5	62.0	63.5	62.0
T_1/S	4.90	6.44	7.80	7.83

T = 353 K	M_τ			
τ/S	α	β	γ	δ
15.0	40.0	41.0	32.6	35.2
13.0	38.5	33.0	27.0	29.6
11.0	34.5	27.0	23.0	24.0
9.0	30.0	22.0	12.0	15.0
7.0	20.0	11.0	3.6	4.5
5.0	6.0	0.0	-5.5	-5.5
3.0	-7.0	-16.0	-17.5	-21.0
1.0	-27.0	-34.0	-36.0	-41.0
M_∞	54.0	59.5	58.5	63.0
T_1/S	7.57	9.01	10.91	10.68

T = 383 K	M_τ			
τ/S	α	β	γ	δ
15.0	37.5	32.0	23.0	31.0
13.0	32.0	25.0	18.0	27.0
11.0	25.0	16.0	8.5	15.5
9.0	16.0	7.5	2.5	10.5
7.0	6.0	1.0	-5.0	-1.0
5.0	0.0	-6.0	-14.0	-11.2
3.0	-11.5	-19.0	-24.0	-30.0
1.0	-28.0	-31.0	-33.5	-47.3
M_∞	53.2	60.0	56.0	65.0
T_1/S	8.74	12.30	14.00	11.64

T = 307 K	M_τ			
τ/S	α	β	γ	δ
0.5	-3803	-4424	-4710	-5032
1.0	-2051	-2689	-2513	-3336
2.0	644	-387	-1169	-1437
3.0	2639	1857	1029	820
4.0	4238	3621	2942	2694
5.0	4395	4694	4111	3906
6.0	6127		5441	5279
7.0	6684			6159
M_∞	8516	9601	10622	10303
T_1/S	3.43	4.24	5.13	5.06
η	1.62	1.49	1.66	1.61

^{119}Sn T_1 and NOE

T = 307 K	
τ/S	M_τ
0.2	-8531
0.5	-7084
1.0	-5755
1.5	-3995
2.0	-2434
2.5	-1121
3.0	247
4.0	2237
5.0	3670
M_∞	10551
T_1/S	4.66
η	-0.43

T_1 and NOE data for ^{119}Sn and ^{13}C nuclei

in nBu_3SnCl (neat)

^{119}Sn T_1 and NOE measured using spectrometer described in Chapter 3

^{13}C T_1 and NOE measured using JEOL FX 100Q

T = 250.7 K	
τ/S	M_τ
0.2	-163.5
0.4	-82.0
0.6	-27.0
0.8	-11.0
1.0	24.0
1.2	72.5
1.4	83.0
1.6	117.5
1.9	150.0
M_∞	256
T_1/S	1.30

T = 257.7 K	
τ/S	M_τ
0.2	-155.5
0.4	-180.0
0.7	-51.0
0.9	-43.5
1.2	0.0
1.5	44.0
1.8	69.0
2.1	81.0
2.5	123.0
M_∞	233.0
T_1/S	1.89

T = 262.9 K	
τ/S	M_τ
0.1	-190.0
0.5	-116.0
1.0	-77.5
1.4	0.0
2.0	46.0
2.5	75.0
3.0	131.0
3.5	146.0
M_∞	248.0
T_1/S	2.30

T = 300.3 K	
τ/S	M_τ
0.1	-183.0
0.5	-166.0
1.0	-150.5
2.0	-82.0
3.0	-45.0
5.0	46.0
6.5	65.0
9.0	111.0
M_∞	195.0
T_1/S	5.74

T = 319.3 K	
τ/S	M_τ
0.2	-149.0
1.0	-134.0
2.0	-75.0
3.0	-32.0
4.0	0.0
5.0	26.5
6.0	53.0
7.0	77.0
8.5	94.0
M_∞	187.0
T_1/S	6.12

T = 338 K	
τ/S	M_τ
0.2	-170.0
0.8	-143.0
1.8	-76.0
2.8	-33.0
3.8	0.0
5.0	42.5
6.0	64.0
7.0	85.5
M_∞	203
T_1/S	5.82

T = 370.7	
τ/S	M_τ
0.2	-179.0
1.0	-108.0
2.0	-40.0
3.0	-6.0
4.0	48.5
5.0	71.0
6.0	103.0
7.0	119.5
M_∞	213.0
T_1/S	4.75

T = 381.5	
τ/S	M_τ
0.1	-178.0
1.0	-108.0
2.0	-36.0
3.0	25.0
4.0	56.0
5.0	82.5
6.0	116.0
7.0	118.0
M_∞	184.0
T_1/S	3.83

T = 390.4	
τ/S	M_τ
0.2	-165.5
0.7	-95.0
1.2	-70.0
2.0	-14.5
3.0	30.5
4.0	67.0
5.0	89.0
7.0	123.0
M_∞	177.0
T_1/S	3.73

T = 410.4	
τ/S	M_τ
0.1	-169.0
0.6	-123.5
1.1	-53.0
1.7	-33.0
2.4	42.0
3.0	52.0
3.5	81.0
4.5	124.0
M_∞	192.0
T_1/S	2.71

^{119}Sn NOE data for nBu_3SnCl

Temp/K	Intensity (gated) Ig	Intensity with NOE Iw	η
253.5	204.0	-68.0	-1.33
266.5	211.5	-54.0	-1.26
276.6	216.0	-35.5	-1.16
285.0	209.5	-18.0	-1.09
300.4	198.0	32.5	-0.84
317.2	215.5	108.0	-0.50
330.6	214.0	148.5	-0.30
341.8	220.5	187.0	-0.15
348.0	198.5	153.0	-0.23
368.3	211.0	144.0	-0.32
394.5	189.0	194.0	0.0

^{13}C Inversion recovery and NOE data

for nBu_3SnCl

T = 307°K	M_τ			
τ/S	α	β	γ	δ
0.1	-3618	-4354	-4522	-4887
0.3	-2106	-3048	-3563	-4049
0.5	-899	-2272	-2731	-3512
0.7	336	-1513	-2237	-3206
1.0	1409	-423	-1171	-2241
1.5	2728	1174	424	-1168
2.0		2369	1364	439
2.5		3272	2268	821
3.0			2947	1671
M_∞	5491	5947	5970	6560
T_1/S	1.13	1.83	2.31	3.40
η	1.90	2.0	2.0	1.88

T_1 and NOE data for ^{119}Sn and ^{13}C nuclei in nPr_3SnCl (neat)

^{119}Sn T_1 and NOE measured using spectrometer described in Chapter 3

^{13}C T_1 and NOE measured using JEOL FX100Q

^{119}Sn T_1 data

T = 279.5 °K	
τ /S	M_τ
0.2	-173.5
0.6	-153.5
1.5	-87.0
2.5	-32.0
4.0	28.5
7.5	111.5
9.0	142.0
M_∞	200.5
T_1/S	4.84

T = 299.3 K	
τ/S	M_τ
0.1	-180.0
0.3	-167.0
0.8	-127.0
1.4	-92.0
2.0	-57.0
3.2	0.0
3.8	27.0
5.0	60.0
6.0	93.5
M_∞	192.0
T_1/S	4.53

T = 313.6 K	
τ /S	M_τ
0.5	-164.0
1.5	-101.0
2.5	-29.0
3.5	6.0
4.5	36.0
5.5	72.0
6.5	106.0
7.5	117.5
M_∞	213.0
T_1/S	5.01

T = 331.2 K	
τ/S	M_τ
0.5	-153.0
1.5	-83.0
2.5	-19.0
3.5	33.5
4.5	79.0
6.5	127.0
7.5	145.0
M_∞	204.0
T_1/S	3.83

T = 344.0 K	
τ/S	M_τ
0.3	-169.5
1.0	-105.0
1.7	-53.5
2.4	0.0
3.0	41.0
3.7	68.0
4.5	114.0
5.4	137.0
M_∞	221.0
T_1/S	3.27

T = 358.9 K	
τ /S	M_τ
0.5	-120.0
1.0	-77.0
1.5	-39.0
2.5	22.0
3.0	56.5
3.5	69.0
4.0	90.0
5.0	124.0
M_∞	194.5
T_1/S	3.05

$T = 385^{o}K$	
τ/S	M_τ
0.2	-170.0
0.5	-115.0
0.8	-66.0
1.4	0.0
2.0	37.0
2.6	94.0
3.1	113.5
3.7	137.0
M	221.0
T_1	2.28

^{119}Sn NOE data

Temp/ K	Intensity (gated) Ig	Intensity with NOE Iw	η
253.5	104.5	-8.0	-1.08
266.5	200.0	50.0	-0.75
276.6	195.5	55.5	-0.72
285.0	209.5	81.0	-0.62
300.4	206.0	137.0	-0.34
317.2	216.0	176.0	-0.19
330.6	220.0	172.0	-0.22
368.3	221.0	209.5	-0.05
394.5	209.0	183.5	-0.12

^{13}C T_1 and NOE data

T = 307 K	M_τ		
τ/S	α	β	γ
0.1	-7369	-7458	-7304
0.2	-6729	-6955	-6662
0.4	-5671	-6193	-6108
0.6	-4533	-5303	-5231
0.8	-3833	-4738	-4804
1.0	-3054	-4116	-4300
1.3	-1629	-2847	-3009
1.6	-684	-1959	-2402
2.0	682	-853	-1505
M_∞	8682	8601	7751
T_1/S	2.77	3.62	3.91
η	1.89	2.00	1.87

T_1 data for ^2H in nBu_3SnD (neat) using spectrometer described in Chapter 3

T = 258 K	
τ/S	M_τ
0.005	-178.0
0.01	-157.0
0.03	-128.0
0.05	-92.0
0.07	-67.0
0.09	-40.0
0.15	30.0
0.18	53.5
0.21	61.0
0.24	83.0
0.28	93.0
M_∞	172.0
T_1/S	0.18

T = 268.4 K	
τ/S	M_τ
0.01	-193.0
0.03	-152.5
0.05	-136.0
0.08	-87.0
0.10	-65.0
0.13	-48.5
0.18	-16.5
0.21	25.0
0.24	41.0
0.27	66.0
0.30	75.5
0.34	95.0
0.4	130.0
M_∞	213.0
T_1/S	0.26

T = 278 K	
τ/S	M_τ
0.01	-196.0
0.05	-148.0
0.10	-94.0
0.15	-58.0
0.20	-23.0
0.24	14.5
0.28	29.0
0.33	51.5
0.38	63.0
0.43	96.0
0.48	105.0
M_∞	198.0
T_1/S	0.33

T = 287.5 K	
τ/S	M_τ
0.01	-184.0
0.015	-170.0
0.021	-155.0
0.05	-138.0
0.10	-111.0
0.16	-77.0
0.22	-45.5
0.28	-20.0
0.35	19.0
0.42	39.5
0.50	65.0
0.58	84.0
0.65	101.5
M_∞	195.0
T_1/S	0.44

T = 298.5 K	
τ/S	M_τ
0.05	-190.0
0.10	-151.0
0.15	-121.5
0.2	-92.5
0.25	-77.0
0.30	-50.0
0.35	-29.0
0.50	36.0
0.55	48.0
0.60	52.0
0.70	80.0
0.80	97.0
0.90	115.0
M_∞	218.0
T_1/S	0.62

T = 311.7 K	
τ/S	M_τ
0.1	-135.0
0.2	-104.0
0.3	-61.0
0.4	-30.0
0.5	0.0
0.6	24.0
0.7	43.0
0.9	66.0
1.1	93.0
1.3	107.0
M_∞	162.0
T_1/S	0.70

T = 323.8 K	
τ /S	M_τ
0.1	-161.0
0.2	-117.0
0.3	-82.0
0.4	-59.0
0.5	-42.0
0.6	-18.0
0.8	31.0
1.1	74.0
1.3	100.5
1.6	122.5
M_∞	199.0
T_1/S	0.96

T = 336.0 K	
τ /S	M_τ
0.1	-166.0
0.2	-125.0
0.3	-96.5
0.4	-84.0
0.5	-51.0
0.6	-33.0
0.7	-14.0
0.9	28.0
1.1	51.5
1.3	70.0
1.5	96.5
M_∞	192.0
T_1/S	1.09

T = 356.0 K	
τ/S	M_τ
0.1	-171.5
0.2	-141.0
0.3	-108.0
0.4	-101.0
0.5	-70.0
0.6	-61.5
0.7	-57.0
0.8	-37.5
0.9	-15.0
1.1	9.0
1.3	35.5
1.5	49.0
1.7	62.5
2.0	78.5
M_∞	161.0
T_1/S	1.35

^{119}Sn T_1 and NOE data for Sn_2Me_6 (neat)

measured using spectrometer described in

Chapter 3

T = 331.5	
τ/S	M_τ
0.1	−101.0
0.3	−58.5
0.5	−34.0
1.0	16.0
1.2	28.0
1.4	53.5
1.6	44.0
1.8	67.0
2.0	81.0
M_∞	125.0
T_1/S	1.26

T = 341.4	
τ/S	M_τ
0.1	−129.0
0.3	−90.0
0.5	−42.0
0.9	22.5
1.1	43.0
1.3	69.0
1.5	86.5
1.7	102.0
2.0	124.0
M_∞	199.0
T_1/S	1.29

T = 347.3	
τ/S	M_τ
0.01	−178.0
0.1	−147.0
0.3	−88.0
0.4	−68.0
0.5	−43.0
0.9	30.0
1.0	50.0
1.2	73.5
1.4	101.0
1.6	123.0
M_∞	212.0
T_1/S	1.10

T = 356.0	
τ/S	M_τ
0.1	−160.0
0.2	−135.0
0.3	−83.0
0.4	−66.0
0.5	−38.0
0.8	30.5
0.9	43.0
1.0	65.5
1.2	88.0
1.4	114.0
M_∞	213.5
T_1/S	0.99

T = 366.0	
τ/S	M_τ
0.01	−190.0
0.1	−144.0
0.2	−108.0
0.3	−73.0
0.4	−58.0
0.5	−17.0
0.7	27.0
0.8	46.0
0.9	59.0
1.1	85.5
1.2	95.0
M_∞	197.5
T_1/S	0.89

T = 388.0	
τ/S	M_τ
0.01	-126.5
0.1	-101.0
0.2	-68.0
0.3	-37.0
0.4	-18.5
0.5	8.5
0.6	27.0
0.7	38.0
0.8	53.5
0.9	60.0
1.0	75.0
M_∞	130.0
T_1/S	0.65

T = 403	
τ/S	M_τ
0.01	-127.5
0.1	-87.0
0.2	-57.0
0.3	-41.0
0.6	33.0
0.7	49.0
0.8	56.0
0.9	67.5
1.0	75.0
M_∞	117.5
T_1/S	0.56

NOE data

Temp/K	Intensity (gated)	Intensity with NOE	η
329.7	210.0	166.0	-0.05
341.8	203.5	199.0	-0.05
368.3	209.0	210.0	0.0

^{13}C T_1 data of $n\text{-}Pr_3SnH$ (neat)

Measured at PCMU on Bruker HX90

T = 273 K	M_τ		
τ/S	α	β	γ
0.75	-37.0	-40.0	-37.0
1.50	-22.0	-25.0	-24.0
3.00	0.0	0.0	0.0
6.00	26.0	28.0	26.5
M_∞	56.0	63.5	50.0
T_1/S	4.66	5.04	4.22

T = 283 K	M_τ		
τ/S	α	β	γ
1.0	-36.0	-39.5	-34.0
2.0	-18.0	-22.0	-20.0
4.0	6.0	4.0	3.5
8.0	34.0	35.0	33.5
M_∞	59.0	64.5	64.5
T_1/S	5.27	5.56	6.03

T = 293 K	M_τ		
τ/S	α	β	γ
1.25	-28.0	-32.0	-29.0
2.5	-15.5	-18.0	-17.5
5.0	5.0	2.5	5.0
10.0	30.0	34.0	29.5
20.0		58.0	50.0
M_∞	55.5	64.0	60.5
T_1/S	7.36	6.73	8.74

T = 307 K	M_τ		
τ/S	α	β	γ
0.75	-36.0	-39.0	-35.0
1.5	-30.0	-31.5	-28.0
3.0	-16.5	-20.0	-16.0
6.0	5.0	3.5	3.0
12.0	31.0	32.0	29.0
24.0	50.0	54.0	49.0
M_∞	58.0	65.0	59.0
T_1/S	9.37	10.28	10.34

T = 318 K	M_τ		
τ/S	α	β	γ
2.0	-29.0	-32.0	-27.5
4.0	-13.0	-14.0	-13.0
8.0	11.5	7.0	8.0
16.0	40.0	39.5	36.0
M_∞	64.0	63.5	62.0
T_1/S	10.32	10.18	11.34

T = 333 K	M_τ		
τ/S	α	β	γ
1.5	-30.0	-35.0	-34.0
3.0	-18.0	-27.0	-21.5
6.0	-5.0	-10.0	-5.5
12.0	15.0	15.0	18.0
24.0	37.0	36.0	39.0
48.0	46.0	52.0	
M_∞	48.5	54.5	53.0
T_1/S	12.64	13.09	12.39

T = 353 K	M_τ		
τ/S	α	β	γ
1.5	-25.0	-26.0	-23.5
3.0	-19.5	-21.0	-16.0
6.0	-4.0	-7.0	-5.0
12.0	8.0	5.0	8.0
24.0	25.0	26.0	22.0
M_∞	42.0	40.0	37.0
T_1/S	16.57	14.63	16.37

^{13}C T_1 and NOE data for Ph_3SnH (90% v/v in toluene d_8)

Measured using Jeol FX100Q

T = 303 K	M_τ		
τ/S	C_o	C_m	C_p
0.01	-5192	-4513	-1129
0.02	-4874	-4401	-949
0.03	-4704	-4151	-762
0.05	-4316	-3817	-423
0.06	-4099	-3681	-296
0.07	-3844	-3602	-159
0.10	-3273	-3136	268
0.13	-2726	-2614	618
0.16	-2279	-2233	886
0.20	-1575	-1717	1129
M_∞	5517	4973	2244
T_1/S	0.468	0.543	0.168
η	1.80	1.71	1.75

T = 303 K	M_τ
τ/S	Carbon adjacent to tin
0.2	-2083
0.5	-1900
1.0	-1481
1.5	-926
2.0	-434
3.0	389
4.0	1145
5.0	1750
7.0	2723
M_∞	5335
T_1/S	6.490
η	1.40

^{119}Sn T_1 and NOE data for neat $nBu_2Sn(OAc)_2$

Measurements at 22.37 MHz using spectrometer described in Chapter 3.

T = 280 K	
τ/S	M_τ
0.05	-193.5
0.10	-115.0
0.15	-49.0
0.25	51.0
0.30	68.0
0.40	112.0
0.45	151.0
0.50	174.0
0.60	206.0
M_∞	288.0
T_1/S	0.32

T = 299.8 K	
τ/S	M_τ
0.1	-173.5
0.3	-83.5
0.5	-26.0
0.8	54.5
1.0	91.5
1.2	116.0
1 4	153.0
M_∞	235.0
T_1/S	0.84

T = 312.7 K	
τ/S	M_τ
0.1	-164.5
0.3	-137.5
0.4	-92.5
0.6	-59.0
1.0	-9.0
1.4	52.5
1.6	79.0
1.8	109.0
1.0	116.0
M_∞	223.0
T_1/S	1.44

T = 319.3 K	
τ/S	M_τ
0.1	-122.0
0.3	-117.0
0.5	-75.5
0.8	-39.0
1.2	0.0
1.5	35.0
1.8	68.0
2.2	93.0
2.6	116.0
M_∞	218.0
T_1/S	2.00

T = 325.8 K .	
τ/S	M_τ
0.1	-179.0
0.5	-111.0
0.8	-89.0
1.1	-54.0
1.5	-17.0
2.0	29.5
2.5	67.0
3.0	89.0
3.5	116.0
M_∞	234.0
T_1/S	2.74

T = 337.5 K	
τ/S	M_τ
0.5	-139.5
1.0	-69.0
1.5	-30.5
2.0	33.0
2.5	65.0
3.0	94.0
4.0	136.0
M_∞	233.0
T_1/S	2.58

T = 350.3 K	
τ/S	M_τ
0.5	-137.0
1.0	-95.0
1.5	-52.0
2.0	-5.0
2.5	35.0
3.0	53.5
4.0	100.5
4.5	123.0
5.0	142.5
M_∞	230.5
T_1/S	3.17

T = 372.0	
τ/S	M_τ
0.5	-144.0
1.0	-113.0
1.5	-59.0
2.5	14.0
3.0	32.0
3.5	64.0
4.0	96.0
4.5	102.0
M_∞	232.0
T_1/S	3.58

T = 402 K	
τ/S	M_τ
0.5	-118.0
1.0	-85.0
1.5	-42.0
2.5	11.5
3.0	48.5
3.5	58.0
4.0	71.0
4.5	97.5
M_∞	203.0
T_1/S	3.67

Temp/K	Intensity (gated)	Intensity (normal)	η
276.6	180.0	117.0	-0.35
284.3	208.0	137.0	-0.34
300.7	228.0	154.0	-0.33
317.2	196.5	131.0	-0.33
348.0	219.0	133.0	-0.39
368.3	219.0	153.0	-0.30

APPENDIX B

74/74 OPT=2 FTN 4.6+428

```
      PROGRAM INERT (INPUT,OUTPUT,TAPE5=INPUT,TAPE6=OUTPUT)
      DIMENSION X(99),Y(99),Z(99),AMASS(99),SYM(6),AFX(6),AFY(6),AHX(6
     1AHY(6),T(3,3),VECA(3),VECB(3),VECC(3),PAT(3,3),TAP(3,3),AM(3,3)
     2AI(3,3),R(99)
      REAL NEWX
      WRITE(6,100)
  100 FORMAT(* HOW MANY ATOMS ARE THERE IN THE MOLECULE*)
      READ(5,101)NATOM
  101 FORMAT(I3)
      WRITE(6,102)
  102 FORMAT(* PLEASE ENTER THE X,Y AND Z COORDINATES OF EACH ATOM *
     1/* FOLLOWED BY ITS ATOMIC MASS.  UNITS TO BE USED AE ANGSTROMS*
     2/* AND A.M.U'S.X,Y,Z.AND MASS FOR EACH ATOM ARE ENTERED AS FOUR
     3/* F9.4 NUMBERS PER LINE*/)
      DO 104 J=1,NATOM
      READ(5,*)X(J),Y(J),Z(J),AMASS(J)
  104  CONTINUE
C     CALCULATE THE CO ORDINATES OF THE CENTRE OF GRAVITY
      CX=0.0
      CY=0.0
      CZ=0.0
      TOT=0.0
      DO 6 K=1,NATOM
      A=AMASS(K)
      TOT=TOT+A
      CX=CX+A*X(K)
      CY=CY+A*Y(K)
    6 CZ=CZ+A*Z(K)
      CX=CX/TOT
      CY=CY/TOT
      CZ=CZ/TOT
      WRITE(6,7)CX,CY,CZ
    7 FORMAT(1X,* FOR THIS MOLECULE THE CENTRE OF GRAVITY HAS CO-ORDS
     1/,F6.3*,*F6.3*,*F6.3)
C     INITIALIZE THE TENSOR MATRIX
      DO 10 K=1,3
      DO 10 J=1,3
   10 T(K,J)=0.0
C     CALCULATE THE ELEMENTS OF THE TENSOR MARIX
      DO 8 K=1,NATOM
      R(K)=(((Y(K)-CY)**2)+((X(K)-CX)**2))+((Z(K)-CZ)**2)
      A=AMASS(K)
      T(1,1)=T(1,1)+A*(R(K)-((X(K)-CX)**2))
      T(1,2)=T(1,2)-A*(X(K)-CX)*(Y(K)-CY)
      T(1,3)=T(1,3)-A*(X(K)-CX)*(Z(K)-CZ)
      T(2,2)=T(2,2)+A*(R(K)-((Y(K)-CY)**2))
      T(2,3)=T(2,3)-A*(Y(K)-CY)*(Z(K)-CZ)
    8 T(3,3)=T(3,3)+A*(R(K)-((Z(K)-CZ)**2))
      T(3,2)=T(2,3)
      T(2,1)=T(1,2)
      T(3,1)=T(1,3)
      TZA=T(1,1)
      TZB=T(1,2)
      TZC=T(1,3)
      TZD=T(2,2)
      TZE=T(2,3)
      TZF=T(3,3)
```

```
74/74   OPT=2                    FTN 4.6+428        19/09/
      WRITE(6,11)
   11 FORMAT(1X*THE TENSOR MATRIX IS *)
      CALL PRINT (T,3,3)
C     CALCULATE THE EIGENVALUES
      D=T(1,1)*T(2,2)*T(3,3)+T(1,3)*T(2,1)*T(3,2)+T(1,2)*T(2,3)*T(3,1)
     1-T(1,3)*T(2,2)*T(3,1)-T(1,1)*T(2,3)*T(3,2)-T(2,1)*T(1,2)*T(3,3)
      B=T(1,1)+T(2,2)+T(3,3)
      C=T(2,3)*T(3,2)+T(2,1)*T(1,2)+T(3,1)*T(1,3)-T(1,1)*T(2,2)
     1-T(1,1)*T(3,3)-T(2,2)*T(3,3)
      OLDX=1.0
    1 NEWX=OLDX-(OLDX*OLDX*OLDX-B*OLDX*OLDX-C*OLDX-D)/(3.0*OLDX*OLDX-
     12.0*OLDX*B-C)
      DELX=NEWX-OLDX
      DELX=ABS(DELX)
      IF(DELX.EQ.0.0) GO TO 2
      OLDX=NEWX
      GO TO 1
    2 IF(OLDX.EQ.0.0)GO TO 3
      GAMMA=OLDX
      GOBBLE=SQRT(ABS(((GAMMA*GAMMA-B*GAMMA)**2)-4.0*GAMMA*D))
      ROOT=GOBBLE/(2.0*GAMMA)
      GO TO 4
    3 ROOT=0.0
      GAMMA=0.0
    4 ALPHA=(B-GAMMA)/2.0+ROOT
      BETA=(B-GAMMA)/2.0-ROOT
      WRITE(6,12)ALPHA,BETA,GAMMA
   12 FORMAT(1X,*THE THREE EIGENVALUES OF THE TENSOR MATRIX ARE*
     1/,E14.8,5X,E14.8,5X,E14.8)
C     CALCULATE THE EIGENVECTOR GENERATED BY ALPHA
      TEST=0.
      CALL EIGEN (TZA,TZB,TZC,TZD,TZE,TZF,GAMMA,VECCA,VECCB,VECCC,TEST)
      PAT(1,1)=VECCA
      PAT(2,1)=VECCB
      PAT(3,1)=VECCC
      CALL EIGEN (TZA,TZB,TZC,TZD,TZE,TZF,BETA ,VECCA,VECCB,VECCC,TEST)
      PAT(1,2)=VECCA
      PAT(2,2)=VECCB
      PAT(3,2)=VECCC
      CALL EIGEN (TZA,TZB,TZC,TZD,TZE,TZF,ALPHA,VECCA,VECCB,VECCC,TEST)
      PAT(1,3)=VECCA
      PAT(2,3)=VECCB
      PAT(3,3)=VECCC
      IF (TEST.GT.0.0)CALL DIG(PAT)
C     FORM THE INVERSE OF PAT IETAP
      DO 39 J=1,3
      DO 39 K=1,3
   39 TAP(K,J)=PAT(J,K)
C     FORM THE PRODUCT OF THE TENSOR MATRIX WITH PAT AND LABEL THE PRODUCT AM
      CALL MATRIX(T,PAT,AM,3,3,3)
C     FORM THE PRODUCT OF TAP WITH AM TO GIVE M.O.I.MATRIX
      CALLMATRIX(TAP,AM,AI,3,3,3)
      WRITE(6,40)
   40 FORMAT(1X,*THE PRINCIPAL AXIS TRANSFORM MATRIX IS*)
      CALL PRINT(PAT,3,3)
      WRITE(6,41)
   41 FORMAT(1X,*THE MOMENT OF INERTIA MATRIX IS*)
```

74/74 OPT=2 FTN 4.6+428

```
      CALL PRINT(AI,3,3)
1000  CONTINUE
      STOP
      END
```

74/74 OPT=2 FTN 4.6+428

```
      SUBROUTINE ZERO(A)
      VALX=A+0.001
      VALM=A-0.001
      IF(VALX)1,2,2
    2 IF(VALM)3,3,1
    3 A=0.
    1 RETURN
      END
```

74/74 OPT=2 FTN 4.6+42

```
      SUBROUTINE EIGEN(A,B,C,D,E,F,EI,V1,V2,V3,TEST)
      ALPHA=C*D-E*B-C*EI
      BETA=E*A-C*B-E*EI
      GAMMA=A*F-C*E-B*EI
      CALL ZERO(ALPHA)
      CALL ZERO(BETA)
      CALL ZERO(GAMMA)
      IF(ALPHA.EQ.0.0.AND.BETA.EQ.0.0.AND.GAMMA.EQ.0.0)GO TO 1
      IF(ALPHA.EQ.0.0.AND.BETA.EQ.0.0) GO TO 2
      GO TO 3
    2 Z=0.0
      X=1.0
      Y=((A-B-EI))*X/(D-B-EI)
      GO TO 4
    3 IF(ALPHA.EQ.0.0.AND.GAMMA.EQ.0.0) GO TO 5
      GO TO 6
    5 X=0.
      Z=1.0
      Y=(F-E-EI)*Z/(D-E-EI)
      GO TO 4
    6 IF(BETA.EQ.0.0.AND.GAMMA.EQ.0.0) GO TO 7
      GO TO 8
    7 Y=0.
      X=1.
      Z=(A-C-EI)*X/(F-C-EI)
      GO TO 4
    8 IF(ALPHA)9,10,9
   10 X=0.
      Z=0.
      Y=1.
      GO TO 4
    9 IF(BETA)11,12,11
   12 Y=0.
      Z=0.
      X=1.
      GO TO 4
   11 IF(GAMMA)13,14,13
   14 X=0.
      Y=0.
      Z=1.
      GO TO 4
   13 X=1.
      Y=BETA*X/ALPHA
      Z=BETA*X/GAMMA
    4 ANORM=SQRT(X*X+Y*Y+Z*Z)
      V1=X/ANORM
      V2=Y/ANORM
      V3=Z/ANORM
      RETURN
    1 V1=0.
      V2=0.
      V3=0.
      CALL SNUG(EI,F,V3)
      CALL SNUG(EI,D,V2)
      CALL SNUG(EI,A,V1)
      AMBER=V1+V2+V3
      IF(AMBER.GT.1.0)TEST=1.0
```

74/74 OPT=2 FTN 4.6+428

```
      RETURN
      END
```

74/74 OPT=2 FTN 4.6+428

```
      SUBROUTINE SNUG(A,B,C)
      D=A-B
      CALL ZERO(D)
      IF(D.EQ.0.0)C=1.0
      RETURN
      END
```

74/74 OPT=2 FTN 4.6+428

```
      SUBROUTINE DIG (P)
      DIMENSION P(3,3)
      DO 1 J=1,3
      DO 1 K=1,3
      P(J,K)=0.
      P(J,J)=1.
    1 CONTINUE
      RETURN
      END
```

74/74 OPT=2 FTN 4.6+428

```
      SUBROUTINE MATRIX (A,B,C,L,M,N)
      DIMENSION A(M,N),B(N,L),C(M,L)
C     THE FIRST TWO DO LOOPS ARE USED TO TAKE EVERY ELEMENT OF THE
      DO 3 J=1,M
      DO 3 K=1,L
C THE THIRD DO LOOP IS USED TO EXECUTE THE SUMMATION  =A(J,N)*B(N,K
C     CLEAR ANSWER MATRIX
      C(J,K)=0.0
      DO 3 NN=1,N
      C(J,K)=C(J,K)+(A(J,NN)*B(NN,K))
    3 CONTINUE
      RETURN
      END
```

74/74 OPT=2 FTN 4.6+428

```
      SUBROUTINE PRINT (A,K,J)
      DIMENSION A(K,J),BORMAT(7),OUTPUT(30)
C     START WITH THE ALPHANUMERIC SYMBOLS TO BE USED IN THE COMPIL AT
C   FORMAT STATEMENT
      DATA(BORMAT(L),L=1,7)/4H(    ,4H2H**,4H,5X,,4HF9.3,4H,//),4H 1H*
     1    /
C     NEXT  CLEAR THE FORMAT ARRAY
      DO 1 I7=1,30
      OUTPUT(IZ)=BORMAT(7)
    1 CONTINUE
C     PLACE OPENING AND CLOSING PARENTHESIS IN YE ARRAY
C     ALSO PUT THE FIRST SPACING SYMBOL
      OUTPUT(1)=BORMAT(1)
      OUTPUT(2)=BORMAT(2)
      OUTPUT(3)=BORMAT(3)
C     INITIATE THE CELL COUNT
      ITEST=4
CYCLE FOR THE  ROWS OF LENGTH J
      DO 2 IK =1,J
C     PLACE IN A F7.2 AND A 5X IN THE NEXT AVAILABLE CELLS
      OUTPUT(ITEST)=BORMAT(4)
      OUTPUT(ITEST+1)=BORMAT(3)
C     INCREMENT THE CELL COUNT
      ITEST=ITEST+2
    2 CONTINUE
C     PUT THE CLOSING     *    TO THE OUT PUT TO SIGNIFY THE END OF A L
      OUTPUT(ITEST+1)=BORMAT(6)
      OUTPUT(ITEST+2)=BORMAT(5)
C     CYCLE OUTPUT FOR THE K ELEMENTS OF THE COLUMN TO ENABLE OUTPUT
      DO 3 KLM=1,K
      WRITE(6,OUTPUT)(A(KLM,N),N=1,J)
    3 CONTINUE
      RETURN
      END
```

APPENDIX C

PROGRAM ANDY 74/74 OPT=2 FTN 4.6+

```
      PROGRAM ANDY(INPUT,OUTPUT,TAPE 1=INPUT,TAPE2=OUTPUT)
      REAL MEANK,K
      DIMENSION A(10),K(10),SP(10),C(10),O(10)
      READ (1,8) D
    8 FORMAT(F10.0)
      DO 300 L=1,6
      T=-200.0
      READ (1,9) TEMP
    9 FORMAT(F10.0)
      WRITE(2,4) TEMP
    4 FORMAT(/,8X*TEMP=*F8.4)
      WRITE(2,51)
   51 FORMAT(///,3X*DELTAO*4X*CONC*)
      DO 102 I=1,3
      READ (1,20) O(I),C(I)
   20 FORMAT(2F10.0)
      WRITE(2,50)O(1),C(1)
   50 FORMAT(///,3X,F10.4,3X,F8.4)
  102 CONTINUE
      J=0
  200 SUMK=0.0
      DO 100 I=1,3
      A(I)=(O(I)-T)/((2.0*D)-T-O(I))
      K(I)=((4.0*A(I)*A(I)*C(I))/(1-A(I);)
      SUMK=SUMK+K(I)
  100 CONTINUE
      SSR=0.0
      MEANK=SUMK/3.0
      DO 101 I=1,3
      SR(I)=(MEANK-K(I))**2
      SSR=SSR+SR(I)
  101 CONTINUE
      SD=SQRT((SSR)/2.0)
      SDR=SD/1.7320508
      ERR=(SUM*100.0)/MEANK
      WRITE (2,5) K(1),K(2),K(3)
    5 FORMAT(///,3X,F8.4,3X,F8.4,3X,F8.4)
      WRITE(2,6) SD,SDM,ERR
    6 FORMAT(//,F8.4,3X,F8.4,3X,F8.4)
      T=T-0.5
      WRITE(2,7) T
    7 FORMAT(/,3X*DELTAT=*F8.2)
      J=J+1
      IF(J.LE.40)GO TO 200
  300 CONTINUE
      STOP
      END
```